METHODS FOR THE ANALYSIS OF ORGANIC CHEMISTRY ON TITAN

Thesis by

Robert Hodyss

In Partial Fulfillment of the Requirements

for the Degree of

Doctor of Philosophy

CALIFORNIA INSTITUTE OF TECHNOLOGY

Pasadena, California

2006

(Defended November 1, 2005)

Acknowledgements

Ron Grimm Heather Sumner Karin Oberg Ryan Julian Daniel Austin Jack Beauchamp Pat Beauchamp Jonathan Lunine Mark Smith Dennis Dougherty Christopher Welch Niladri Sarker Chu-Ha Oh Gary Hansen Karl Hibbits Nathan Daleska Rick Gerhart Mike Echevarria

Abstract

Tholins are brownish, sticky residues formed by the energetic processing of mixtures of gases abundant in the cosmos, such as CH_4, N_2, and H_2O, either with ultraviolet light or electrical discharge. This thesis describes investigations of the tholins produced by the processing of mixtures of N_2 and CH_4, as a model of photochemical processes occurring in the atmosphere of Titan. These compounds are mixed with liquid water during impacts or cryovolcanism, in melt pools which eventually freeze. The melt pools are interesting sites for astrobiological research, containing a wealth of organic material interacting over long time periods in a liquid water solvent. Studies of the near infrared reflectance spectrum and the fluorescent properties of the tholins are presented, yielding information on the composition of the tholins and a means of finding organic deposits on the surface of Titan. Tholin decomposition on heating is extensively investigated, partly to ascertain the utility of pyrolysis as a technique for tholin characterization. Tholins are found to undergo significant chemical change at temperatures as low as 100 °C, releasing large quantities of ammonia, while at higher temperatures, cyclizing and aromatizing reactions occur. Pyrolysis is thus not a good technique for the characterization of tholins. The development of two instruments for tholin characterization are also discussed: a gas chromatograph with an ultraviolet absorption detector, for functional group analysis of the tholins, and sensors designed for the determination of enantiomeric excess.

Table of Contents

Acknowledgements iii

Abstract iv

1 Introduction 1-1

1.1 References 1-5

2 Titan as a laboratory for prebiotic chemistry 2-1

2.1 Introduction 2-1

2.2 Tholins 2-3

2.3 Impacts on Titan 2-4

2.4 Recent data from Cassini 2-5

2.5 Conclusions 2-6

2.6 References 2-7

3 Infrared reflectance spectra of tholins at cryogenic temperatures 3-1

3.1 Introduction 3-1

3.2 Experimental..... 3-2

3.3 Near infrared reflectance spectra of tholins 3-4

3.4 Conclusions 3-10

3.5 References 3-11

4 Heat-induced chemical change in tholins: the case against pyrolysis 4-1

4.1 Introduction 4-1

4.2 Thermal gravimetric analysis and differential scanning calorimetry of tholins..... 4-3

4.3 Headspace gas chromatography of heated tholins..... 4-6

4.4 Laser desorption ionization mass spectrometry of heated tholin residues. 4-9

4.5 Thermal analysis of tholins by UV absorption spectroscopy of desorbed species 4-13
4.6 Conclusions 4-28
4.7 References 4-30

5 Complexation of tholins by 18-crown-6: identification of primary amines 5-1
5.1 Introduction 5-1
5.2 Experimental 5-2
5.3 Complexation of 18-crown-6 with tholins 5-3
5.4 Conclusions 5-7
5.5 References 5-8

6 Fluorescence spectra of Titan tholins: *in-situ* detection of astrobiologically interesting areas on Titan's surface 6-1
6.1 Abstract 6-1
6.2 Introduction 6-2
6.3 Experimental 6-3
6.4 Three-dimensional fluorescence spectra 6-5
6.5 Thin-layer chromatography 6-8
6.6 Fluorescence spectra of tholins at 77K 6-11
6.7 Conclusions 6-13
6.8 Acknowledgements 6-14
6.9 References 6-15

7 Gas chromatography-ultraviolet detection for tholin analysis 7-1
7.1 Introduction 7-1
7.2 Experimental 7-2
7.3 GC-UV of tholin pyrolysis products 7-5
7.4 Conclusions 7-9
7.5 References 7-13

8 Detectors for the determination of enantiomeric excess 8-1
8.1 Introduction 8-1
8.2 Experimental..... 8-2
8.3 Results and discussion 8-8
8.4 Conclusions 8-10
8.5 References 8-11

Appendices

A Multi-Dimensional Detection of Nitro-organic Explosives by Gas Chromatography-Pyrolysis-Ultraviolet Detection (GC-PUD) A-1
A.1 Abstract A-1
A.2 Introduction A-1
A.3 Experimental..... A-4
A.4 Results and Discussion..... A-7
A.5 Conclusions A-9
A.6 Acknowledgements..... A-10
A.7 References A-10

B Simple Optical Sensor for Amine Vapors Based on Dyed Silica Microspheres B-1
B.1 Abstract B-1
B.2 Introduction B-1
B.3 Experimental..... B-4
B.4 Results and Discussion..... B-8
B.5 Conclusions B-19
B.6 Acknowledgements..... B-20
B.7 References B-20

List of Figures

1

1.1 LDI mass spectrum of tholins 1-2

2

2.1 Reactor for tholin production 2-3

3

3.1 Infrared reflectance spectra of tholins 3-5

3.2 Mid-IR region of the IR reflectance spectra of tholins 3-7

3.3 Infrared reflectance spectrum of polyacrylonitrile 3-10

3.4 Difference spectrum between 123 K and 303 K 3-10

4

4.1 Thermal gravimetric analysis of tholins 4-4

4.2 Differential scanning calorimetry of tholins 4-5

4.3 GC-MS chromatograms of tholin headspace gases 4-7

4.4 LDI mass spectra of heated tholin residues 4-10

4.5 Magnified view of spectra in Figure 4.4 4-11

4.6 Experimental arrangement for UV spectroscopy of evolved gases 4-14

4.7 Heating curve for UV spectroscopy experiments 4-15

4.8 Thermal degradation of tholins 4-16

4.9 Thermograms for tholins 4-18

4.10 Thermal degradation of hydrolyzed tholins 4-19

4.11 Thermograms for hydrolyzed tholin 4-20

4.12 Thermal degradation of polyacrylonitrile 4-21

4.13 Thermograms for polyacrylonitrile 4-22

4.14 Thermal degradation of polyallylamine 4-25

4.15 Thermal degradation of polypyrrole 4-26

4.16 Thermal degradation of polyethyleneimine 4-27

5

5.1 ESI mass spectrum of tholin and 18-crown-6 5-4

5.2 CAD spectrum of 416 m/z 5-5

5.3 Source CAD of tholin-crown ether complexes 5-6

6

6.1 Experimental arrangement for fluorescence 6-4
6.2 3-D fluorescence spectrum of tholin..... 6-6
6.3 Fluorescence of TLC plates..... 6-9
6.4 3-D fluorescence spectrum of spot 1 6-10
6.5 Fluorescence spectra of tholins in ice 6-12

7

7.1 Pyrolysis-GC-UV system..... 7-3
7.2 Lab-built low temperature pyrolyzer 7-4
7.3 GC-MS chromatogram of tholin pyrolysis products 7-6
7.4 3-D GC-UV chromatogram of tholin pyrolysis products 7-7
7.5 Spectrum of the peak at 90 s 7-8
7.6 Spectrum of the peak at 125 s..... 7-10
7.7 Spectrum of the peak at 250 s..... 7-10
7.8 Gas-phase ultraviolet spectrum of 1-hexene 7-11
7.9 Gas-phase ultraviolet spectrum of 5-hexenenitrile..... 7-11
7.10 Gas-phase ultraviolet spectrum of tert-butylamine..... 7-12
7.11 Gas-phase ultraviolet spectrum of diethylamine 7-12
7.12 Gas-phase ultraviolet spectrum of triethylamine..... 7-13

8

8.1 Block diagram of the QCM apparatus 8-5
8.2 Colpitts oscillator..... 8-6
8.3 Response of the QCM to methyl lactate vapor..... 8-9
8.4 Response of SAW sensor to methyl lactate vapor..... 8-10

A

A.1 Block diagram of GC-PUD system A-5
A.2 3-D GC-PUD chromatogram..... A-6
A.3 Peak area vs. mass of analyte A-8

B

B.1 Schematic diagram of the optical sensor system..... B-5

B.2 Diffuse reflectance spectrum of the LED..... B-6
B.3 Bromocresol green and its conjugate base..... B-8
B.4 Absorbance spectra of the sensor B-9
B.5 Absorbance versus time at different temperatures..... B-12
B.6 Absorbance curves for different concentrations of t-butylamine..... B-13
B.7 Successive sensor response for triethylamine B-14
B.8 Relationship between absorbance and concentration B-15
B.9 Absorbance versus time at 620 nm..... B-17
B.10 Detector response for 1.4 ppb tert-butylamine..... B-18

List of Tables

2

2.1 Selected components of Titan's atmosphere 2-2

3

2.1 Frequencies and assignments for tholins in the IR 3-9

B

B.1 Table of pK_a and gas phase basicities B-10

Chapter 1. Introduction

The term "tholin" was coined by Carl Sagan in 1979 (Sagan and Khare, 1979), to describe the products obtained by the energetic processing of mixtures of gases abundant in the cosmos, such as CH_4, N_2, and H_2O. Tholin comes from the Greek, meaning "muddy", an apt description for the brownish, sticky residues formed by such experiments. These experiments, using either electrical discharges or ultraviolet irradiation, are the natural extensions of the well-known Miller-Urey experiment (Miller and Urey, 1959). While the Miller-Urey experiment focused on an atmosphere meant to be like that of the early Earth, Sagan and others attempted to simulate the atmospheres of other planets and moons in the Solar System, such as Titan, Triton (McDonald*,* et al., 1994), and Jupiter (Khare and Sagan, 1975).

As one would expect, tholins are a very complex mixture of organics, and are a great challenge for most analytical methods. A laser desorption ionization mass spectrum of a tholin created by electrical discharge of an N_2/CH_4 mixture is shown in Figure 1.1. There are literally thousands of distinct compounds represented here, and an even larger number of isomers will exist that cannot be separated by mass spectrometry. But there is still order apparent in the mixture. The spectrum shows groups of peaks differing by 14 m/z, the mass of a methylene unit. This kind of pattern gives us hope that a more detailed understanding of the structure of the tholins is possible.

Since our interest is in Titan, the focus of this thesis is on the Titan tholins, those made from mixtures of N_2 and CH_4, the predominant components of Titan's atmosphere.

Titan is of great interest as an astrobiological target because it is a unique place in the Solar System. Titan has a dense atmosphere, and so is thought to have a great abundance of organics on its surface, the result of photochemical reactions in the upper atmosphere.

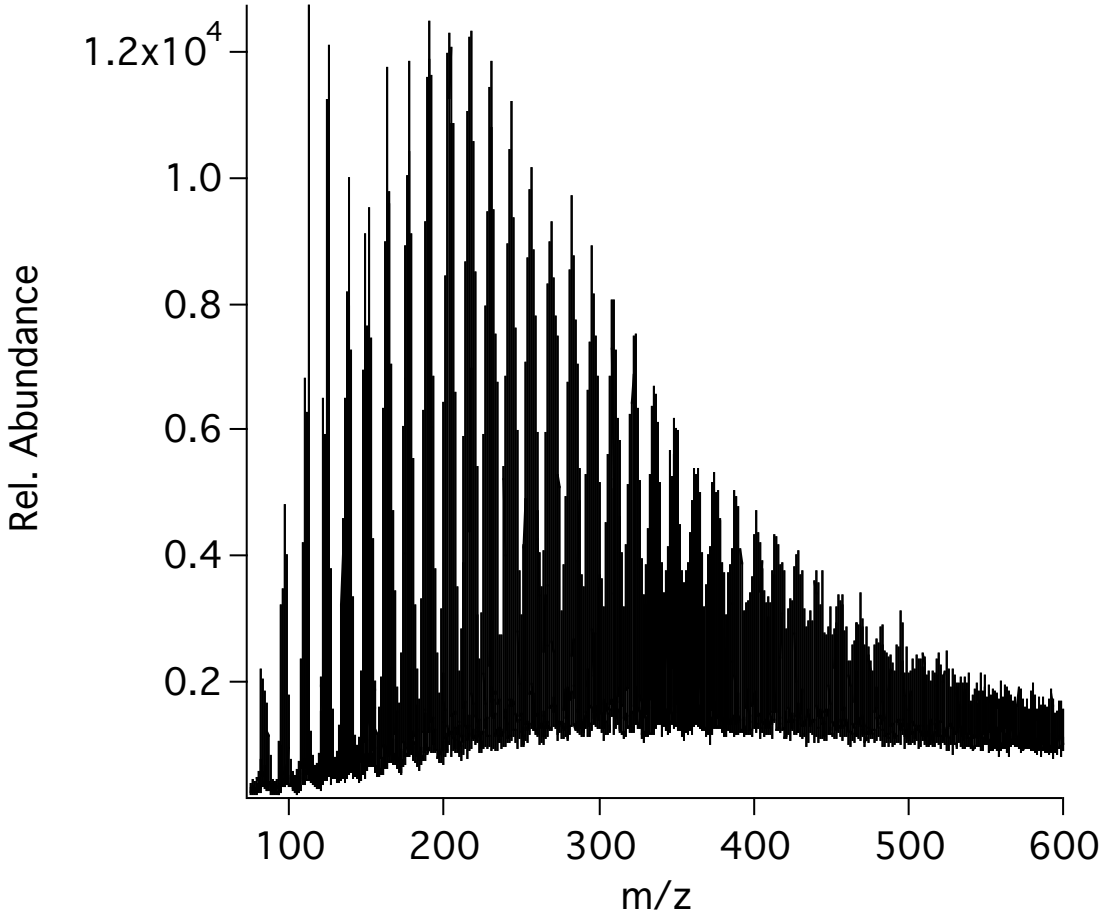

Figure 1.1 Laser desorption ionization mass spectrum of CH_4 + N_2 tholins.

Titan also has a surface expected to be composed primarily of water ice, with a surface temperature of ~90 K. Impactors or cryovolcanism would result in a mixture of organics

and liquid water, which would eventually freeze (Artemieva and Lunine, 2003; Artemieva and Lunine, 2005). Each impact site or volcanic event represents an individual experiment in prebiotic chemistry, preserved by the cold for later study. Chapter two discusses the promise of Titan as a laboratory for prebiotic chemistry in greater detail.

This thesis explores two broad themes. The first is the characterization of Titan tholins. While many researchers characterize their tholin materials as a matter of course, using infrared spectroscopy and mass spectrometry, we have instead concentrated on techniques that have been more infrequently used for tholin analysis, and we hope this approach has led to a greater understanding of the nature of the tholins.

Chapter three is a detailed study of the near infrared reflectance spectrum of tholins at temperatures close to those of Titan's surface. Few studies of the spectrum exist between 1 and 5 microns, and these spectra help fill that gap. Near-infrared spectra of tholins are useful in models of the albedo of asteroids and other small interplanetary bodies, and may prove of value in the future exploration of Titan.

Chapter four discusses the chemical changes that occur when tholins are heated. A variety of techniques have been used here; thermal gravimetric analysis, differential scanning calorimetry, headspace GC-MS, LDI-MS, and ultraviolet evolved gas analysis. The results of these techniques are synthesized into the beginning of an understanding of the processes that occur when the tholins are heated. While it is impossible to ever have a complete understanding of the processes that occur in a material as complex as the

tholins, we have discovered that they are very unstable when heated, releasing large amounts of ammonia at only 100 °C, and as heating continues, cyclizing and aromatizing. These results have implications for the further study of tholins, especially by pyrolytic techniques, and for the surface of Titan as well.

Chapter five uses mass spectrometry to separate a particular portion of the tholins for analysis. Electrospray ionization mass spectrometry is used to introduce the tholins into the gas phase in association with 18-crown-6, a molecule that forms a strong non-covalent complex with protonated primary amines. Two related homologous series of ions are seen complexed with the crown ether. This is the first identification of these molecules in the tholin mixtures.

Chapter six separates another subset of the tholins for study: the fluorescent components. Three-dimensional fluorescence spectra and thin layer chromatography are used to classify the fluorescent components. Tholins are highly fluorescent, and several distinct fluorophores can be identified.

Chapter six also begins the exploration of our second theme, the development of instrumentation for the future exploration of the chemistry of Titan. Spaceflight instrumentation must meet stringent limitations on power, weight and size, and so the design of equipment for chemical analysis can be challenging. In Chapter six, we use our knowledge of the fluorescent properties of the tholins to construct a small fiber optic spectrometer that can examine the fluorescent properties of ices. Tholin in a water ice matrix is shown to have a fluorescence distinct from the aqueous or solid phases. Such

an instrument incorporated into a Titan probe would be able to locate areas where tholins had been exposed to liquid water, and then frozen. These areas would be of great astrobiological interest.

Chapter seven discusses the use of an unusual instrument, a gas chromatograph with a gas phase far-ultraviolet absorption detection system. The use of far-ultraviolet spectroscopy as a detection method for gas chromatography (GC) allows for the identification of functional groups by their characteristic absorptions. We demonstrate the use of the system on the pyrolysis products of the tholins. GC-UV has the advantage over GC-MS systems in weight and power requirements, since a vacuum system is not required.

Chapter eight discusses our efforts to build enantiomerically selective detectors. The detection of enatioenrichment on Titan would be a step towards understanding the role enantioenrichment played in the origin of life. We have chosen quartz crystal microbalances as the transduction device, and use derivatized self-assembled monolayers as the sensing medium.

Finally, the appendices present some instruments that were developed along the way, although they have no direct application to Titan chemistry. Appendix A shows the utility of GC-UV (with minor modifications) for the detection of explosives. Appendix B is a detailed study of the characteristics of a simple, highly sensitive amine and ammonia detector developed in our labs.

1.1. References

Artemieva, N., and J.I. Lunine (2003), Cratering on Titan: impact melt, ejecta, and the fate of surface organics, *Icarus*, *164*, 471-480.

Artemieva, N., and J. I. Lunine (2005), Impact cratering on Titan - II. Global melt, escaping ejecta, and aqueous alteration of surface organics, *Icarus*, *175*, 522-533.

Khare, B. N., and C. Sagan (1975), Cyclic octatomic sulfur - possible infrared and visible chromophore in clouds of jupiter, *Science*, *189*, 722-723.

McDonald, G. D., et al. (1994), Chemical investigation of Titan and Triton tholins, *Icarus*, *108*, 137-145.

Miller, S. L., and H. C. Urey (1959), Organic compound synthesis on the primitive Earth, *Science*, *130*, 245-251.

Sagan, C., and B. N. Khare (1979), Tholins - organic chemistry of interstellar grains and gas, *Nature*, *277*, 102-107.

Chapter 2. Titan as a Laboratory for Prebiotic Chemistry

2.1. Introduction

Titan is the largest moon of Saturn, and in fact, one of the largest moons in the Solar System. Discovered by Christian Huygens in 1655, it is larger in diameter than the planets Mercury and Pluto. This alone would make Titan an intriguing target for exploration, and Titan was visited by the Voyager 1 spacecraft in 1980, and more recently by the Cassini/Huygens mission to Saturn. Additionally, Titan possesses a thick nitrogen/methane atmosphere, shrouded in haze that obscures the surface.

Clearly, the atmosphere has been the primary focus for planetary scientists studying Titan. Early spectroscopic measurements found methane at concentrations of a few percent, and later higher hydrocarbons such as acetylene and propane were observed. Table 2.1 gives the mole fraction of some select species in Titan's atmosphere [Lewis, 2004]. Of course, the concentration of these compounds vary by latitude and altitude [Flasar*, et al.*, 2005]. Nitrogen containing species, such as HCN, were also discovered. These compounds are the result of photochemistry in the upper reaches of the atmosphere. Photochemistry also results in aerosols which form a haze at high altitudes (>300 km) [Imanaka*, et al.*, 2004]. The aerosols eventually fall to the surface, during which condensation of organics onto the aerosol may occur. The temperature at the surface of Titan is about 90 K. The compounds that reach the surface are thus frozen and trapped on the surface.

Table 2.1 Selected components of the atmosphere of Titan

Species	Mole fraction
N_2	~.94
CH_4	0.06
H_2	2×10^{-3}
CO	5×10^{-5}
C_2H_6	2×10^{-5}
C_2H_2	2×10^{-6}
HCN	2×10^{-7}

The chemistry that occurs in the upper atmosphere drives interest in Titan as a laboratory for prebiotic chemistry. The compounds formed in the upper atmosphere eventually fall down to the surface, where impacts and cryovolcanism will mix them with liquid water. The melt pools will freeze, and preserve the products of hydrolysis for later examination. Each frozen pool represents a separate experiment in prebiotic chemistry on a scale that is unavailable on Earth. The direct exploration of the surface of Titan, and of these frozen pools, would contribute greatly to our understanding of prebiotic chemistry, and perhaps ultimately to an understanding of how life arose on Earth.

2.2. Tholins

Any attempt to understand the complexity of the chemical reactions occurring in the atmosphere of Titan will require an experimental approach that can simulate these

reactions. The current approach uses an electrical discharge in a gas mixture of nitrogen and methane representative of the atmosphere of Titan, using reactors like that in Figure 2.1. A number of workers have performed these kinds of experiments, utilizing a variety of experimental conditions, varying temperature, pressure, and the form of the discharge, either microwave, DC, or AC.

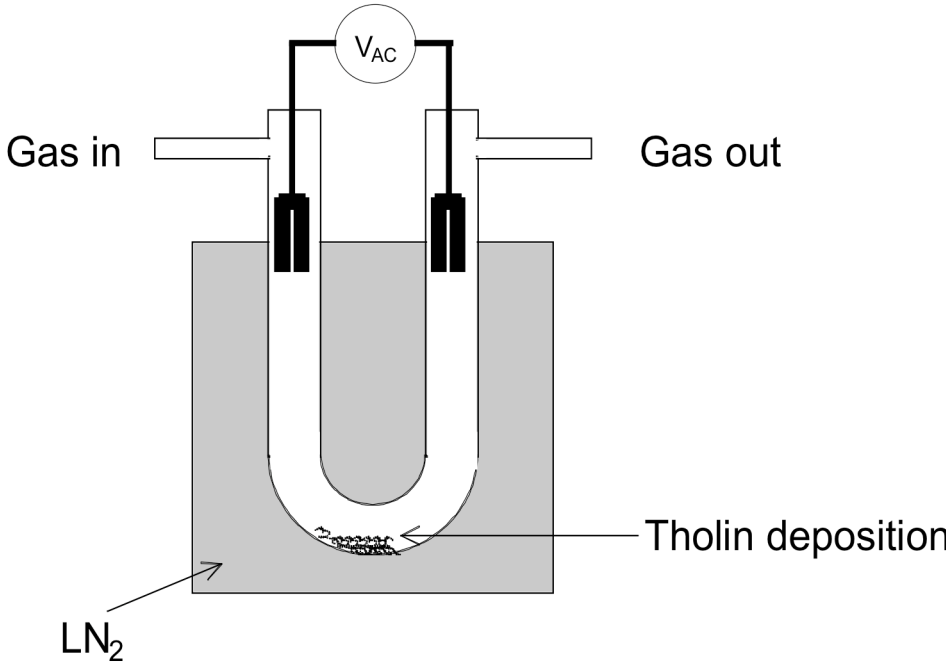

Figure 2.1. Plasma reactor for the production of tholins.

In all cases, however, these experiments yield a reddish brown or orange polymeric material, coined by Carl Sagan as "tholin," from the Greek, meaning "muddy" [Sagan and Khare, 1979]. Figure 2.2 is a diagram of the kind of plasma reactor used to produce the tholins discussed in this thesis. The details of the production of the tholin are described elsewhere [Sarker, *et al.*, 2003]; [Somogyi, *et al.*, 2005].

Chemically, the tholins are composed of CHN compounds, usually with C/N ratios of around 2, and C/H ratios of around 0.75 [Sarker, *et al.*, 2003]. Infrared analysis indicates that the material possesses basically all the functional groups one might expect, such as amines, nitriles, alkenes, and imines. Electrospray mass spectral analysis shows many thousands of compounds. The sheer complexity of the material makes the tholins highly intractable to most analytical methods.

Several workers have performed hydrolysis of the tholins, mainly reporting on the yield of amino acids produced. Hydrolysis in acid produces amino acids in yields between 0.2 and 7 mg/g tholin [Mcdonald, *et al.*, 1994]. Obviously, a large number of other kinds of molecules, including urea [Khare, *et al.*, 1986], are formed during hydrolysis as well. Hydrolysis may also produce carboxylic acids, alcohols, or possibly even purines and pyrimidines.

2.3. Impacts on Titan

Like all planetary bodies, Titan is occasionally hit by an impactor of a size large enough to survive passage through the atmosphere and hit the surface. Artemieva and Lunine have modeled the result of such impacts [Artemieva and Lunine, 2003; [Artemieva and Lunine, 2005]. Restricting their modeling to comets, they find that projectiles smaller than 100-200 m will not reach the surface intact, and that impactors larger than 1 km in diameter are basically unaffected by the atmosphere. This is important since projectiles smaller than this will experience enough atmospheric drag to significantly alter the impact velocity and thus crater size. Assuming the surface is composed of water ice, a 2 km diameter icy projectile impacting at a velocity of 7 km/s or

higher, at an angle of impact between 30° and 45°, will generate 2-5% melt by volume within the crater [Artemieva and Lunine, 2003].

Not unexpectedly, much of the surface organics will be heavily shocked and ejected from the crater. However, the impact modeling shows that a significant percentage of the organics are deposited in the melt at the bottom of the crater [Artemieva and Lunine, 2003]. Furthermore, the liquid will ice over quite rapidly, and then proceed to freeze downward. The timescale for complete freezing of the melt pool is surprisingly long. Several hundred or even thousands of years (if there is a significant amount of ammonia, as seems likely) would be required for complete freezing. This is plenty of time for significant aqueous alteration of the organic material.

Modeling of cratering rates shows that there should be hundreds of craters greater than 100 km in diameter on the surface of Titan [Artemieva and Lunine, 2005]. Many will likely be covered and obscured by organic deposits, but the more recent craters should be more visible. In any event, over the entire planet a very large quantity of organics would have been processed by water during the history of the Solar System.

2.4. Recent data from Cassini-Huygens

The Cassini-Huygens mission arrived at Saturn on June 30, 2004. Several close flybys of Titan have already been completed, and many more are planned in the coming years. As well, the Huygens probe successfully penetrated the atmosphere of Titan and landed on the surface in January 2005. While analysis of the data is ongoing, some intriguing results relevant to the question of organic surface chemistry have been obtained.

Two separate features seen on the surface are relevant to this discussion. Data obtained with the radar imager aboard the probe has revealed a large (180 km in diamter) circular feature, possibly a volcanic dome or an old impact scar [Elachi*, et al.*, 2005]. Channels that appear to carry material away from the center radiate from the feature. The radar imager also shows that the surface of Titan is rather young; few impact features are visible in the radar strip obtained [Elachi*, et al.*, 2005]. This could be the result of coverage by organics produced in the atmosphere.

The Visible and Infrared Mapping Spectrometer aboard Cassini has also revealed a feature best interpreted as a cryovolcano [Sotin*, et al.*, 2005]. The putative volcanic dome is 30 km in diameter, and appears to be releasing volatiles. Eruptions of ammonia-water liquids from such a volcano would undoubtedly lead to mixing of the surface organics with the liquid.

2.5. Conclusions

Titan is one of the most intriguing bodies in the Solar System. Possessed of a thick nitrogen-methane atmosphere, photochemistry in the upper atmosphere leads to the production of a wide variety of organic compounds which eventually settle to the surface. Impacts or cryovolcanism would then lead to the mixing of the organics with liquid water, or ammonia-water mixtures. Hydrolysis of the organics produces a range of oxygenated organic compounds, including amino acids. When the melt pools freeze, they preserve the products of hundreds or thousands of years of complex organic chemistry. Each melt pool is an individual experiment in prebiotic chemistry waiting for analysis. Exploration of Titan, with a particular emphasis on the organic chemistry of the

surface, would provide a new insight into the origin of life that would be unobtainable on Earth.

2.6. References

Artemieva, N., and J. Lunine (2003), Cratering on Titan: impact melt, ejecta, and the fate of surface organics, *Icarus*, *164*, 471-480.

Artemieva, N., and J. I. Lunine (2005), Impact cratering on Titan - II. Global melt, escaping ejecta, and aqueous alteration of surface organics, *Icarus*, *175*, 522-533.

Elachi, C., et al. (2005), Cassini radar views the surface of Titan, *Science*, *308*, 970-974.

Flasar, F. M., et al. (2005), Titan's atmospheric temperatures, winds, and composition, *Science*, *308*, 975-978.

Imanaka, H., et al. (2004), Laboratory experiments of Titan tholin formed in cold plasma at various pressures: implications for nitrogen-containing polycyclic aromatic compounds in Titan haze, *Icarus*, *168*, 344-366.

Khare, B. N., et al. (1986), Amino-Acids Derived from Titan Tholins, *Icarus*, *68*, 176-184.

Lewis, J. (2004), *Physics and Chemistry of the Solar System*, San Diego: Elsevier.

Mcdonald, G. D., et al. (1994), Chemical Investigation of Titan and Triton Tholins, *Icarus*, *108*, 137-145.

Sagan, C., and B. N. Khare (1979), Tholins - Organic-Chemistry of Inter-Stellar Grains and Gas, *Nature*, *277*, 102-107.

Sarker, N., et al. (2003), Titan aerosol analogues: Analysis of the nonvolatile tholins, *Astrobiology*, *3*, 719-726.

Somogyi, A., et al. (2005), Organic environments on Saturn's moon, titan: Simulating chemical reactions and analyzing products by FT-ICR and ion-trap mass spectrometry, *Journal of the American Society for Mass Spectrometry*, *16*, 850-859.

Sotin, C., et al. (2005), Release of volatiles from a possible cryovolcano from near-infrared imaging of Titan, *Nature*, *435*, 786-789.

Chapter 3. Infrared Reflectance Spectra of Tholins at Cryogenic Temperatures

3.1. Introduction

Infrared spectroscopy is one of the cornerstone techniques for molecular structure determination. Because of the relation between infrared absorption and structure, the infrared is a preferred region for use in remote sensing applications, in order to acquire compositional information on the surfaces of astronomical bodies. Prior to remote sensing, though, careful laboratory work is required in order for the results to be interpretable. Remote detection of solar system bodies is necessarily a reflectance technique in the near and mid-infrared, and so for laboratory studies to be relevant to remote sensing applications, spectra should be taken in the reflectance mode. It is also important to obtain comparison spectra at a temperature as close as possible to that of the body being studied, since infrared spectra may change as a function of temperature.

Infrared spectra of tholins are useful not just as a means of broadly characterizing the material. They also serve as a proxy for organic material on many Solar System bodies, in addition to being the closest available analog to Titan atmospheric aerosols. The infrared spectral features of tholins have been used to model the reflectance spectrum of asteroids (Roush and Dalton, 2004), and explain absorption features seen on Iapetus and the rings of Uranus (Cruikshank*, et al.*, 1991). While most workers obtain mid-infrared spectra of their tholins as a matter of course (Khare*, et al.*, 2002; Sarker*, et al.*, 2003), few engage in a detailed examination and assignment of the spectra, and even

fewer studies in the near infrared have been published. Imanaka et al. (Imanaka*, et al.*, 2004) made a detailed study of the variation in the mid-infrared spectrum of tholins as a function of pressure in the discharge reactor, and thoroughly studied the complex nitrile band. Only two papers containing the near-infrared spectrum of tholins have been published. Cruikshank (Cruikshank*, et al.*, 1991) published spectra of the near- and mid-infrared spectra of tholins, with a special emphasis on the first nitrile overtone band. Roush and Dalton (Roush and Dalton, 2004) have also published a near-infrared spectrum, using a "hydrated" tholin sample to examine the effect of added water on the spectrum. A near-infrared transmittance spectrum has also been published (Coll*, et al.*, 2001), but no interpretation of the features is offered.

In order to assist future studies of the surface of Titan, we have obtained the near and mid-IR reflectance spectra of tholins at cryogenic temperatures. A number of strong features are seen in the near-IR, resulting from overtone bands of nitriles, methyl and methylene groups. No significant temperature dependence is seen. The spectra are consistent with previously published work.

3.2. Experimental

Tholin samples were produced by Mark Smith at the University of Arizona, using a plasma discharge reactor, the details of which are given elsewhere (Sarker*, et al.*, 2003). The gas mixture used was 2% CH_4 in nitrogen, at a pressure of approximately 10^2 bar. The reactor was not cooled, and so remained at room temperature. Tholin was recovered by scraping from the reactor walls in a dry, oxygen-free glove box, and stored in dry, oxygen-free environment until needed. Polyacrylonitrile was purchased from Aldrich and used as received.

For these experiments, it was necessary to use tholins produced at room temperature, even though this is not representative of the temperature in the upper reaches of Titan's atmosphere (195 K) where photochemistry occurs. Tholins produced at low temperatures are sticky and difficult to handle, while room temperature tholins are a flaky, harder material that can easily be powdered. A powdery material was necessary to load into the sample cell for these experiments, and so room temperature tholins were chosen. We do not expect that the infrared reflectance spectra will be greatly influenced by the temperature at which the tholins are produced, since mass spectral data of room temperature and 195 K tholins are similar.

The sample was mounted in a small aluminum cup, approximately 2 cm in diameter and 0.5 cm deep, fitted with a sapphire window sealed to the cup with a gasket. The sample was loaded into the cup in a nitrogen-purged glove bag. The sample cup was mounted to a liquid nitrogen cooled cryostat, and the temperature of the sample was measured with a thermocouple in close mechanical contact to the cup. The cryostat head and sample were mounted in a chamber pumped to 10^{-6} torr by a turbomechanical pump. The chamber was fitted with quartz windows for optical access, and two CaF_2 lenses were arranged within the chamber to focus the light onto the sample, and to focus the light scattered from the sample onto the detector. The geometry of the sample and detector were arranged so that diffuse reflectance, and not specular reflectance spectra were obtained. The angle between the detector and spectrometer was approximately 105°.

Spectra were acquired with an Analect Diamond-20 Fourier transform infrared spectrometer, equipped with a separate EG&G BXK-625 detector. The region from 0.5

to 5 microns was scanned. Reference spectra using a gold diffuse reflectance standard were periodically taken during each experimental run, and typically were composed of 5000 averaged scans. Spectra were taken of the tholin sample as the sample was cooled, and at room temperature. Each spectrum was made up of 1000 co-added scans.

Spectra of tholins taken in transmission mode in a KBr pellet were prepared by grinding a few milligrams tholin with dry KBr, and pelletizing with a hand press. The spectrometer used was a BioRad Excalibur FTS 3000.

3.3. Near infrared reflectance spectra of tholins

Figure 3.1 compares the spectra of tholin at room temperature (303 K) and at cryogenic temperatures (123 K), and the mid-infrared region, between 2000 and 4000 cm^{-1} is shown in an expanded form in Figure 3.2. Table 1 summarizes the band positions and their assignments. A number of features are worth noting. The mid-infrared region is dominated by nitrile and amine stretches, as expected from a polymeric CHN material like tholin. This region is compared to a spectrum obtained by transmission with the tholin prepared in a KBr pellet. The spectra are identical. The nitrile band is complex, with at least four distinct peaks. Imanaka et al. (Imanaka*, et al.*, 2004) extensively studied the infrared spectrum of tholin, and thoroughly assigned peaks in the nitrile region. The spectra obtained here are very similar to Imanaka's and we can assign peaks according to the type of CN bond as he did. The peaks are assigned as aliphatic nitriles (2241 cm^{-1}), conjugated nitriles, i.e., a nitrile on a carbon that is doubly bonded to another carbon (2174 cm^{-1}), isocyanides (2139 cm^{-1}), and ketene imines (R-C=C=N-R) and diazo compounds (2100 cm^{-1}).

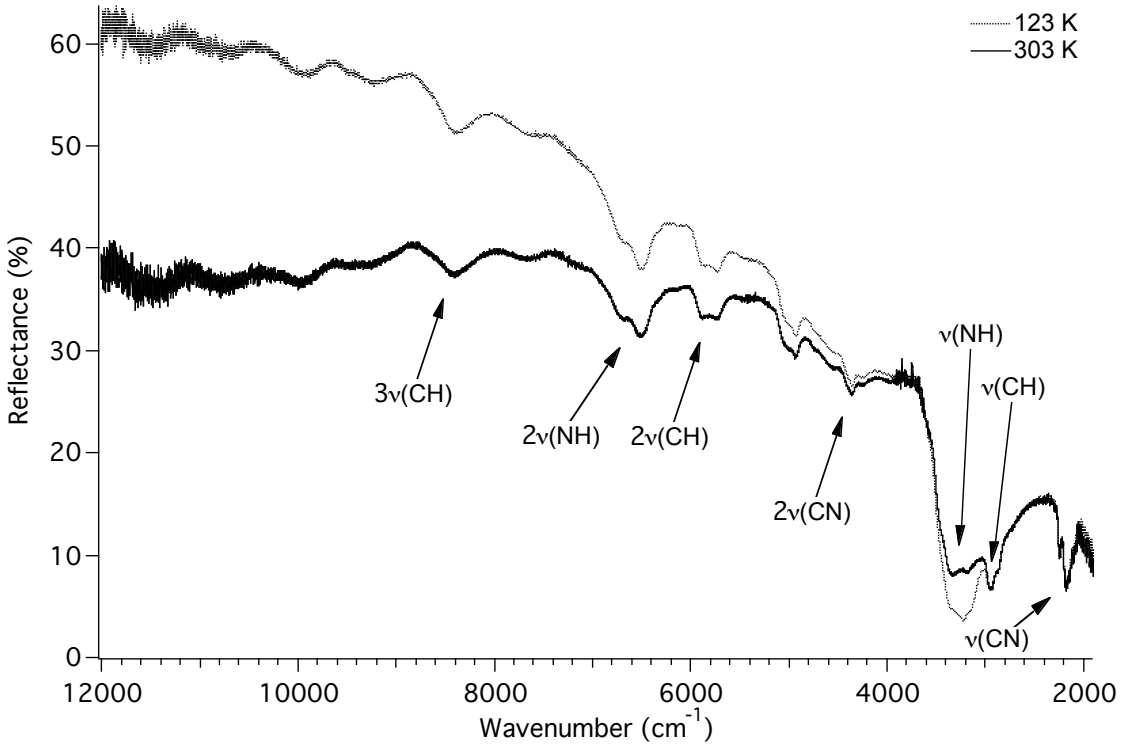

Figure 3.1. Near and mid infrared reflectance spectra of tholins at room temperature (303 K) and at 123 K.

At 10,000 cm^{-1} and above, a sinusoidal ripple in the spectrum is apparent. This is an artifact caused by a small amount of specular reflection in the signal. Between 4000 and 10,000 cm^{-1} is the near infrared region, useful to planetary science since it is amenable to remote detection. Several overtone bands of the CH, CN, and NH stretches are clearly identifiable, along with some as yet unidentified bands. The splitting in the CH bands is assigned to the methyl ($-CH_3$) and methylene ($-CH_2$) stretching modes, with the methyl stretches at higher frequencies (Hildrum*, et al.*, 1992).

We can compare the spectra shown here with those obtained by Cruikshank (Cruikshank*, et al.*, 1991). In the mid-infrared region, the nitrile fundamental is seen at

2169 cm^{-1}, but exhibits no structure. Cruikshank's spectra appear to have a lower resolution than ours, but detailed experimental procedures were not given, so we cannot be certain. A very broad peak centered at 3 μm (3333 cm^{-1}) can be assigned to NH and CH stretches. In the near-infrared, Cruikshank's spectra show the first nitrile overtone to occur at about 4545 cm^{-1}, almost 100 cm^{-1} higher in frequency than in the spectra we obtained. This is an odd finding. Since the nitrile fundamental is at 2169 cm^{-1}, its

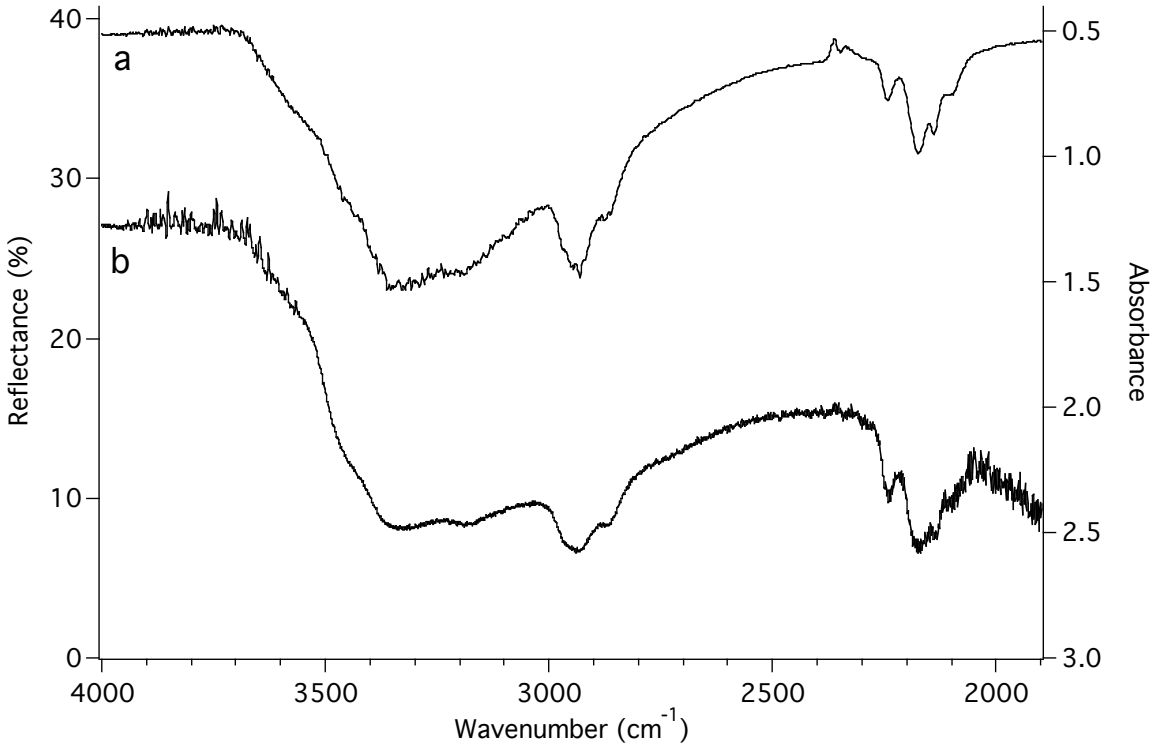

Figure 3.2. Expanded view of the mid-IR region of the reflectance spectrum of tholins (b) compared to a spectrum obtained by transmission in a KBr pellet (a).

overtone should occur at slightly less than twice this frequency (due to anharmonicity), i.e., around 4338 cm^{-1}, consistent with the nitrile overtone we observe. The reason for

this discrepancy is unknown. The other major features seen in our spectra are also visible in Cruikshank's spectra, although the CH overtones are far less pronounced.

Roush and Dalton (Roush and Dalton, 2004) examined the near infrared spectra of "hydrated" tholins, old material that had been exposed to atmosphere and absorbed some water vapor. Not surprisingly, the spectrum is dominated by water features. However, the first nitrile overtone is clearly visible at around 4445 cm^{-1}, and the first CH stretch overtone is at about 5880 cm^{-1}, consistent with the spectra we obtained, although the nitrile overtone frequency is a bit high.

There are two significant differences between the spectrum obtained at room temperature and the spectrum obtained at 123 K. The difference between the two spectra is shown in Figure 3.3. The broad band at 3229 cm^{-1}, corresponding to an increase in absorbance in the low temperature spectrum, is the most notable feature. This band is due to water ice (Baratta*, et al.*, 1991), which condensed from residual water in the vacuum chamber onto the cold window of the sample cup. Some smaller features, corresponding to CH overtones, are also apparent. Also, the low temperature spectrum appears to be generally brighter at shorter wavelength than the room temperature spectrum. In the current experimental set-up, the slope of the baseline at shorter wavelengths is not reproducible, and no significance should be ascribed to this feature. The IR spectrum of tholins does not appear have a large temperature dependence.

For comparison, the near IR reflectance spectrum of polyacrylonitrile is shown in Figure 3.4. Easily identifiable are the nitrile stretch (2243 cm^{-1}), the CH stretch (2943 cm^{-1}), and the first overtone of the CH stretch, 2ν(CH), (5925 cm^{-1}, 5763 cm^{-1}). The first overtone of the nitrile stretch, 2ν(CN), is visible at 4407 cm^{-1}, and a nearby peak, 4296

cm^{-1}, can be attributed to a methylene combination band, formed from the combination of the symmetric stretch and scissoring modes. The features at 3526 cm^{-1}, 3621 cm^{-1}, and 5235 cm^{-1} can be assigned to residual water adsorbed on the polyacrylonitrile sample. Since this sample was not loaded into the cell under nitrogen, but in ambient air, some adsorption of water is not unexpected.

Table 3.1 Frequencies and assignments of spectral features of tholins in the IR

Assignment	Frequency (cm^{-1})
ν(CN)	2100 2139 2174 2241
ν(CH)	2865 2940
ν(NH)	3196 3330 3461
2ν(CN)	4355
unassigned	4930
2ν(CH)	5735 5883
2ν(NH)	6511 6692
3ν(CH)	8403

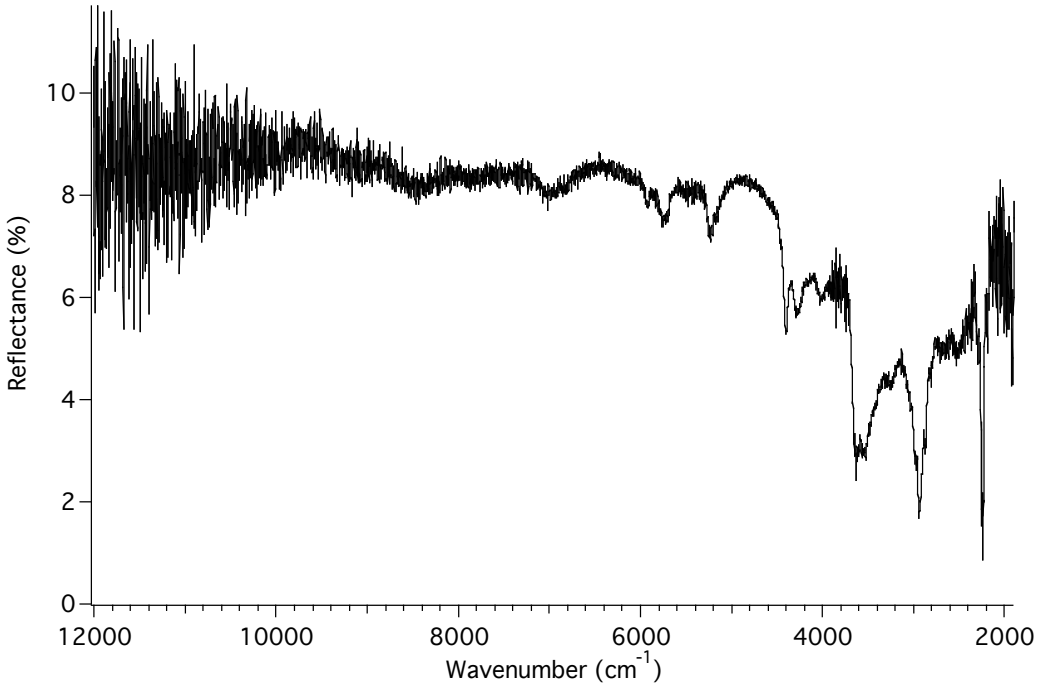

Figure 3.3. Infrared reflectance spectrum of polyacrylonitrile.

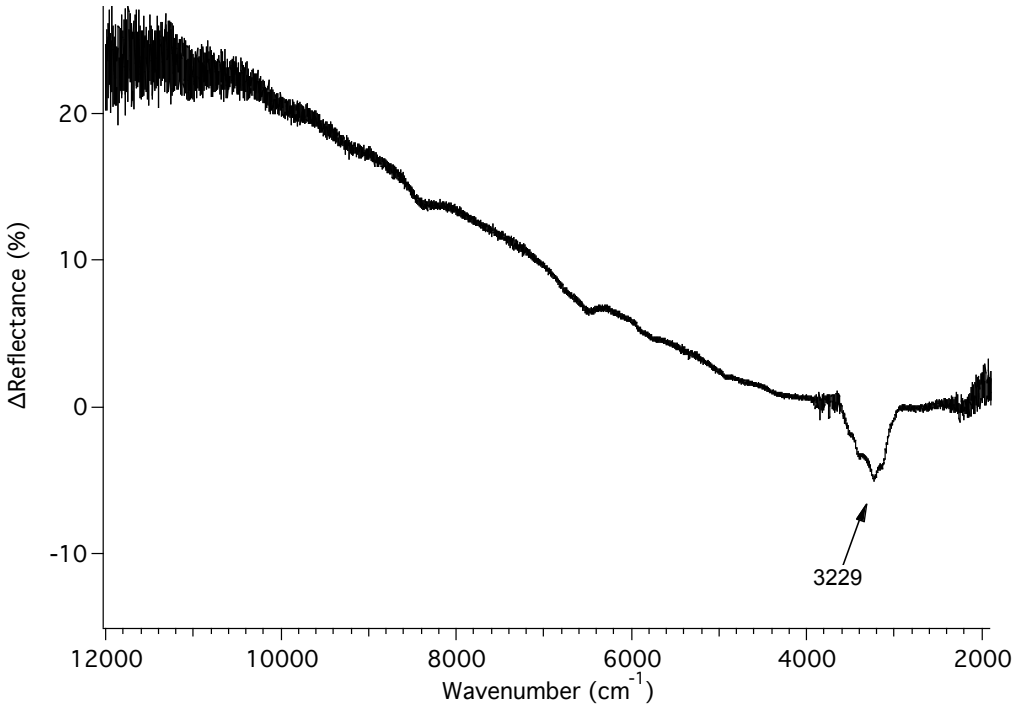

Figure 3.4. Difference between the reflectance spectrum obtained at 123 K and the spectrum obtained at 303 K.

3.4. Conclusions

The near infrared spectrum of tholins is complex, consisting of a number of overtone bands attributable to nitrile, methyl, and methylene functional groups. The mid infrared reflectance spectrum is identical to that obtained by transmission, down to approximately 2000 cm^{-1}. No temperature dependence between room temperature and 123 K is observed. The near infrared spectrum of polyacrylonitrile is an interesting comparison, and possesses a simple structure that allows easy assignment of all the spectral features.

The near infrared spectrum presented here should be useful for the modeling of the reflectance spectra of outer Solar System bodies, as well as for future studies of the surface of Titan. Further work should involve obtaining the near infrared reflectance spectrum of tholins mixed with water ice, and mixed with water-ammonia ices, which should be prevalent on the surface of Titan. Also, careful examination of the near infrared spectrum of tholins may be able to provide insight on the structure of the tholins themselves. For instance, the first CH stretch overtone can be used to determine relative concentrations of primary CH_3, secondary CH_2 and aromatic CH groups, and is more useful than the fundamental CH stretch region, since it does not overlap with the amine stretches, as the fundamental does. These experiments would require higher resolution spectra of the overtone region than those obtained here, and careful calibration experiments, but could provide additional functional group information for tholins.

3.5. References

Baratta, G. A., et al. (1991), The 3.1 Mu-M Feature in Ion-Irradiated Water Ice, *Astronomy and Astrophysics*, *252*, 421-424.

Coll, P., et al. (2001), Chemical and optical behaviour of tholins, laboratory analogues of Titan aerosols, *Space Life Sciences: Life in the Solar System: Prebiotic Chemistry, Chirality and Space Biology*, *27*, 289-297.

Cruikshank, D. P., et al. (1991), Solid Cn Bearing Material on Outer Solar-System Bodies, *Icarus*, *94*, 345-353.

Hildrum, K. I., et al., eds. (1992), *Near Infra-Red Spectroscopy*, Ellis Horwood, New York.

Imanaka, H., et al. (2004), Laboratory experiments of Titan tholin formed in cold plasma at various pressures: implications for nitrogen-containing polycyclic aromatic compounds in Titan haze, *Icarus*, *168*, 344-366.

Khare, B. N., et al. (2002), Analysis of the time-dependent chemical evolution of Titan haze tholin, *Icarus*, *160*, 172-182.

Roush, T. L., and J. B. Dalton (2004), Reflectance spectra of hydrated Titan tholins at cryogenic temperatures and implications for compositional interpretation of red objects in the outer Solar System, *Icarus*, *168*, 158-162.

Sarker, N., et al. (2003), Titan aerosol analogues: Analysis of the nonvolatile tholins, *Astrobiology*, *3*, 719-726.

Chapter 4. Heat-induced Chemical Changes in Tholins: the Case Against Pyrolysis

4.1. Introduction

Pyrolysis is a common technique for the analysis of organic polymers, since it enables the volatilization of high molecular weight species, allowing gas chromatography and mass spectrometry to be used. Many hundreds of polymers have been analyzed by pyrolysis [Haken, 1998]; [Haken and Iddamalgoda, 1996], and a number of variations have appeared, such as Curie-point pyrolysis and thermochemolytic techniques [del Rio, *et al.*, 1998] .

It is thus inevitable that pyrolysis would be applied to the examination of tholins. From the beginning of work on tholins, it was noted that the material was particularly intractable to analysis [Ehrenfreund, *et al.*, 1994]; [Pietrogrande, *et al.*, 2001]. Pyrolysis-GC, however, gives a wealth of peaks, and so became a favored method of analysis. A pyrolyzer has been included on the Huygens probe to examine the atmospheric aerosols and analyze the products by GC-MS [Israel, *et al.*, 1997].

The compounds obtained from the pyrolysis of tholins gives a wide range of nitriles, alkenes, and aromatic compounds, but all the studies agree broadly with one another. For instance, benzene and acetonitrile are seen in large quantities by most researchers [Coll, *et al.*, 1999]; [Israel, *et al.*, 1997]. However, there are some differences. In particular, the quantity of nitrogen heterocycles observed varies widely between reports [Coll, *et al.*, 1998]. These differences may reflect differences in tholin composition, due to the conditions under which it was produced, or exposure to oxygen.

Also, different pyrolysis and chromatographic conditions will affect the type of products that are observed.

Pyrolysis relies on a fundamental assumption, that the pyrolytic fragments are substructures (or easily accounted for reactive products) of the original polymer. While this assumption is probably valid for homogeneous polymers, a material like the tholins, which is composed of thousands of different compounds, not necessarily structurally alike, is not a good candidate for pyrolysis as a means of structure determination. Reactions between components of the tholins, as well as fragmentation, will obscure any structural information that can be gained.

We have examined in detail the process of the thermal decomposition of tholins. Thermal gravimetric analysis and differential scanning calorimetry reveal that tholins begin to degrade at relatively low temperatures, and eventually pyrolyze to a hard, insoluble material. Headspace gas chromatography of heated tholins enables us to identify some of the products of heating, which turn out to be mostly small nitriles. Laser desorption ionization of the residue from these experiments shows an increase in unsaturation occurs with heating, suggesting crosslinking or aromatization. Further experiments using evolved gas analysis investigate the facile release of ammonia at temperatures as low as 100 °C, and attempt to relate this unusual behavior to a particular functional group. Tholins undergo a drastic chemical change beginning at 100 °C, releasing large quantities of ammonia and small organics. Pyrolysis cannot be used to infer the structure of tholins, since these changes will occur before pyrolysis can volatilize components of the tholin. The instability of tholins to heat should also be taken into account in studies of the surface of Titan.

4.2. Thermal gravimetric analysis and differential scanning calorimetry of tholins

Thermal gravimetric analysis is a commonly used technique in the analysis of polymeric materials. The experiment is simple. A small amount of sample, on the order of a few milligrams, is placed in a small pan and weighed as the temperature is increased at a constant rate. This procedure is usually conducted under inert atmosphere (N_2), although in principle any gas can be used. As the sample is heated, it changes chemically, and components will desorb, leading to a decrease in mass. Information on the amount of desorbed volatiles and on the heat-induced degradation of a polymer can be obtained [Campbell*, et al.*, 2000].

Differential scanning calorimetry is a related, but more powerful technique. The sample and a reference are placed in individual pans with separate provisions for heating. The power required to keep the sample and reference at the programmed temperature is monitored. From this data, the enthalpy changes associated with sample transformations, such as melting or glass transitions, can be calculated [Campbell*, et al.*, 2000].

We performed thermal gravimetric analysis and differential scanning calorimetry on tholin samples as a first step in our studies of the behavior of tholins at elevated temperatures. A Netzsch STA 449C TGA-DSC was used to perform simultaneous TGA and DSC measurements. 3.32 mg of tholins (sample MS133A) was loaded into the instrument. A purge gas of N_2 was used at a flow rate of 50 mL/min, and the sample was heated from room temperature to 950 °C at a rate of 10°C/min.

The residue remaining after the TGA/DSC scan was performed was obtained. The residue is shiny, black, and reminiscent of asphalt, and consisted of spherical

globules, indicating that the tholins had melted at some stage during the scan. Further analysis of the residue was eventually abandoned, due to the insolubility of the residue in any common solvent.

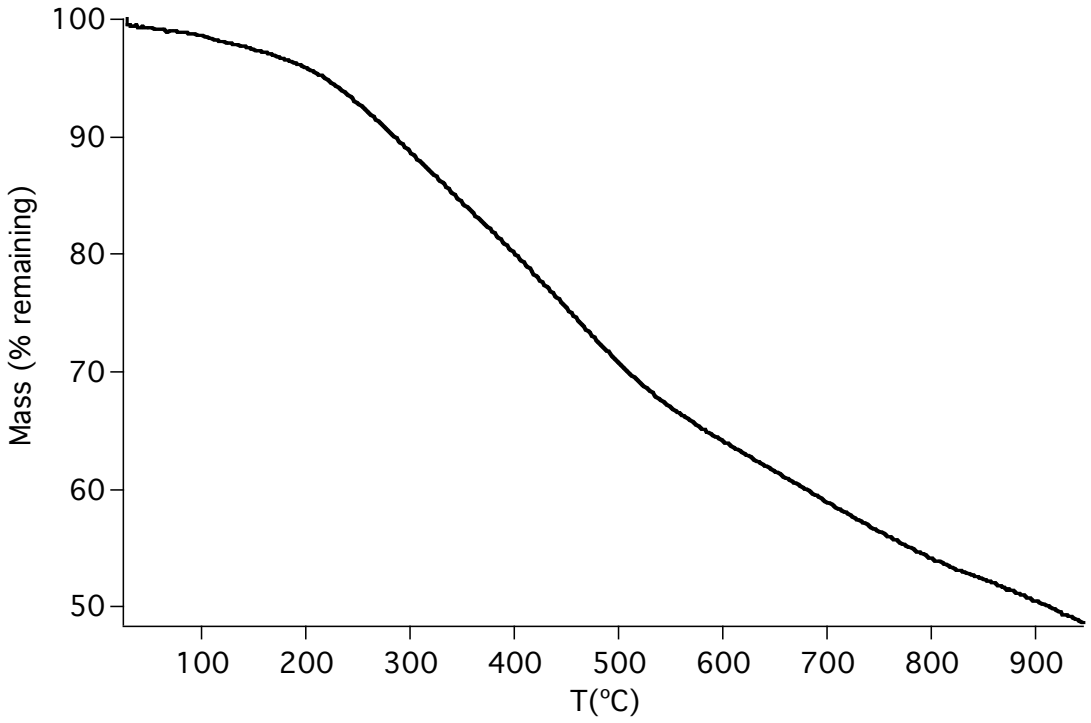

Figure 4.1. Thermal gravimetric analysis of tholins.

The results of the thermal gravimetric analysis are shown in Figure 4.1. There is a clear onset of mass loss that occurs at around 210 °C. At approximately 550 °C, a change in the slope of the mass loss is visible, suggesting that a difference in the process leading to desorption is occurring. Overall, only 50% of the mass of the sample was lost on heating to 950 °C. Tholins have a rather high thermal stability, although it must be remembered that the material that remains at 950 °C will be chemically quite distinct from pristine tholin. This stability to high temperatures was noted by other workers who

performed thermal analysis of the tholins.

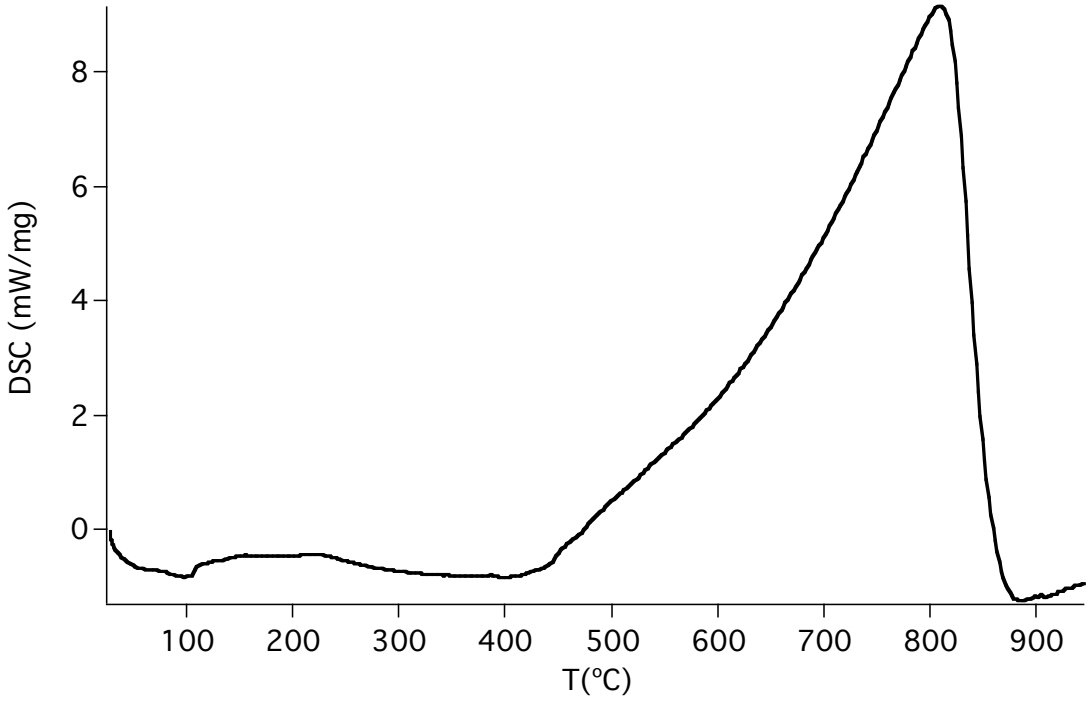

Figure 4.2. Differential scanning calorimetry of tholins.

Figure 4.2 gives the results from differential scanning calorimetry. A large exothermic feature peaking at 800 °C dominates the graph. The onset of this peak roughly coincides with change of slope we see in the TGA trace at around 500 °C, suggesting the two features are related. This is most likely due to an exothermic reaction of some kind, leading to the desorption of material at a different rate than seen previously. Another possibility is melting as the cause of the exothermic peak, although it seems unlikely melting would not have already occurred at such a high temperature. The DSC trace is relatively featureless at lower temperatures, although the small endothermic peak at around 100 °C is reproducible. The origin of this feature is unknown.

4.3. Headspace gas chromatography of heated tholins

The TGA and DSC experiments lead inevitably to one question: What is the nature of the compounds desorbing from the tholins as it is heated? While there are numerous means to characterize the evolved gases, we initially chose to perform gas chromatography on the headspace gases that remain after the tholin is heated in a sealed vial.

Approximately 1-2 mg of tholins (sample NS27) was placed in three small (1 mL) vials sealed with septum caps. The vials were flushed with nitrogen, and then heated at 100 °C, 200 °C, and 300 °C, respectively, for 10 minutes. The vials were allowed to cool, and 50 μL of the headspace gas was injected in to the gas chromatograph, an HP 5890 with a 5972 MS detector, using an RTX-5MS column. The temperature program was as follows: -50 °C for 3 min, then ramped at 8 °C/min to 30 °C, then ramped at 30 °C/min to 150 °C, which was held for 2 minutes. The low initial temperature was achieved with liquid nitrogen cooling of the GC oven.

Figure 4.3 shows the chromatograms obtained for the tholin samples heated at 100, 200 and 300 °C. The identity of the peaks was determined by examination of their

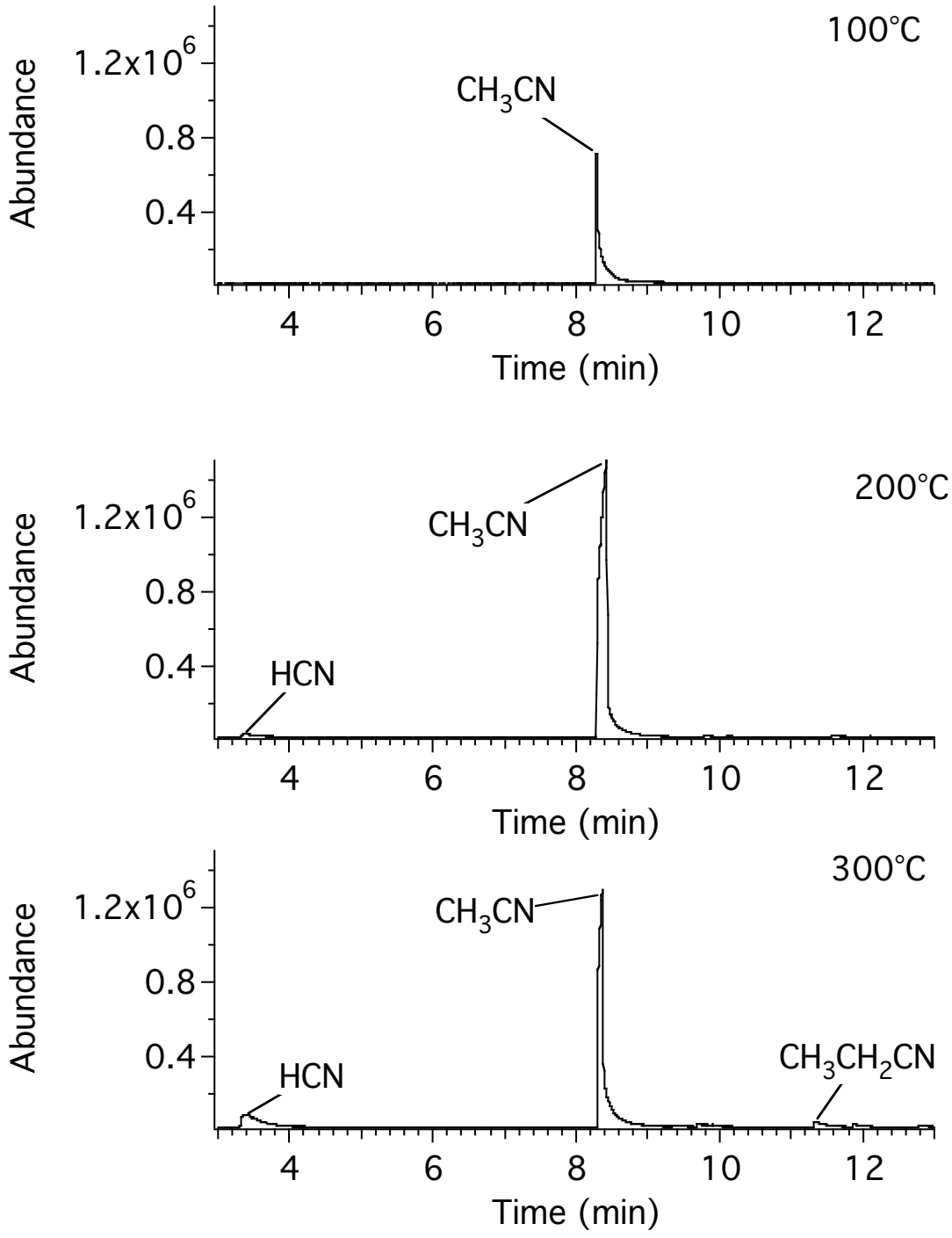

Figure 4.3. GC-MS chromatograms of the headspace gases of tholin heated for 10 minutes at the indicated temperature.

mass spectra, and comparison to the NIST database [Linstrom and Mallard, 2005]. Acetonitrile is seen as the major peak at all three temperatures. As the temperature increases, HCN, and then propionitrile begin to evolve from the tholin sample. Other small peaks are apparent in the 300 °C sample. These correspond to other small organic nitriles. It is unlikely that such large quantites of acetonitrile are trapped in the tholin matrix. The tholins are undergoing a degradation reaction that releases acetonitrile, as well as other small organic nitriles, and HCN. The evolution of such large quantities of acetonitrile at 100 °C suggest that this reaction is facile, and underscores the thermal instability of the tholins.

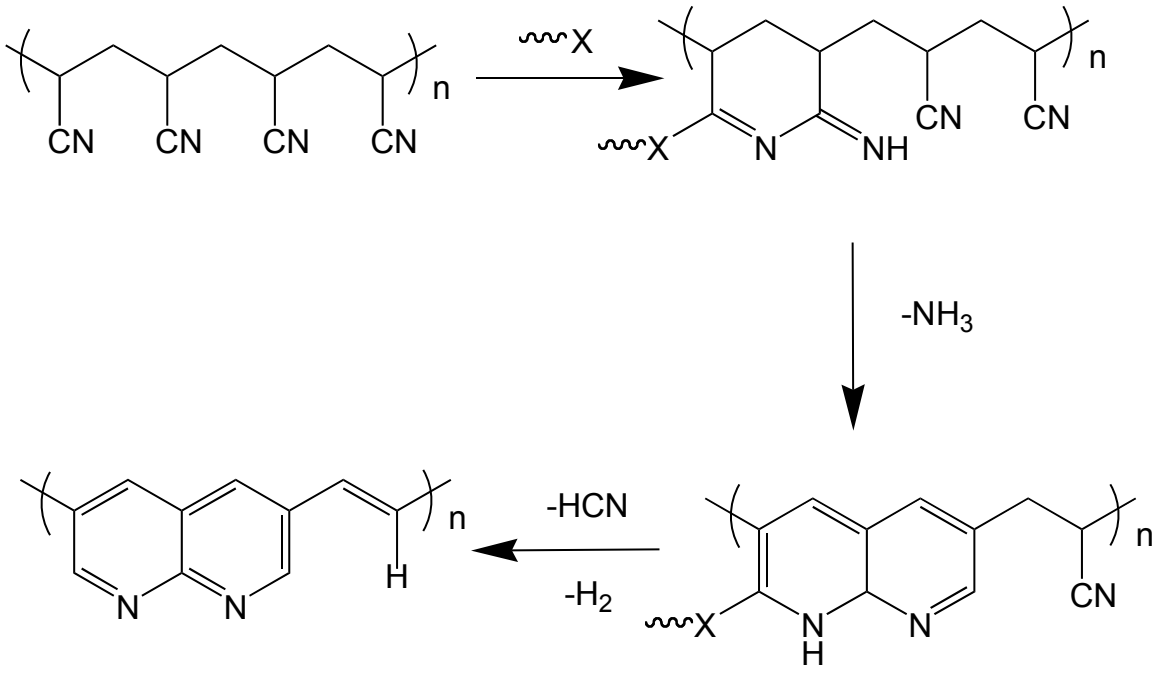

Scheme 4.1. Thermal degradation of polyacrylonitrile. X refers to any possible nucleophile, including nitriles.

Once again, polyacrylonitrile (PAN) can serve as a useful model system to compare to the tholins, and the thermal degradation of PAN is well studied [Mellottee

and Vovelle, 1982]. The evolution of HCN and NH_3 is seen to begin at 160 °C. The mechanism is quite complicated, but involves cyclization and aromatization of the polymer, followed by release of HCN [Xue*, et al.*, 1997]. A simplified overview of the process is shown in Scheme 4.1. The end result of the thermal degradation of polyacrylonitrile is an extensively cyclized aromatic chain. This type of material would likely have properties similar to that seen in heated tholins residues: black, shiny and insoluble. Acetonitrile has also been seen in the products of the thermal degradation of polyacrylonitrile [Surianarayanan*, et al.*, 1998]. Acetonitrile could be produced by a mechanism similar to the one that produces HCN. Tholins do contain nitriles, and it is likely that some of the processes occurring in the thermal decomposition of polyacrylonitrile occur in tholins as well.

4.4. Laser desorption ionization mass spectrometry of heated tholin residues

It is now apparent that tholins are a thermally unstable material, releasing large quantities of small nitriles, especially acetonitrile, on heating. The evolution of these gases from the tholins may occur via a mechanism similar to those that occur in the thermal degradation of polyacrylonitrile. The next step is to examine the residues left behind after these gases have evolved.

Since the residual material is largely insoluble, we chose laser desorption ionization (LDI) mass spectrometry as a means of studying the residue. This technique is well suited to the study of polymeric materials. The residues left in the sample vials after the headspace analysis were finely ground in a mortar and pestle, and the resulting

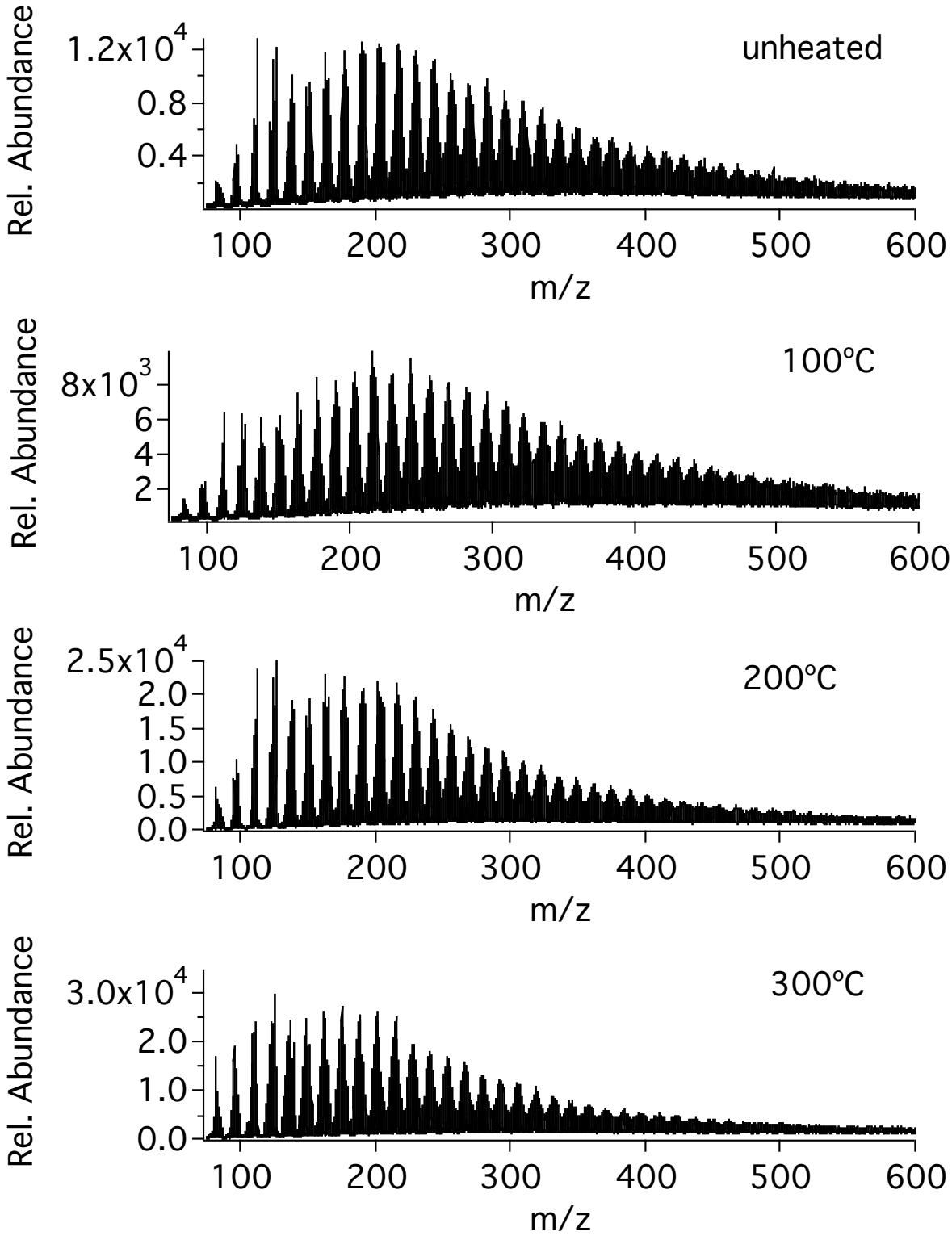

Figure 4.4. Laser desorption ionization mass spectra of heated tholin residues.

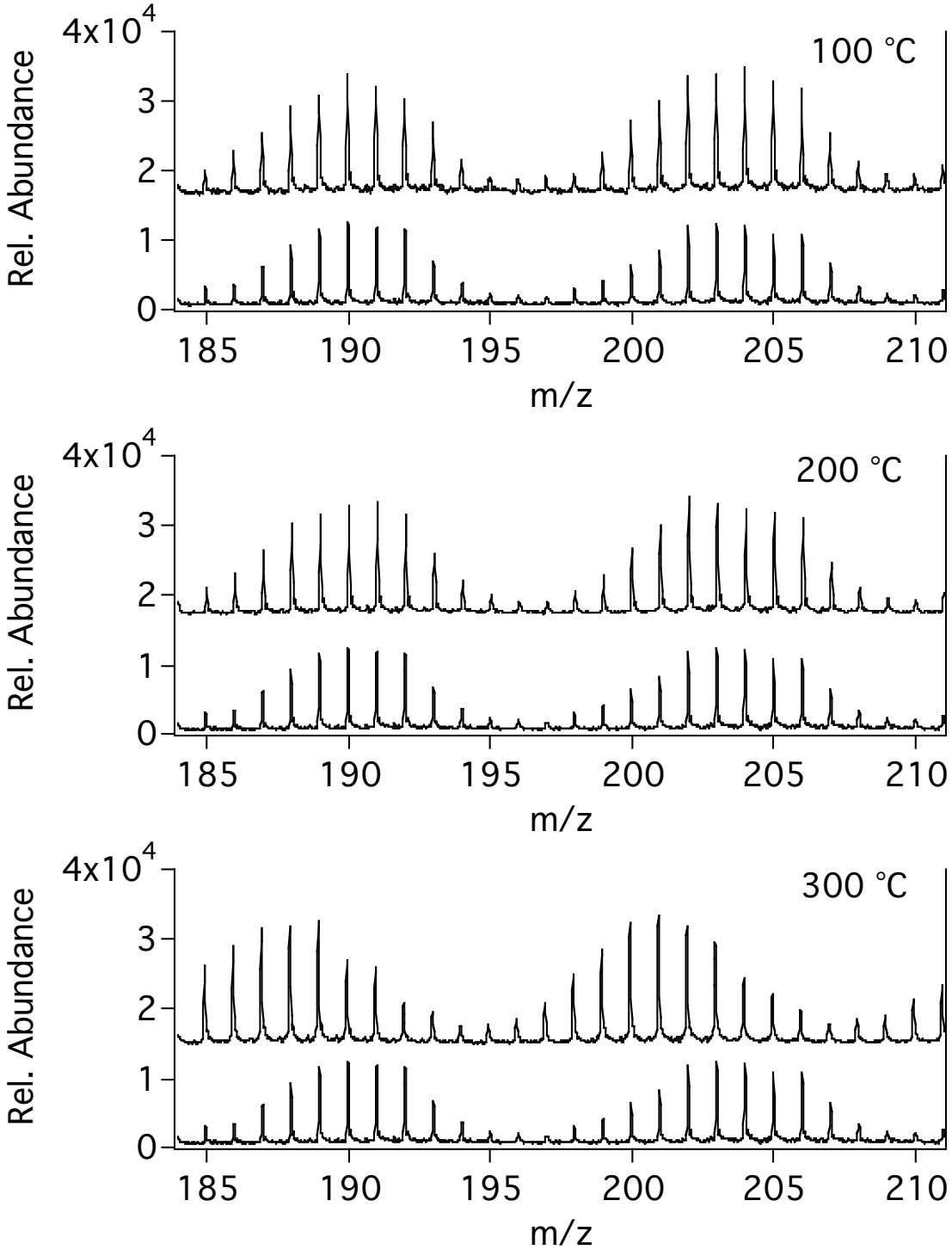

Figure 4.5. Magnified view of the spectra presented in Figure 4.4. In each panel, the lower trace is the spectrum obtained from unheated tholin, while the upper trace is the spectrum obtained from tholin that was heated to the indicated temperature.

powder was applied to a piece of double-sided sticky carbon tape, which was affixed to the sample plate of a Voyager DePro time of flight mass spectrometer. The laser power was adjusted for the best signal, and between 300 and 500 shots were averaged for each spectrum.

The results are presented in Figure 4.4. At first glance, the spectra are all quite similar. They all exhibit the characteristic polymeric distribution of the tholins, clusters of peaks spaced 14 mass units apart. Some small differences are are apparent. In the material heated to 200 °C and 300 °C, the distribution peaks just before 200 m/z, while in the unheated and 100 °C material, the distribution peaks at around 225 m/z. This is in agreement with the loss of small molecules on heating noted in the previous section. A closer inspection of the spectra reveals more definitive differences.

Figure 4.5 is a magnified view of a region of the spectra shown in Figure 4.4. The spectrum obtained from residue heated to the indicated temperature is compared to the spectrum of unheated tholin. At 100 °C and 200 °C, the spectra of the residue and of unheated tholin are basically identical. However, at 300 °C, the spectra of the residue undergoes a shift to lower masses. Each cluster of peaks is shifted about two mass units lower. The loss of H_2, from an increase in unsaturation, would lead to this result.

The LDI spectra corroborate the results obtained from headspace gas chromatography, discussed in the previous section. As they are heated, the tholins are chemically altered. Small molecules, such as acetonitrile, are evolved, and the residual material is less saturated than pristine tholins. A mechanism similar to that which occurs in the thermal degradation of polyacrylonitrile is likely at work. The tholins become increasingly cyclized and aromatic, resulting in a black, insoluble material. Since the

LDI spectra exhibit an overall shift to lower masses (Figure 4.4) on heating, the cyclization reactions are predominantly intramolecular, and little intermolecular crosslinking seems to be occurring.

4.5. Thermal analysis of tholins by UV absorption spectroscopy of desorbed species

Further studies were undertaken to elucidate the role of the evolved gases in the thermal degradation of tholins, and as a possible means of studying tholin-like materials on Titan. Evolved gas analysis has been performed by infrared absorption spectroscopy [Materazzi and Curini, 2001b], mass spectrometry [Materazzi and Curini, 2001a], and a number of other techniques [Xie and Pan, 2001]. Here we use ultraviolet absorption spectroscopy to identify the gases evolved from tholins as they are heated. In some cases, we can also quantify the amount of evolved gas, and use this information to expose some aspects of the structures of the tholins.

The experimental arrangement used in these experiments in shown in Figure 4.6. A few milligrams of tholins (sample PNNL 1) is placed in a small vial (1 mL) fitted with a septum cap. The vial is supported in an aluminum block that can be heated with heating tape, controlled by a Variac. Figure 4.7 gives the heating curve produced by this arrangement. The Variac setting was kept constant for all experiments described in this section, so the heating curve is also the same for all experiments. The temperature is recorded by a thermocouple positioned in contact with the bottom of the vial. A continuous flow of He at 100-200 mL/min is passed over the tholins and into an ultraviolet absorption cell. The cell consists of two aluminum blocks supporting a quartz

tube (3 mm OD) between them, with silica windows on either side. The tube serves as both a light pipe and a conduit for the gaseous products. The cell has a pathlength of ~6 cm. The light from a 30 W deuterium lamp (Oriel 63163) is coupled into the cell using silica lenses. Unfocused light exiting the cell is directed into a Chromex 250is imaging spectrograph equipped with an Apex SPH-5 CCD detector. The resolution of the system is approximately 0.5 nm. The

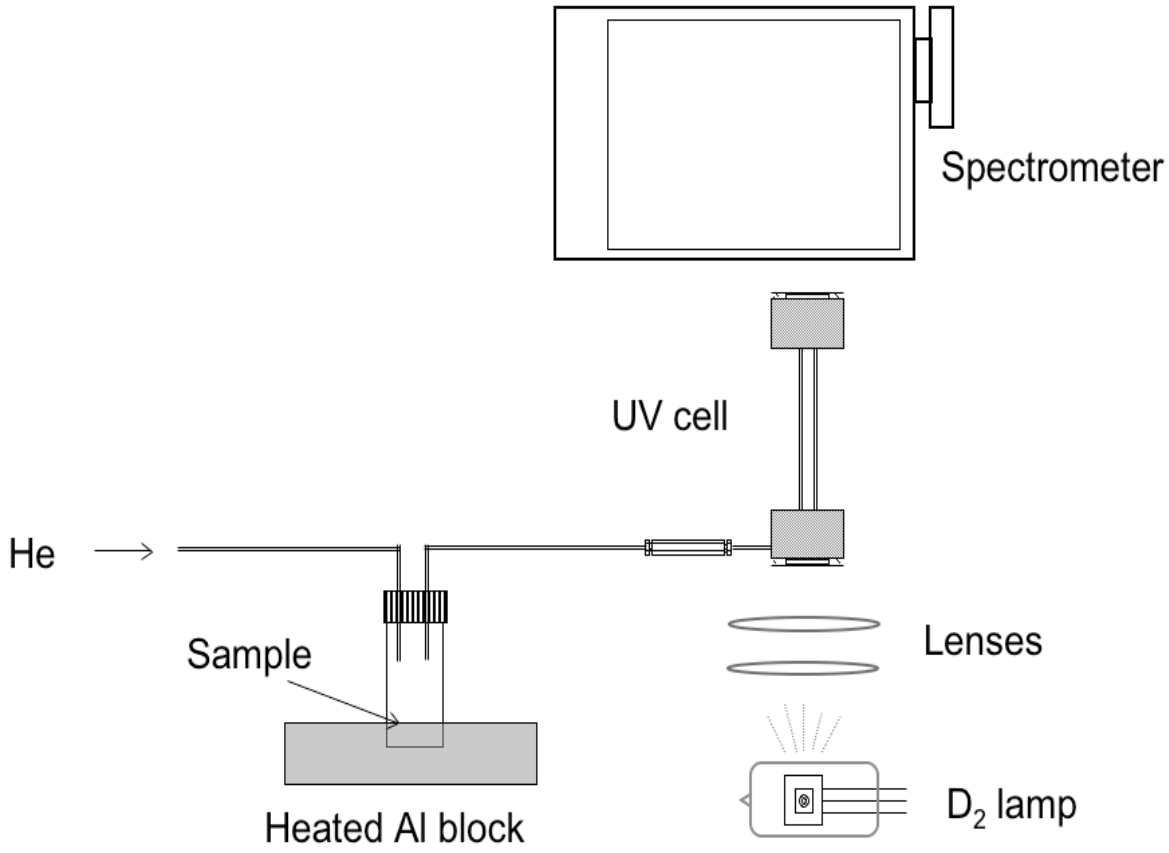

Figure 4.6. Experimental arrangement for UV absorption spectroscopy of gases evolved during tholin thermal degradation.

entire optical path, including the spectrometer, is purged with nitrogen to allow operation below 200 nm. Spectra from 180-240 nm are acquired approximately every 1.5 seconds, with an integration time of 1 s.

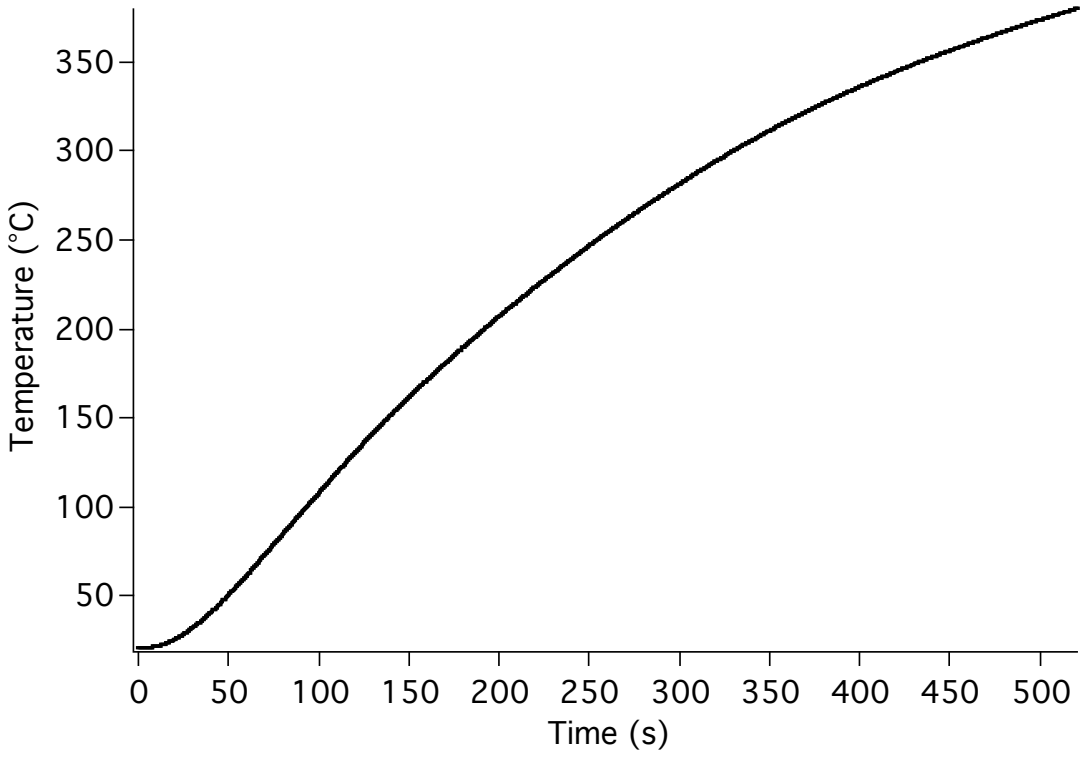

Figure 4.7. Heating curve for UV absorption spectroscopy experiments.

A three-dimensional graph of the data obtained with an 11.6 mg tholin sample is shown in Figure 4.8a. There are a number of ways to present this data. Here, we show wavelength on the x-axis, time on the y-axis, with darker shades of gray indicating increased absorbance. Figure 4.8b and c are cuts through the three-dimensional graph in Figure 4.8a at the indicated time. The graph exhibits a banded feature, peaking in intensity at around 150 seconds, which is an excellent match for the absorption spectrum of ammonia [Chen, *et al.*, 1999]. Ammonia was not seen in the gas chromatography

experiments, probably because the column used was unsuitable for ammonia analysis. This spectrum is shown in the cut labeled 4.8b. At later times (and thus higher temperatures) a broad feature peaking at around 210 nm can be seen overlapping the ammonia spectrum, as shown in

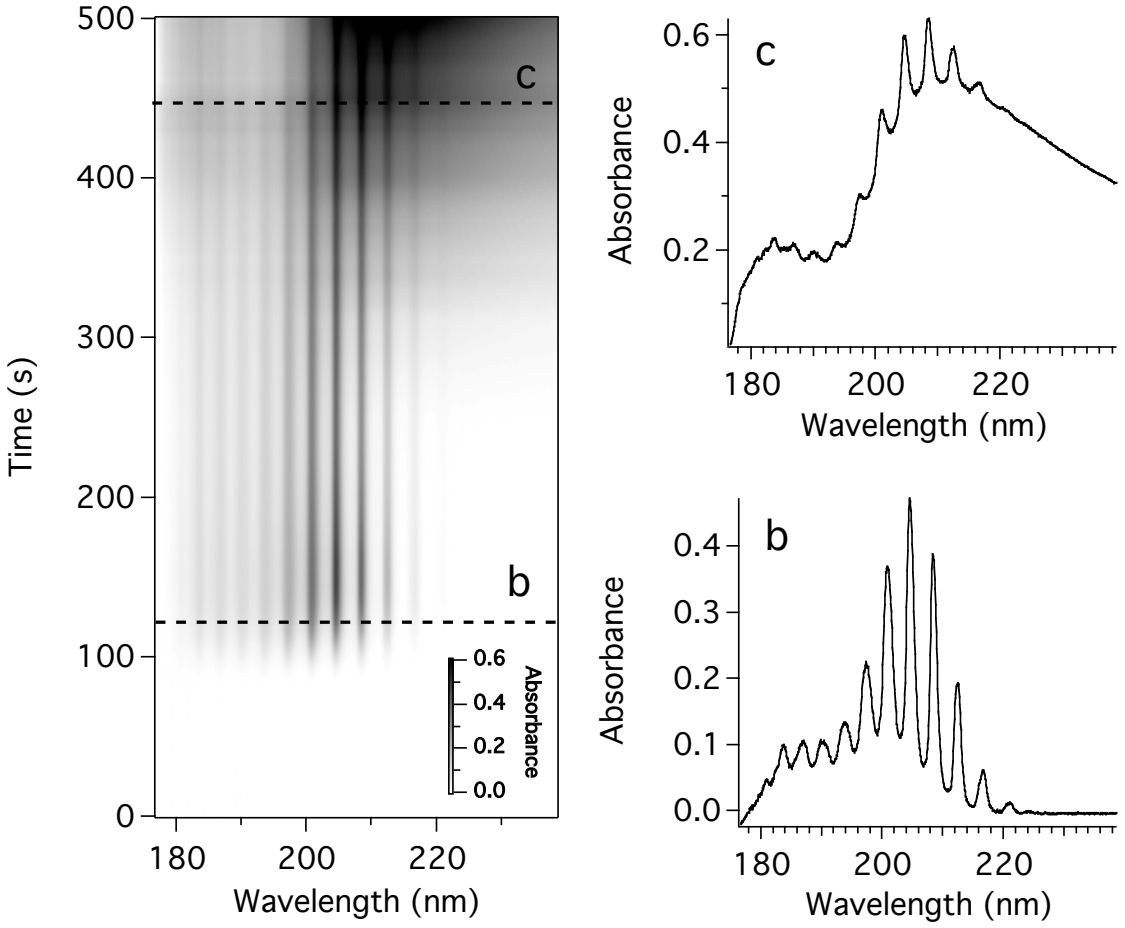

Figure 4.8. a) Three-dimensional graph of the ultraviolet absorption of the gases evolved during the thermal degradation of tholin. b) Cut through a) at the indicated time (~120 s). c) Cut through a) at the indicated time (~450 s).

Figure 4.8c. This is likely due to small organics, probably nitriles, as seen in the headspace gas chromatography experiments. The samples were weighed before and after the experiment, and showed an average mass loss of 26%. It is unlikely such a a large amount of mass could be lost from the tholin without significant structural rearrangement.

Using the heating curve, we can make a graph of the absorbance at a certain wavelength against the temperature. By choosing a wavelength that corresponds to the absorption of a particular species, we can graph the dependence of the evolution of this molecule against temperature. We hereafter refer to such a graph as a "thermogram." Two such thermograms are shown in Figure 4.9. In Figure 4.9a, the absorbance at 204 nm is plotted against temperature, giving the thermogram for ammonia. Ammonia begins evolving from the tholin sample at a very low temperature, only 100 °C. Ammonia evolution reaches a peak at 160 °C, declines and begins to rise again at around 300 °C, although much of this rise can be attributed to the overlapping broad absorption that begins to emerge at around 250 °C. The broad absorption feature can be tracked by monitoring the absorbance at 240 nm; this thermogram is shown as Figure 4.9b.

Ehrenfreund et al. [Ehrenfreund*, et al.*, 1994] performed evolved gas analysis with mass spectrometry on a sample of tholin produced by corona discharge. They report the evolution of compounds beginning at approximately 260 °C, and identified ammonia, hydrogen cyanide, and acetonitrile as some of the evolved products. The ammonia signal peaks at around 410 °C, and then declines. The acetonitrile signal peaks later, around 490 °C. Although the temperatures are different, the behavior of the ammonia and

acetonitrile evolution is similar in our system. However, the samples were not protected from oxidation, and also showed the release of CO_2 and acetamide.

An experiment to determine the amount of ammonia that can be lost at low temperatures was undertaken. A sample of tholin was heated at 120 °C while monitoring the absorbance due to ammonia. After 30 minutes, the absorbance spectrum of ammonia was no longer apparent, and the sample was weighed, yielding a mass loss of 9%.

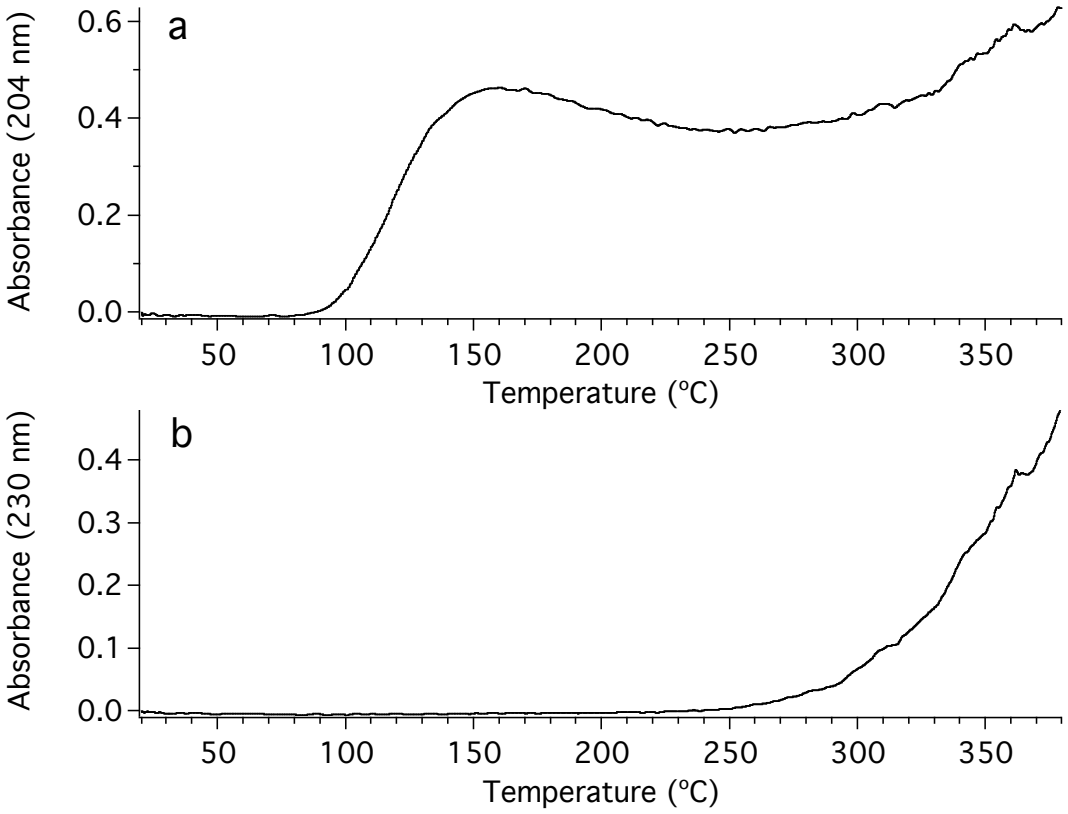

Figure 4.9. Thermograms for a) ammonia and b) the broad nitrile absorption.

The experiment was performed on a 15.0 mg sample of tholins that had been hydrolyzed in an ammonia-water solution. Approximately 20 mg tholin was sealed in a

vial with a Teflon cap with 1 mL concentrated ammonia, and the solution was heated at 100 °C for 12 hours. The residue was dried under vacuum before use.

A graph of the data is shown in Figure 4.10. The strong ammonia features are still present, but the broad feature seen at later times in the data obtained for pristine tholins is diminished. This is more obvious in an examination of the relevant thermograms, shown in Figure 4.11.

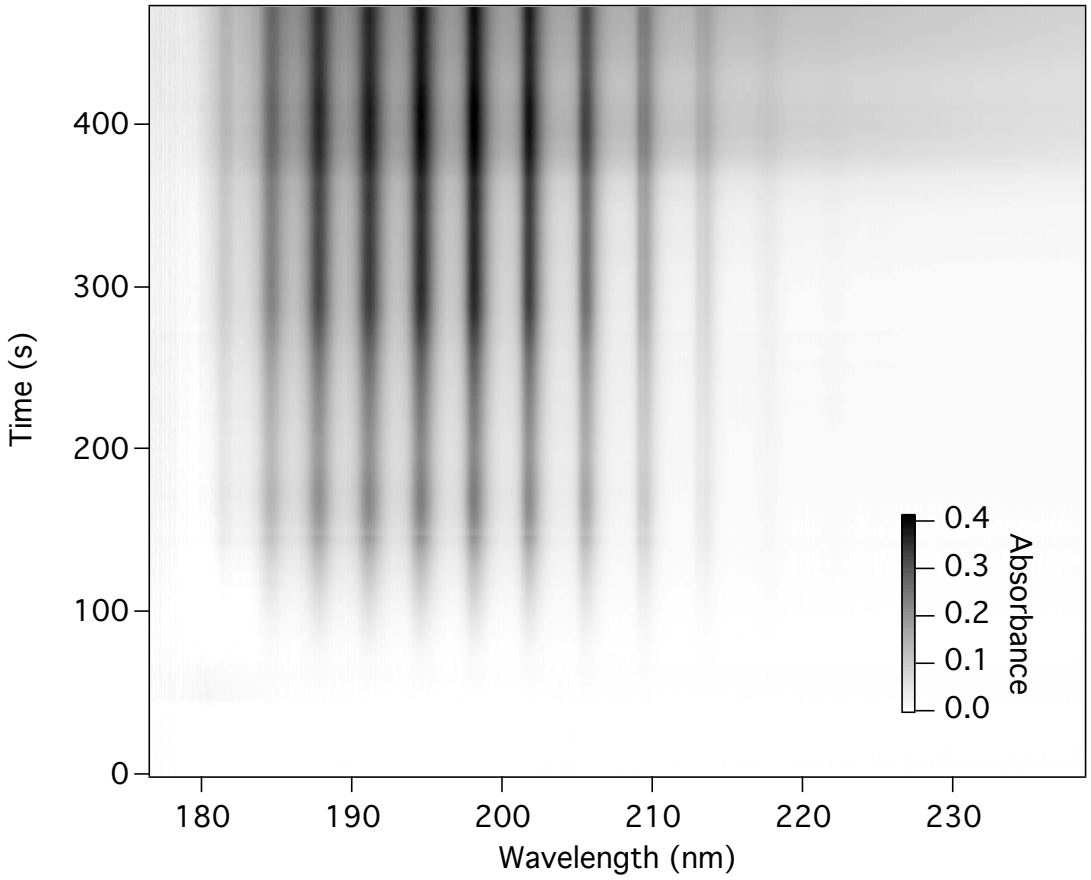

Figure 4.10. Three-dimensional graph of the ultraviolet absorption of the gases evolved during the thermal degradation of hydrolyzed tholin.

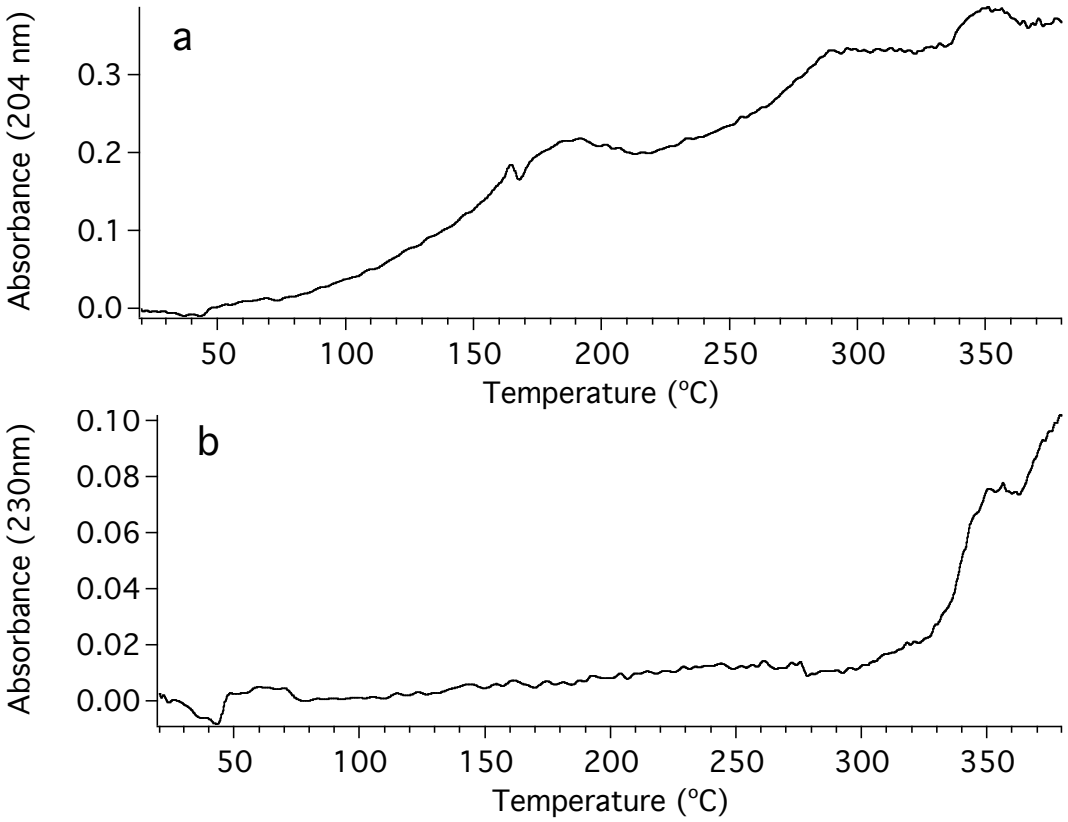

Figure 4.11. Thermograms for a hydrolyzed tholin sample. a) ammonia thermogram. b) Organic nitrile thermogram.

As before, the thermogram of ammonia is obtained by graphing the absorbance at 204 nm against temperature. The small amount of ammonia that evolves beginning at 50 °C is probably due to residual ammonia left by the hydrolysis procedure trapped in the tholin matrix. The ammonia release peaks at around 190 °C, declines and then rises again, as before. The thermogram for the broad feature is shown in Figure 4.11b. This is the same in shape as with the pristine tholins, but of much diminished intensity. If this feature is indeed due to the evolution of small nitriles, hydrolysis of the nitriles themselves may be responsible for the loss of this signal.

Once again, data from model polymers is useful as a comparison to the tholins. The data for PAN is shown in Figure 4.12, and the thermograms for polyacrylonitrile are shown in Figure 4.13. We see that this sample of PAN evolves ammonia beginning at much higher temperatures than the tholins, along with other organics that lead to a broad absorption feature. The low temperature evolution of ammonia from the tholins is thus not due to the presence of nitrile functionalities, but must be the result of the decomposition of another nitrogen containing moiety.

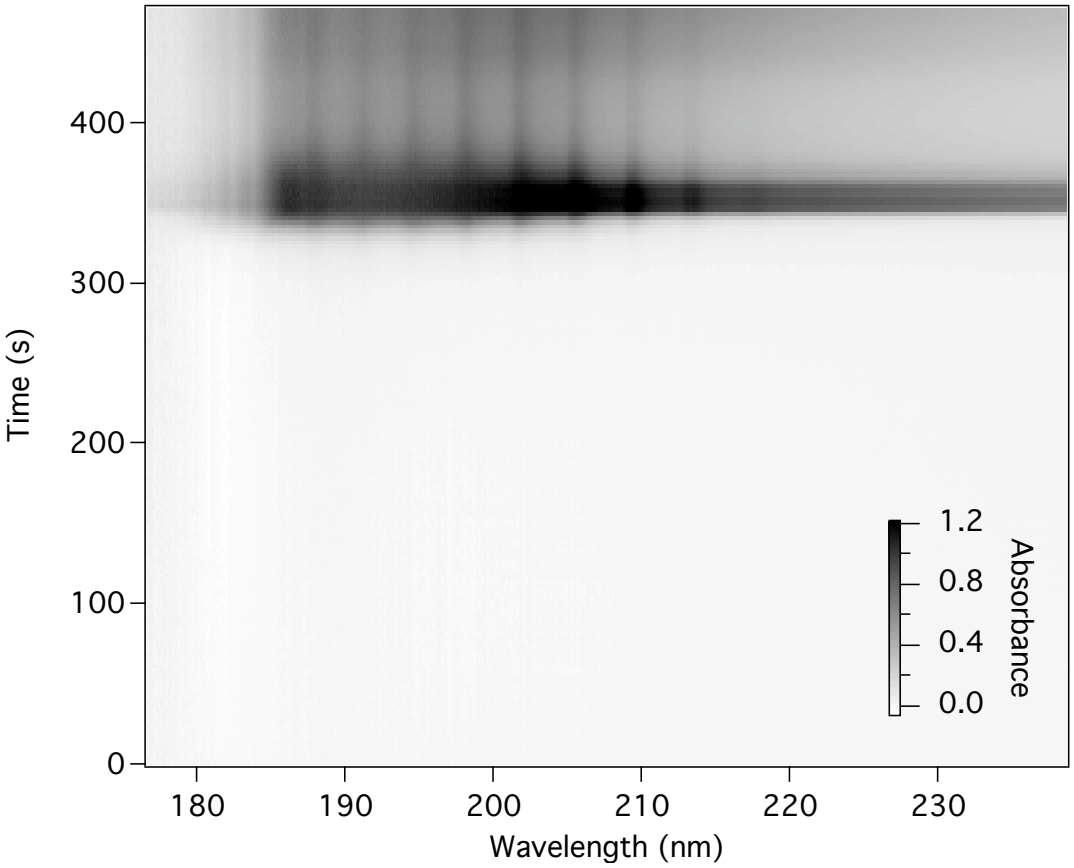

Figure 4.12. Ultraviolet absorption spectra of the gases evolved during the heating of polyacrylonitrile.

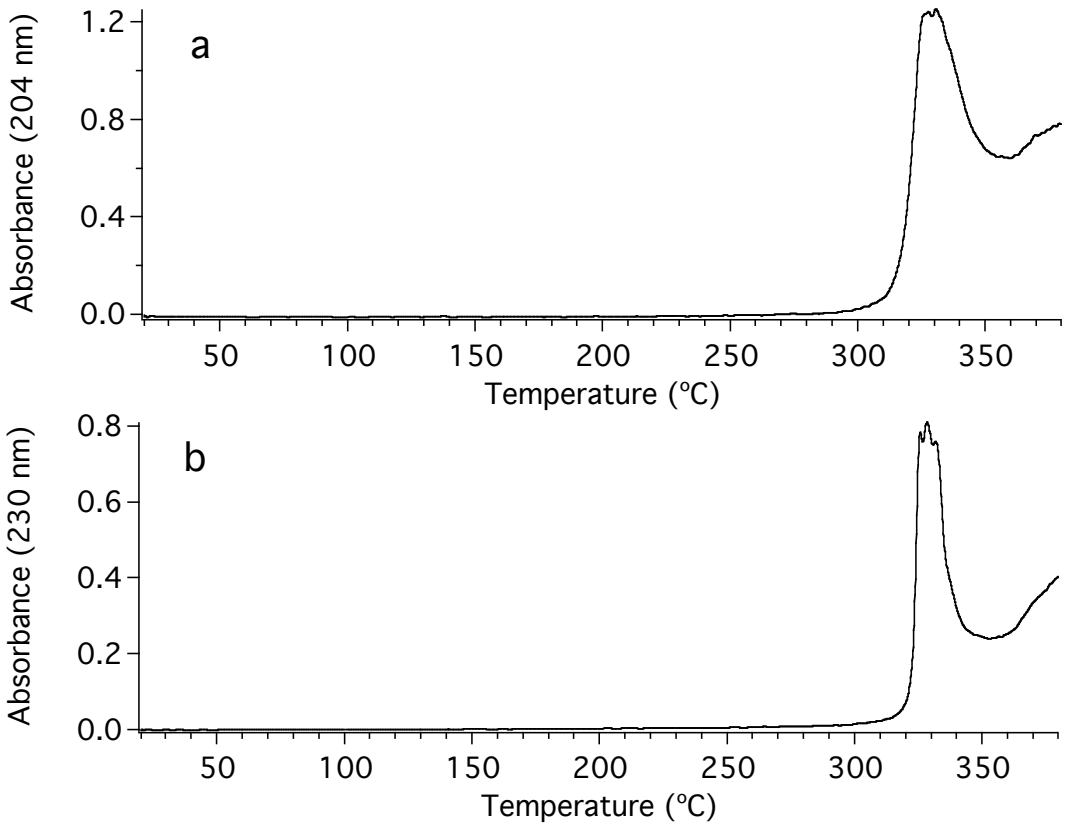

Figure 4.13. Thermograms for a) ammonia and b) organics obtained from the thermal decomposition of PAN.

In order to try to determine the nature of this other nitrogenous functional group or groups, several other polymers were subjected to the same experimental procedure. The structure of these polymers, and of PAN, is shown in Scheme 4.2. The polyethyleneimine (Aldrich) sample had an average molecular weight of 423, and a boiling point of 250 °C, and so the sample was heated to only 225 °C. Polyallylamine (CarboMer, Inc.) was obtained as a 20% solution in water, and had an average molecular weight of 10,000. The water was removed under vacuum before the experiment.

Polypyrrole (Aldrich) was obtained doped onto carbon black. The sample also contained a "proprietary organic acid." Unfortunately, pure polypyrrole was not available.

Data for the thermal decomposition of polyallylamine is shown in Figure 4.14. We see immediately that the evolution of ammonia begins at much longer times (and thus higher temperatures) than in the tholin samples, and we can conclude that amine groups are not responsible for the ammonia signal in tholins.

Figure 4.15 gives the thermal decomposition pattern for polypyrrole. In contrast to polyacrylonitrile and polyallylamine, ammonia evolution is apparent beginning around 100 s (which corresponds to approximately 100 °C), as in the tholin samples. However, the amount of ammonia produced is far lower, as can be seen in the far smaller scale for absorbance. The carbon black on which the polypyrrole is doped may be absorbing some of the ammonia. A group of bands appears between 210 and 225 nm at approximately 150 °C. The compound responsible for this absorption is unknown, but it may be a product of the sulfonic acid doping agent added to the composite.

Data for polyethyleneimine is shown in Figure 4.16. The polymer could only be heated to 225 °C, as its boiling point is 250 °C. As with polypyrrole, we observe slight evolution of ammonia at low temperatures, but the amount is negligible. Towards the top of the plot, the broad absoption is likely due to polyethyleneimine itself.

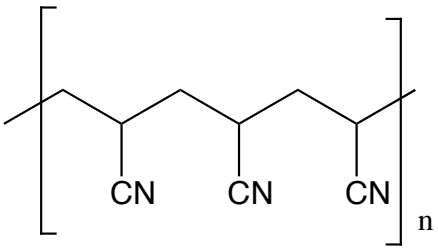

polyacrylonitrile

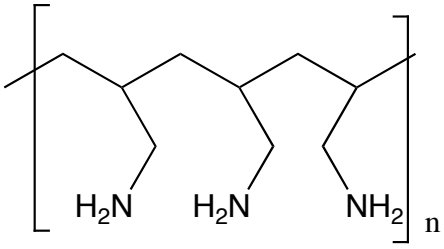

polyallylamine

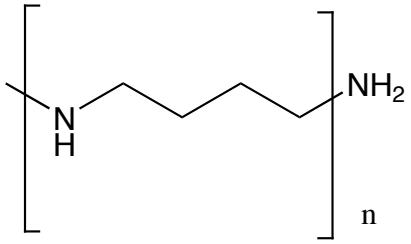

polyethyleneimine

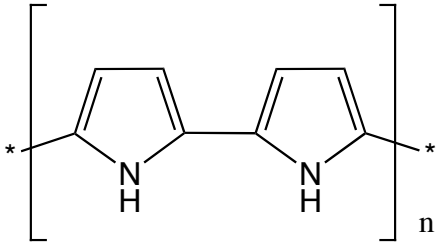

polypyrrole

Scheme 4.2. Nitrogen containing polymers used for comparison to tholins.

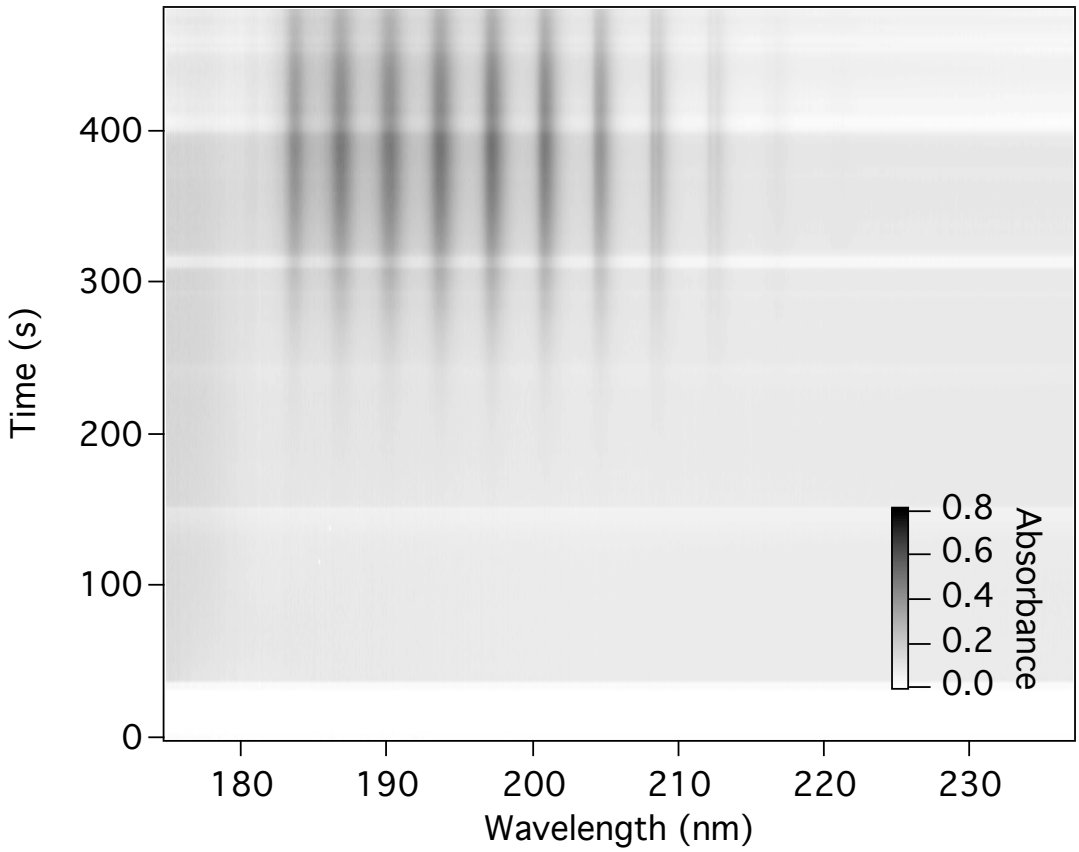

Figure 4.14. Ultraviolet absorption data for the thermal decomposition of polyallylamine.

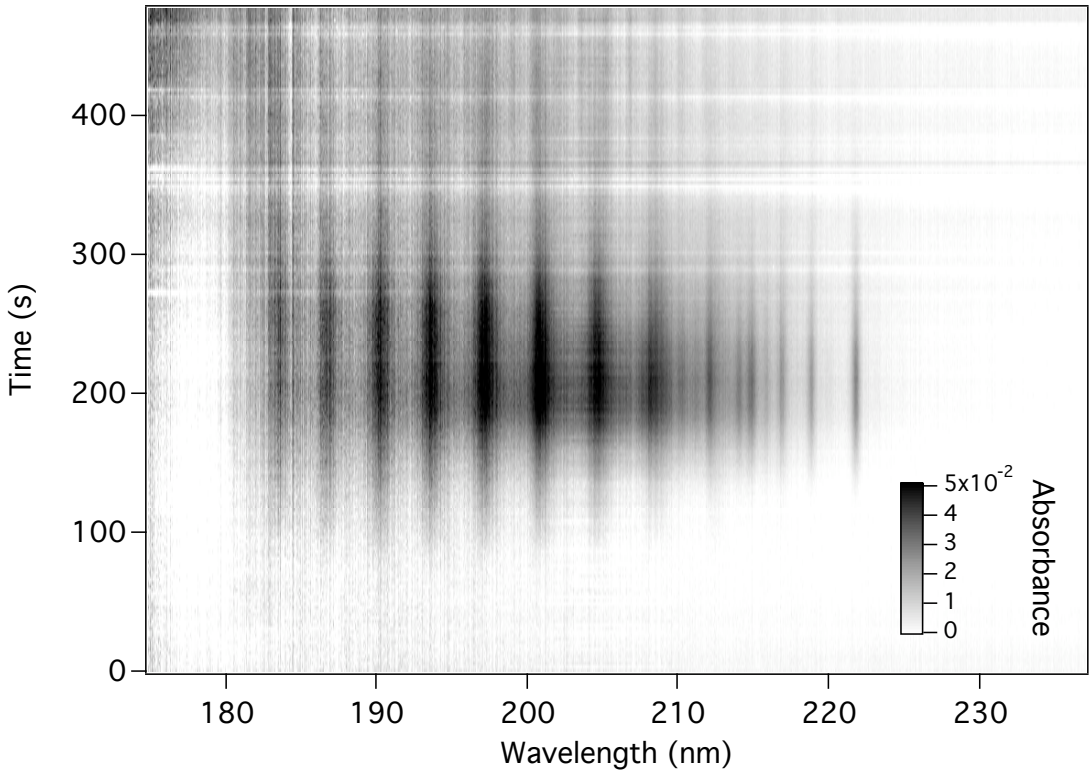

Figure 4.15. Thermal evolved gas ultraviolet spectra of polypyrrole. The horizontal banding is an artifact caused by variations in the output of the D_2 lamp.

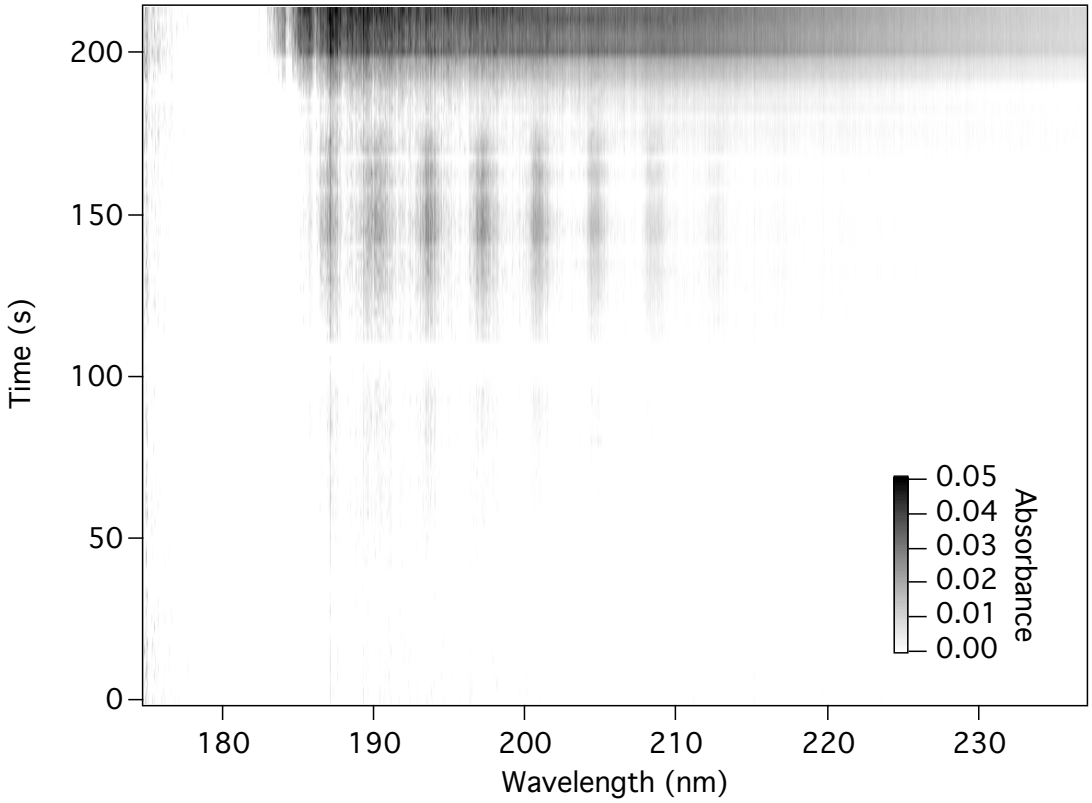

Figure 4.16. Ultraviolet spectra from the thermal decomposition of polyethyleneimine. Note that the polymer was heated for a shorter length of time, as its boiling point is 250 °C.

4.6. Conclusions

The thermal decomposition of tholins is a complex process, beginning at fairly low temperatures (~100 °C). A key property of the decomposition is the release of large quantities of ammonia, easily detected by ultraviolet absorption spectroscopy of the evolved gases. Thermal gravimetric data and differential scanning calorimetry show that the decomposition occurs in several stages. Hydrogen cyanide and small organic nitriles, especially acetonitrile, evolve from the tholins as well. The residual material left after heating is chemically distinct from unheated tholin. LDI mass spectrometry studies show an increase in unsaturation, and a movement towards products of lower mass, consistent with the evolution of volatiles.

The thermal decomposition of tholins proceeds as follows. Beginning at 100 °C, ammonia begins to evolve. This low energy decomposition pathway is the primary means of decomposition until around 250 °C, where small organics, mostly nitriles, begin to dominate. This corresponds approximately to the temperature at which a dramatic change in slope is seen in the TGA data. As well, LDI mass spectrometry data on heated residues shows an increase in unsaturation between material that had been heated to 200 °C and 300 °C, supporting a transition in the mechanism of decomposition flanked by these two temperatures. Both the loss of ammonia and small organics continues as the temperature is increased, until a highly carbonized and glassy material remains. Only 50% of the mass of tholin is lost on heating to 950 °C under N_2.

The nature of the functional groups that release volatiles at such low temperatures is still a mystery. The evolution of HCN and acetonitrile can be explained through a mechanism similar to the one by which polyacrylonitrile thermally degrades, involving

cyclization and aromatization. Experiments with model polymer systems rule out nitrile and amine functionalities as the source of the ammonia. At 100 °C, secondary amines release very small amounts of ammonia; polypyrrole releases somewhat more. Nitrogen containing rings such as pyrrole or pyridine may be the source of the ammonia, but more work is necessary to confirm this hypothesis. Observing the volatiles released from the thermal degradation of additional nitrogenous polymers would be useful.

The poor thermal stability of tholins has several implications for further research, and for Titan itself. On Titan, impactors would raise the temperature locally well above 100 °C, for brief period of time. This would both change the structure of the Titan aerosols, as well as release large quantities of ammonia. This ammonia would eventually either condense onto the cold surface, or dissolve into melt-water formed by the impact. Either way, there would be a likely be a noticeable influence on the local environment as a result of the additional ammonia.

Pyrolysis is not a good method for the volatilization of tholins, since significant changes to the material occur at low temperatures. This renders the usual assumption of pyrolysis, that the fragments are structurally related to the polymer, invalid, since the polymer appears to condense, and lose a great deal of nitrogen as ammonia in the pyrolysis process. However, tholins are difficult to volatilize by other means. Chemical derivatization may be a viable alternative. Thermochemolytic methods, which involve simultaneous pyrolysis and chemical derivatization, may also be useful. Analytical methods other than gas chromatography, such as HPLC and mass spectrometric methods, should also be pursued in the future.

4.7. References

Campbell, D., et al. (2000), *Polymer Characterization: Physical Techniques*, Stanley Thomas, Cheltenham, UK.

Chen, F. Z., et al. (1999), Low and room temperature photoabsorption cross sections of NH3 in the UV region, *Planetary and Space Science*, *47*, 261-266.

Coll, P., et al. (1998), Review and latest results of laboratory investigations of Titan's aerosols, *Origins of Life and Evolution of the Biosphere*, *28*, 195-213.

Coll, P., et al. (1999), Experimental laboratory simulation of Titan's atmosphere: aerosols and gas phase, *Planetary and Space Science*, *47*, 1331-1340.

del Rio, J. C., et al. (1998), Structural characterization of bio- and geo-macromolecules by off-line thermochemolysis with tetramethylammonium hydroxide, *Journal of Chromatography A*, *823*, 433-448.

Ehrenfreund, P., et al. (1994), Analytical Pyrolysis Experiments of Titan Aerosol Analogs in Preparation for the Cassini Huygens Mission, *Life Sciences and Space Research XXV (4)*, *15*, 335-342.

Haken, J. K. (1998), Pyrolysis gas chromatography of synthetic polymers - a bibliography, *Journal of Chromatography A*, *825*, 171-187.

Haken, J. K., and P. I. Iddamalgoda (1996), Degradative polymer analysis by chromatography, *Journal of Chromatography A*, *756*, 1-20.

Israel, G., et al. (1997), The Aerosol Collector Pyrolyser (ACP) Experiment for Huygens, in *Huygens: Science, Payload and Mission*, ESA Publications Division, Noordwijk, The Netherlands.

Materazzi, S., and R. Curini (2001a), The coupling of mass spectrometry with thermoanalytical instruments: Applications of evolved gas analysis, *Applied Spectroscopy Reviews*, *36*, 169-180.

Materazzi, S., and R. Curini (2001b), On-line evolved gas analysis by infrared spectroscopy coupled to thermoanalytical instruments, *Applied Spectroscopy Reviews*, *36*, 1-9.

Mellottee, H., and C. Vovelle (1982), Pyrolysis of Polyacrylonitrile.1. Study by Thermogravimetry and the Analysis of Free Gases, *European Polymer Journal*, *18*, 999-1006.

Linstrom, P.J., and Mallard, W.G. (Eds.) (2005), *NIST Chemistry WebBook, NIST Standard Reference Database Number 69*, National Institute of Standards and Technology, Gaithersburg, MD.

Pietrogrande, M. C., et al. (2001), Analysis of complex mixtures recovered from space missions - Statistical approach to the study of Titan atmosphere analogues (tholins), *Journal of Chromatography A*, *939*, 69-77.

Surianarayanan, M., et al. (1998), Spectroscopic investigations of polyacrylonitrile thermal degradation, *Journal of Polymer Science Part a-Polymer Chemistry*, *36*, 2503-2512.

Xie, W., and W. P. Pan (2001), Thermal characterization of materials using evolved gas analysis, *Journal of Thermal Analysis and Calorimetry*, *65*, 669-685.

Xue, T. J., et al. (1997), The thermal degradation of polyacrylonitrile, *Polymer Degradation and Stability*, *58*, 193-202.

Chapter 5. Complexation of Tholins by 18-crown-6: Identification of Primary Amines

5.1. Introduction

Electrospray ionization (ESI) is an excellent technique for the ionization of complex mixtures, since it is soft enough that only molecular ions are formed, and the confusion caused by overlapping fragments can be avoided. In conjunction with ion traps [Julian, *et al.*, 2003a]; [Julian, *et al.*, 2003b] capable of MS^n experiments, the necessity for chromatography of mixtures before analysis can sometimes be avoided. ESI has been applied to the investigation of such analytically difficult substances as crude oil [Hughey, *et al.*, 2002] and humic acids [Cooper, *et al.*, 2002]; [Stenson, *et al.*, 2002].

To date, only Mark Smith's group at the University of Arizona has used ESI for the analysis of tholins. In combination with high-resolution mass spectrometry, empirical formulas for hundreds of tholin components have been obtained [Sarker, *et al.*, 2003]. MS^n and H/D exchange experiments have also been used to obtain structural information for a number of these components [Somogyi, *et al.*, 2005].

Electrospray is soft enough that even non-covalent complexes can be brought into the gas phase. For instance, 18-crown-6 (Scheme 5.1) forms strong non-covalent complexes with protonated amines that can be transferred into the gas phase. In our laboratories, 18-crown-6 has been used to tag protonated amines in proteins and peptides, as a way to identify lysine residues [Julian and Beauchamp, 2001], and to create gas phase biomimetic reagents that bind to lysine side chains.

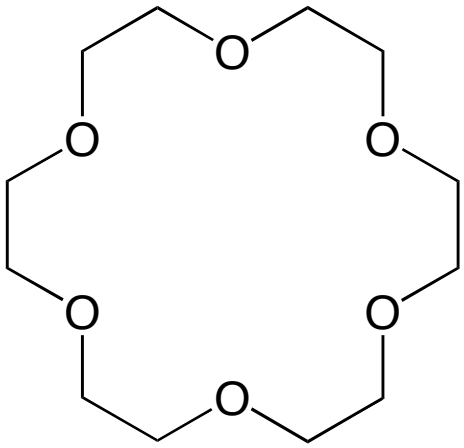

Scheme 5.1. 18-crown-6.

Here, tholins are electrosprayed in the presence of 18-crown-6, and complexes are formed with the components of the tholins that contain amines. Two major ion series that contain primary amines are present. Both appear to the linear aliphatic molecules, one based on aminoacetonitrile, the other on an ion with mass 110 Da. The implications of these species for the formation of the tholins is discussed.

5.2. Experimental

All experiments were performed on a ThermoElectron LCQ Deca ion trap mass spectrometer. Tholin (sample CH154) was dissolved in dichloromethane at a concentration of 2 mg/mL. Assuming an average molecular weight of 250 amu, the concentration is approximately 8 mM. 18-crown-6 was then added to the solution at a concentration of 1-2 mM. The LCQ tuning parameters were adjusted to maximize the species of interest. It is important to note that a high electrospray needle voltage (6.5 kV) was necessary in order to obtain a sufficient abundance of tholin-crown ether complexes.

5.3. Complexation of 18-crown-6 with tholins

Figure 5.1 is the mass spectrum obtained by electrospray of a solution of tholins with 18-crown-6 in dichloromethane. The largest peaks in the spectrum are assigned to protonated 18-crown-6 (MH^+) and a cluster of 18-crown-6, a proton and water ($[M+H_3O^+]^+$). At m/z values below that of MH^+ (264), the normal distribution of tholins obtained by electrospray is apparent. This consists of a series of groups of peaks differing by 14 m/z, the mass of a methylene unit. At masses higher than that of crown ether, complexes of 18-crown-6 with other components of the solution are apparent. The series of peaks separated by 14 m/z must be tholins complexed with 18-crown-6. Two major ion series are present complexed to the crown ether. The first corresponds to the formula $CN(CH_2)_n(NH_3)^+$, where n = 1-6. This series, based on aminoacetonitrile, is marked with triangles in Figure 5.1. The regularity of the distribution in intensity of this series suggests that methylene units are added as a linear chain. Branching would likely lead to steric effects that would alter the ability of the crown ether to bind, and thus alter the intensity distribution.

The other major series is based on an ion with mass 110 Da, plus between zero and four methylene groups. This series is marked with circles in Figure 5.1. The structure of this ion is uncertain, but it also has a regular intensity distribution, and so is probably a linear, rather than branched, structure.

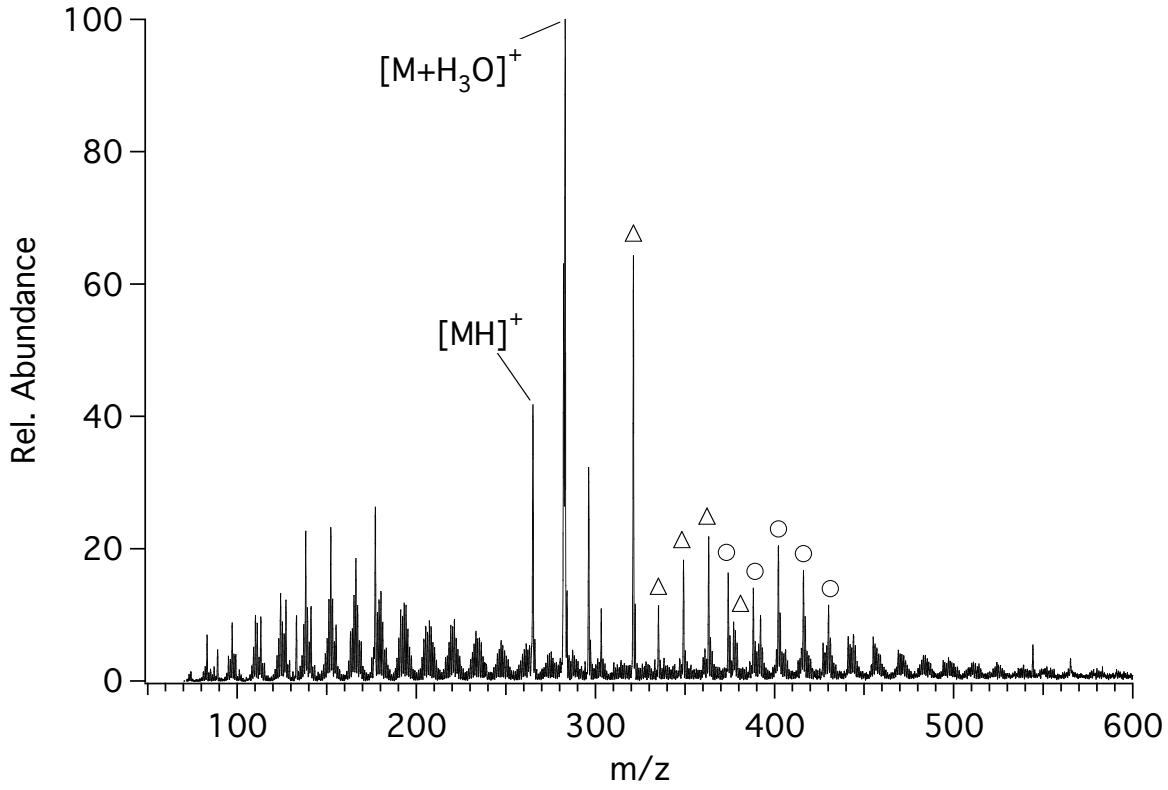

Figure 5.1. ESI mass spectrum of tholin complexed with 18-crown-6. Triangles, aminoacetonitrile series; Circles, 110 Da series.

We can confirm that the series are indeed crown ether adducts by isolating and fragmenting some of these ions. Figure 5.2a is the collisionally activated (CAD) mass spectrum of the ion at 416 m/z. The spectrum shows a mass loss of 264 Da, the mass of 18-crown-6, to give the ion at 152 m/z. The two other peaks in the spectrum, at 265 m/z and 283 m/z, correspond to protonated 18-crown-6 and 18-crown-6 complexed with hydronium ion. The hydronium ion peak is the result of protonated 18-crown-6 associating with background water vapor in the trap. The other peaks in the series have analogous CAD spectra. Figure 5.2b is the CAD spectrum of the ion at 153 m/z formed from the dissociation of 416 m/z. On activation, this ion loses small neutral molecules

such as HCN, NH_3, and acetonitrile. These kinds of losses are characteristic of the tholins.

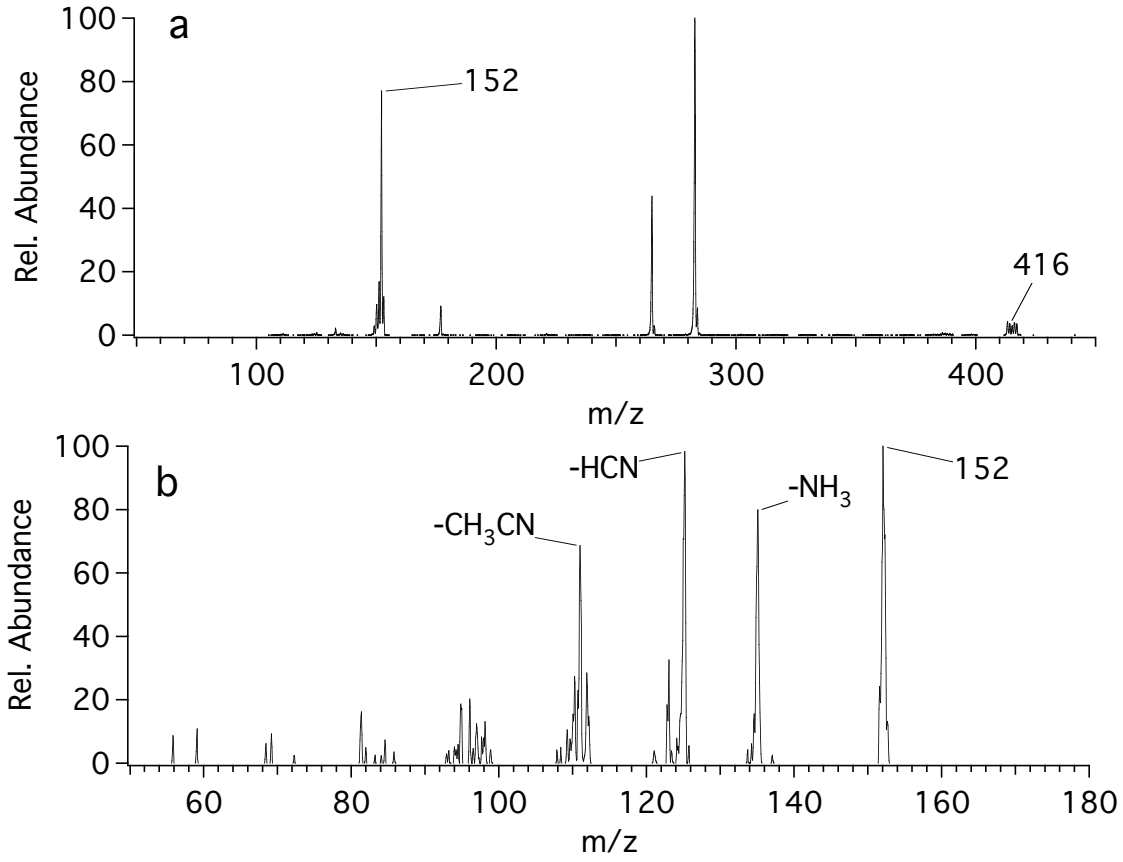

Figure 5.2. a) CAD spectrum of the ion at 416 m/z. b) CAD spectrum of the ion at 152 m/z from a).

The ion at mass 152 m/z has been extensively investigated by high resolution mass spectrometry and H/D exchange [Somogyi*, et al.*, 2005]. High resolution data reveals two peaks at a nominal m/z value of 152. The ions have the empirical formulae $C_8H_{14}N_3$ and $C_6H_{10}N_5$, and show seven and eight exchangeable protons, respectively. The 152 m/z ion is the fourth in the series we observe. Subtracting three methylene

groups from the above formulae leaves $C_5H_8N_3$ and $C_3H_4N_5$. Both ions may be capable of complexation with 18-crown-6.

To remove the possibility of non-specific binding of the crown ether to other positively charged groups that are present in the tholins, such as protonated imines, the source CAD capabilities of the LCQ were utilized. In this mode, voltage is applied to the octapole ion guide that feeds ions into the trap so as to provide a low level of collisional activation prior to trapping. This collisional activation should dissociate more weakly bound non-covalent complexes, leaving the more strongly bound complexes intact.

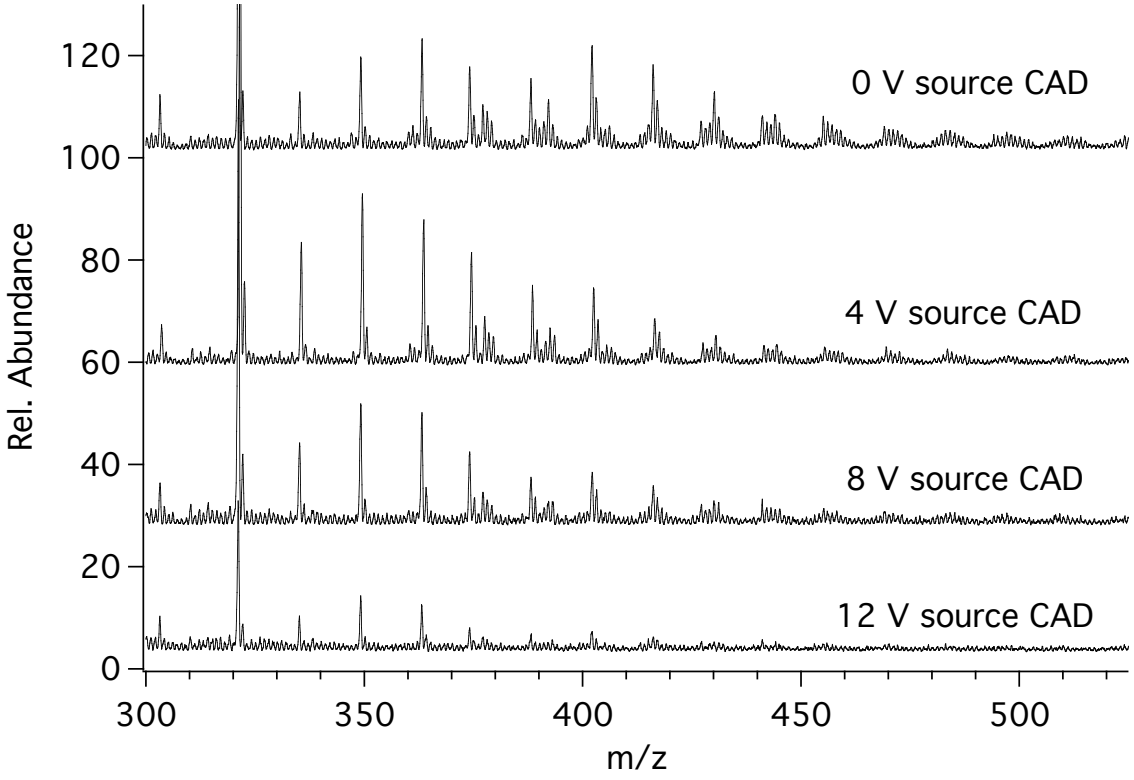

Figure 5.3. Source CAD of tholin-crown ether complexes.

Data from a range of CAD collision voltages is shown in Figure 5.3. None of the adducts in the two predominant ion series is particularly weakly bound, and so represent

protonated primary amines. The aminoacetonitrile series is more strongly bound to the crown ether than the $C_6H_{10}N_2$ series. For instance, the peak at 363 m/z (part of the aminoacetonitrile series) drops to half of its initial intensity at 12 V, while the ion at 402 m/z (part of the $C_6H_{10}N_2$) series has dropped to half its initial intensity by only 8 V.

No complexes are seen that contain more than one crown ether adduct. This suggests that most of the compounds that make up the tholins have either a single primary amine group or none at all. Perhaps primary amines are particularly reactive to the other components of the plasma in which the tholins are produced, and are converted into other functional groups, such as secondary or tertiary amines, during tholin production.

5.4. Conclusions

Electrospray ionization of tholins in the presence of 18-crown-6 enables the formation of complexes of 18-crown-6 with components of the tholins that possess primary amines. Two series of ions predominate in forming complexes with 18-crown-6. One series has the formula $CN(CH_2)_nNH_3^+$, where n = 1-6, which is assigned to aminoacetonitrile (n = 1) and analogs with additional methylene groups. The regularity of the distribution of this series suggests that methylene units are added as a linear chain. The other series is composed of ions of mass 110 + $(CH_2)_n$, where n = 0-4. The structure of this ion is uncertain. The aminoacetonitrile series is shown to be more strongly bound to the crown ether than the mass 110 series.

The use of 18-crown-6 to separate primary amines from a complex mixture is not limited to the analysis of tholins. The technique could also prove useful in analyzing the

amine content of crude oils, and in the tagging of lysine-containing peptides in tryptic digests.

5.5. References

Cooper, W. T., et al. (2002), Identification of individual humic molecules by electrospray ionization and ion cyclotron resonance mass spectrometry, *Abstracts of Papers of the American Chemical Society*, *223*, U514-U514.

Hughey, C. A., et al. (2002), Resolution of 11 000 compositionally distinct components in a single Electrospray ionization Fourier transform ion cyclotron resonance mass spectrum of crude oil, *Analytical Chemistry*, *74*, 4145-4149.

Julian, R. R., and J. L. Beauchamp (2001), Site specific sequestering and stabilization of charge in peptides by supramolecular adduct formation with 18-crown-6 ether by way of electrospray ionization, *International Journal of Mass Spectrometry*, *210*, 613-623.

Julian, R. R., et al. (2003a), Biomimetic approaches to gas phase peptide chemistry: combining selective binding motifs with reactive carbene precursors to form molecular mousetraps, *International Journal of Mass Spectrometry*, *228*, 851-864.

Julian, R. R., et al. (2003b), Molecular mousetraps: Gas-phase studies of the covalent coupling of noncovalent complexes initiated by reactive carbenes formed by controlled activation of diazo precursors, *Angewandte Chemie-International Edition*, *42*, 1012.

Sarker, N., et al. (2003), Titan aerosol analogues: Analysis of the nonvolatile tholins, *Astrobiology*, *3*, 719-726.

Somogyi, A., et al. (2005), Organic environments on Saturn's moon, Titan: Simulating chemical reactions and analyzing products by FT-ICR and ion-trap mass spectrometry, *Journal of the American Society for Mass Spectrometry*, *16*, 850-859.

Stenson, A. C., et al. (2002), Ionization and fragmentation of humic substances in electrospray ionization Fourier transform-ion cyclotron resonance mass spectrometry, *Analytical Chemistry*, *74*, 4397-4409.

Chapter 6. Fluorescence Spectra of Titan Tholins: *in-situ* Detection of Astrobiologically Interesting Areas on Titan's Surface

6.1. Abstract

We report the three-dimensional fluorescence spectra of Titan tholins in water and acetonitrile, and separate some of the fluorescent components of tholins using two-dimensional thin layer chromatography. In acetonitrile, tholins exhibit a broad fluorescence with a maximum at 471 nm, and an excitation maximum at 410 nm. The fluorescence spectrum of a water extraction displays a more complicated spectrum with multiple peaks. TLC results indicate the presence of at least three distinct fluorescent species. In addition, we obtained the two-dimensional fluorescence spectrum of tholins in water ice at 77K, close to the surface temperature of Titan. The fluorescence of tholins in a 77K ice matrix is red-shifted in comparison to a water solution, and undergoes a further red-shift when the water solution is heated prior to freezing. These results suggest that a simple fluorescence probe could be used on the surface of Titan to identify sites where tholins have been mixed with water, and possibly reveal information about the extent of heating the tholin-water mixture has undergone. This would be useful for a future mission with the goal of examining the organic chemistry of Titan.

6.2. Introduction

Titan, the largest moon of Saturn, is one of the most astrobiologically interesting targets in the Solar System. Photochemistry in the upper reaches of a thick N_2/CH_4 atmosphere produces a wealth of organic compounds that eventually fall to a surface composed primarily of water ice. Once there, impacts or volcanism (Lorenz 1996) melt the surface ice, mixing the organics with liquid water in melt pools that may last for hundreds or thousands of years (Lorenz et al. 2001; Artemieva and Lunine 2003), adequate time for a complex organic chemistry to develop. Titan's frozen melt pools represent a collection of individual experiments in prebiotic chemistry preserved by the frigid temperatures of the surface.

With the arrival of the Cassini/Huygens mission in 2004, interest in the properties of Titan's tholins has experienced a resurgence. Analysis has naturally been limited to laboratory analogs produced by electrical discharge or UV irradiation of N_2/CH_4 mixtures (Coll *et al.* 1999). The products of these reactions are numerous, and vary from low molecular weight alkanes, alkenes and nitriles (Coll *et al.* 1999) to a reddish-brown polymeric material, the substance known as tholins. While a good deal of information on the spectral properties and elemental composition of the tholins has been obtained (Khare et al. 2002; Coll et al. 2001; Sarker et al. 2003), structural information is still lacking. We report the first 3-D fluorescence spectra of Titan tholins, as well as the first low-temperature observations of the fluorescence properties of tholins (cf. Sagan et al. 1993). Three-dimensional fluorescence spectra like those obtained can be used as a "fingerprint" of these complex mixtures. Of particular interest are the fluorescence spectra of tholins extracted into water, and the fluorescence of tholins in a water ice matrix at temperatures

similar to those on the surface of Titan, approximately 94 K (Lorenz et al. 2001). We discuss how these results might be applied to the future exploration of Titan's surface and chemistry.

6.3. Experimental

The tholin samples were produced in a plasma discharge reactor, the details of which are given elsewhere (Sarker et al. 2003). The gas mixture used was 2% CH_4 in nitrogen at 7 torr, with the entire discharge cell cooled to 195 K in a dry ice-isopropanol bath. The sample was recovered as a saturated solution in acetonitrile and contained a tholin mixture the components of which ranged in mass between 100 and 500 amu as determined by electrospray ionization-Fourier transform mass spectrometry. Samples were isolated in a dry, oxygen free glove box, and stored in a dry, oxygen free environment until needed.

Three-dimensional fluorescence spectra were obtained on a Hitachi F-4500 FL spectrophotometer. The excitation and emission slits were set at 5 nm, and both excitation and emission were scanned in 5 nm intervals at 12000 nm/min. The acetonitrile sample was a ten-fold dilution of a saturated solution of tholins in acetonitrile. To prepare the water sample, an aliquot of the saturated acetonitrile solution was dried under vacuum to yield 17.6 mg of solid. This was extracted with 3 mL of water, and then filtered through a 0.2 μm syringe filter. This solution was diluted ten-fold for use in the spectrophotometer.

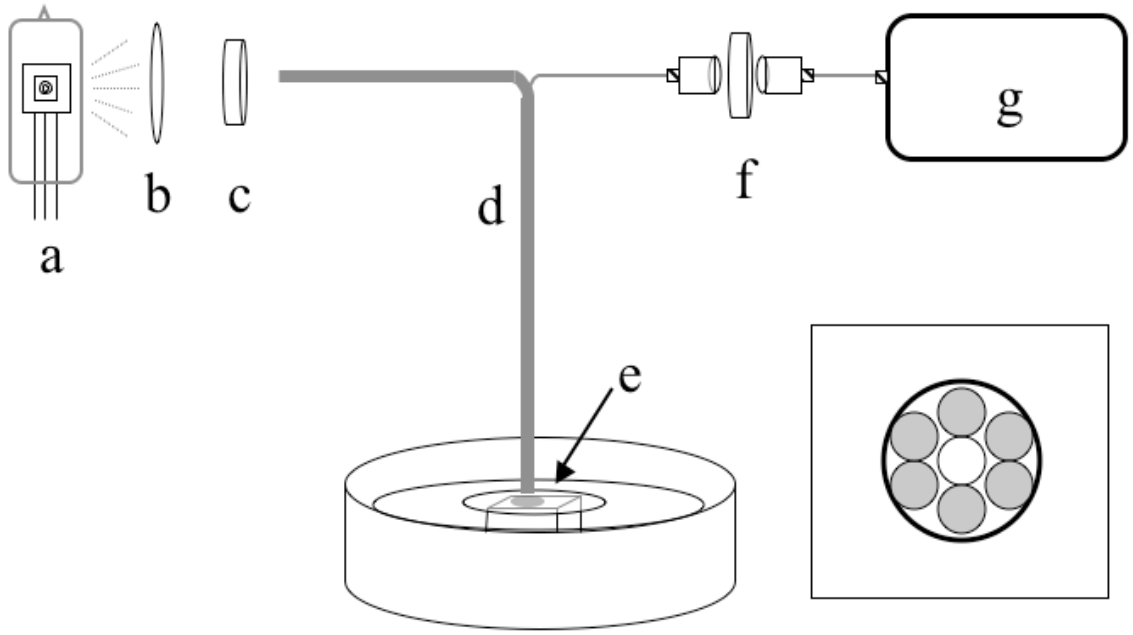

Figure 6.1. Experimental arrangement for obtaining fluorescence spectra of tholin at 77 K. a) deuterium lamp, b) lens, c) 365 nm bandpass filter, d) six-around-one fiber optic probe, e) ice sample supported on an aluminum block immersed in LN_2, f) 400 nm lonpass filter, g) Ocean Optics S2000 fiber optic spectrometer. Inset: End-on view of the six-around-one fiber optic probe. Six illumination fibers (gray) surround one read fiber (white).

Fluorescence spectra of tholins in ice are obtained using the arrangement shown in Figure 6-1. A 30 W deuterium lamp is used as the excitation source. The output of the lamp is passed though a 360 nm filter with a FWHM bandpass of 45 nm (Hoya U-360) and focused into the excitation bundle of a six-around-one fiber optic probe. The end of the probe is held a few millimeters above the ice sample. The ice is kept at approximately 77K by placing the glass slide with the ice sample on an aluminum block

immersed in LN_2. Fluorescence collected by the read fiber of the probe is passed through a 400 nm longpass filter (Schott GG400) to remove the excitation light, and is analyzed with a fiber optic spectrometer (Ocean Optics S-2000). The inset of Figure 6.1 shows a view of the end of the fiber optic probe facing the sample. Six illumination fibers surround a single read fiber.

Two-dimensional thin-layer chromatography was performed on 60 μm silica gel plates (Merck silica gel 60). Plates were prewashed with methanol:dichloromethane overnight, and dried at 100 °C before use. Approximately 1 μL of tholin in acetonitrile was spotted onto the plate for each chromatograph. Plates were developed with either dimethylformamide and then methanol, or ethanol and then acetonitrile. Spots on the plates were scraped off with a razor blade, and the silica gel was extracted with acetonitrile for analysis with the Hitachi F-4500 FL spectrophotometer. Separate plates were developed in an identical manner for staining. $KMnO_4$ solution for staining was prepared from 1 g $KMnO_4$ and 2 g Na_2CO_3 dissolved in 100 mL water.

6.4. Results and discussion

6.4.1. Three-dimensional fluorescence spectra

Three-dimensional fluorescence spectra of tholins in acetonitrile and water are given in Figure 6.2. The acetonitrile solution spectrum is broad and featureless, with an emission maximum at 471 nm, and an excitation maximum at 410 nm.

At least two distinct fluorophores are present in the water extraction. The emission is blue-shifted relative to the acetonitrile spectrum, with a maximum at 397 nm. The excitation maximum is also blue-shifted, peaking at 335 nm. Molecules with similar

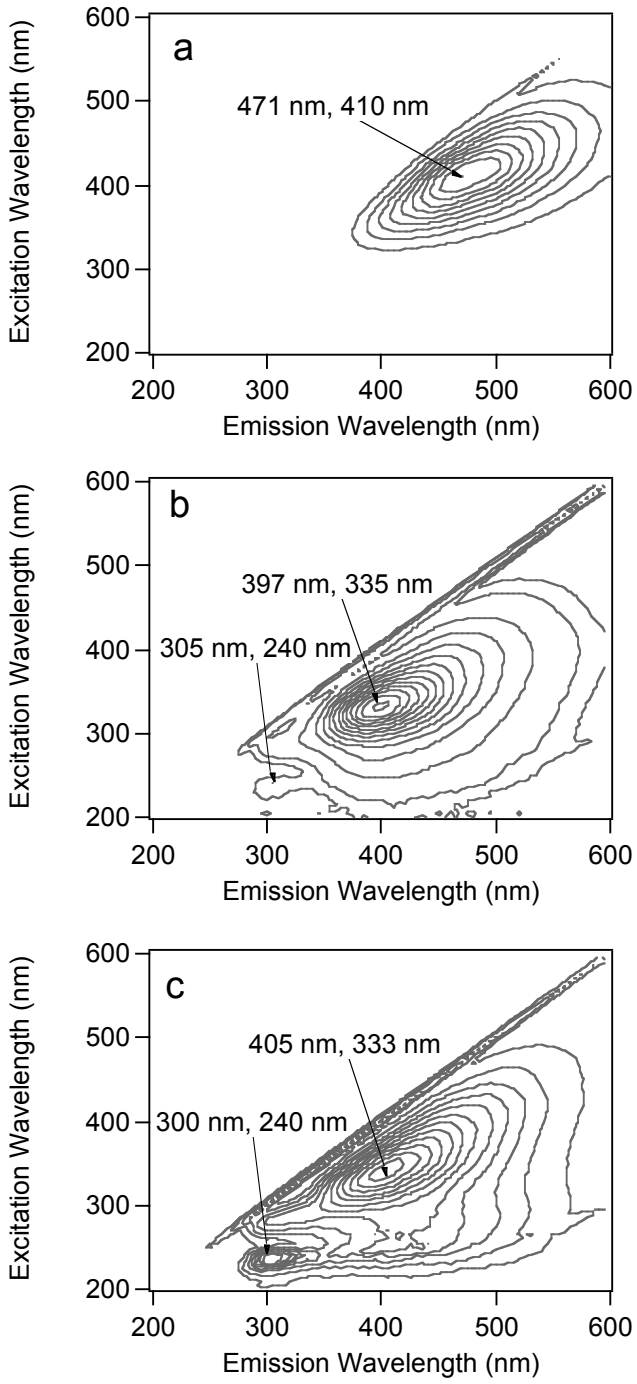

Figure 6.2. a) The 3-D fluorescence spectrum of tholin in acetonitrile. b) The 3-D fluorescence spectrum of a water extract of tholin. c) The 3-D fluorescence spectrum of the chromatographically separated fluorescent fraction of tholin. The prominent diagonal lines in b and c are due to Rayleigh scatter from the sample.

fluorescence maxima include several polycyclic aromatic hydrocarbons (PAHs) with 4-5 rings, including pyrene, benzopyrene, and benzanthracene derivatives (Dean 1992). Sagan et al. (1993) have previously detected PAHs in Titan tholins. Nitrogen containing PAHs were detected in tholins as well (Imanaka et al. 2004), and should display fluorescence properties similar to normal PAHs. Linear conjugated systems of 8-10 atoms, such as octatetraene, also have similar emission and excitation maxima (D'Amico et al. 1980). The water spectrum displays a second, fainter peak, with an emission maximum of 305 nm, and an excitation maximum of 240 nm. Fluorescence emission in the UV is suggestive of a small molecule. Monocyclic aromatics such as benzene, toluene, and aniline have emission maxima in this region (Berlman 1971).

Figure 6.2c is the spectrum of the fluorescent fraction of the saturated acetonitrile solution, separated chromatographically on a silica gel column with acetonitrile. The separation was followed with a UV lamp. The spectrum is strikingly similar to that of the water sample (Figure 6.2b). The emission peak at 305 nm is more strongly represented, however.

Solvent effects on fluorescence spectra are complex, but in general emission maxima shift to longer wavelengths as solvent polarity increases (Lakowicz 1999). The opposite apparent trend is observed in the tholin spectra in Figures 6.2a (in acetonitrile) and 6.2b (in water). In addition, the spectrum of the chromatographically-separated tholins in acetonitrile (Figure 6.2c) is essentially the same as that of the water extraction (Figure 6.2b), despite the difference in solvent. This indicates that the differences in the excitation and emission wavelengths between Figures 6.2a and 6.2b are probably not due to solvent effects.

The chromatographic separation results indicate, rather, the presence of a fluorophore that, when separated from other chemically distinct components of the bulk tholin solution by silica gel chromatography, undergoes a shift to the blue in excitation and emission maxima. This could be the result of intermolecular interactions between this fluorophore and one or more non-fluorescent components of the bulk tholins. These interactions could result in an intermolecular complex with lower-energy excited states, and red-shifted fluorescence relative to the isolated fluorophore. The difference in spectra between acetonitrile and water solutions would suggest that the non-fluorescent component is essentially insoluble in water, but soluble in acetonitrile, or that water prevents the formation of the complex.

While no structural information about the fluorophores can be gleaned from these spectra, they are a fingerprint of the tholin sample. Producing laboratory tholins under various conditions would establish a library of spectra useful as a reference for future missions to Titan that may collect fluorescence data.

6.5. Thin-layer chromatography

Figure 6.3a is a photograph of the native fluorescence of tholins, spotted from an acetonitrile solution, separated on a TLC plate developed in the first dimension with dimethylformamide, and in the second dimension with methanol. Development with these solvents causes the majority of the fluorescent components to migrate to the upper right corner of the plate. Polar solvents such as methanol and dimethylformamide are necessary to move the tholins on the polar silica gel, indicating that the fluorescent compounds are polar themselves. The spot labeled 1 reacts with $KMnO_4$, indicating the

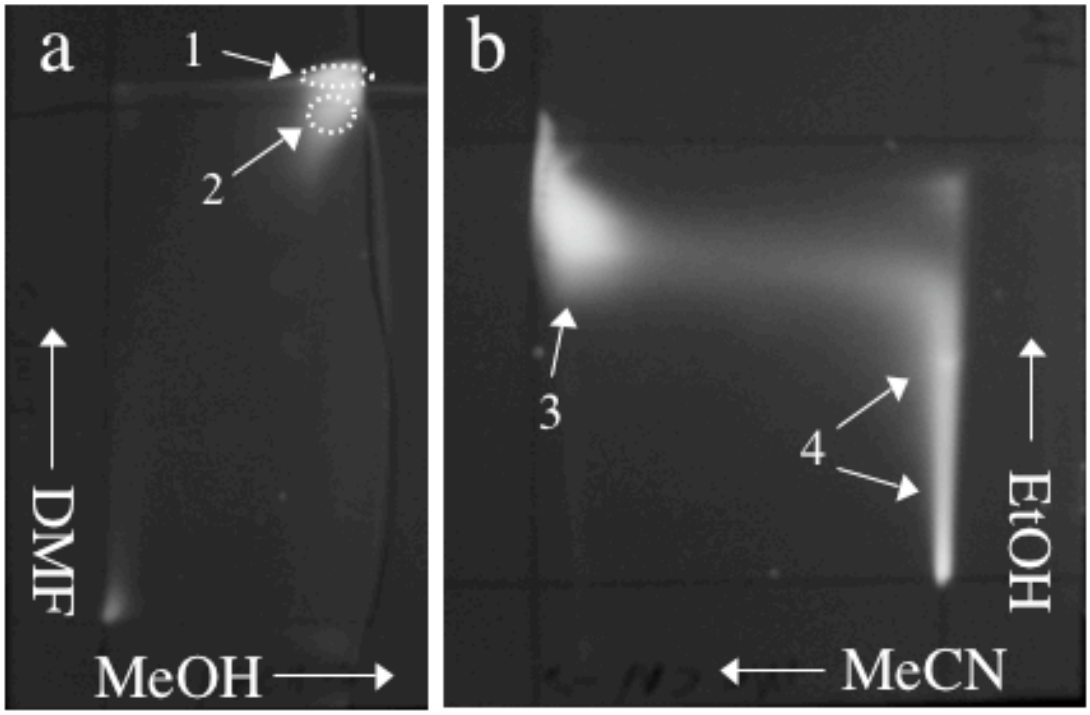

Figure 6.3 . a) Photograph of the fluorescence of the TLC plate developed with DMF and methanol. b) Photograph of the fluorescence of the TLC plate after development with ethanol and acetonitrile. Both plates were illuminated with a 366 nm UV lamp. Light areas are fluorescent tholin components.

presence of double bonds. $KMnO_4$ does not react with aromatic systems. Spot 1 exhibits a greenish fluorescence, and the 3D fluorescence spectrum is shown in Figure 6.4. The group of peaks between 400 and 500 nm emission is the result of vibrational structure in the fluorophore. This kind of structure is usually observed in the fluorescence of aromatic or conjugated systems. The spacing between the peaks is approximately 1300 cm^{-1}, characteristic of skeletal C-C stretching modes (Coates 2000). The data supports the conclusion that this spot represents a linear conjugated molecule, such as decapentaene or one of its derivatives.

The spot labeled 2 exhibits a blue fluorescence, with a fluorescence excitation maximum at 340 nm, and an emission maximum at 400 nm. This is the same fluorescence seen in the water extraction of the tholins, and so we assume that the fluorophore is the same.

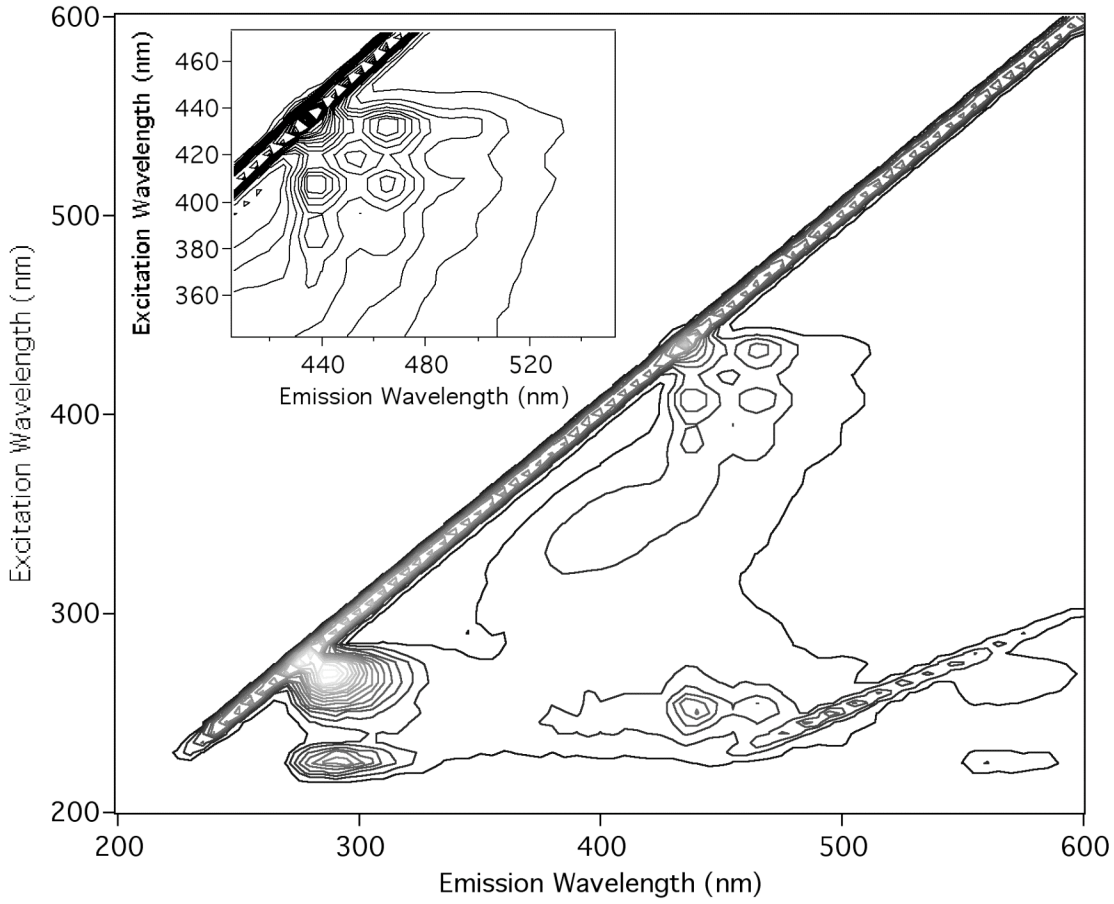

Figure 6.4. 3-D fluorescence spectrum of the acetonitrile extract of spot 1. The inset shows detail in the region between 410 and 550 nm emission, and 340 and 470 nm excitation. The prominent diagonal lines are due to Rayleigh scatter.

Figure 6.3b is a photograph of the native fluorescence of tholins developed in the first dimension with ethanol, and in the second dimension with acetonitrile. The

fluorescence is split into two major groups, a large, irregular spot labeled 3 and a long streak labeled 4. The 3D fluorescence spectrum of spot 3 reveals an excitation maximum at 340 nm, and an emission maximum at 400 nm, characteristic of the blue, water soluble component. 3D fluorescence spectra of different regions of the streak labeled 4 all showed similar fluorescence: an excitation maximum at 285 nm, and an emission maximum at 340 nm. The emission displays a long tail to ~500 nm, explaining the blue color visible to the naked eye.

Streak 4 in Figure 6.3b represents a class of compounds with blue fluorescence distinct from the blue fluorophore of spot 3. These compounds are distinct in structure as well; streak 4 is formed from components with varying affinity for silica gel relative to ethanol, and a great affinity for silica gel relative to acetonitrile. This suggests a group of polymers that share a common fluorescent moiety, perhaps a pendant polycyclic aromatic structure. Spot 3 shows little affinity for silica relative to both ethanol and acetonitrile. The thin-layer chromatography results indicate the presence of at least three distinct fluorescent species: (1) a linear, conjugated molecule with a green fluorescence (spot 1 of Figure 6.3), (2) the water soluble, blue-fluorescent compound that is the primary fluorophore of the water extract, and (3) a blue-fluorescent class of polymeric compounds with a common fluorescent group.

6.6. Fluorescence spectra of tholins at 77K

Figure 6.5 gives the fluorescence spectra of several different tholin samples acquired at approximately 77K. Tholins in pure water ice at this temperature exhibit a single fluorescence peak with a maximum at 520 nm. At the excitation wavelength used

in these experiments (~360 nm), the fluorescence of a water extract of tholin peaks at 430 nm. The fluorescence in ice is significantly red-shifted relative to the fluorescence in liquid water. Further experiments in which the ice sample was allowed to melt and then refrozen showed no changed in the fluorescence properties. This indicates that the observed red-shift is the result of a change in the environment of the fluorophore, and not the result of a chemical transformation.

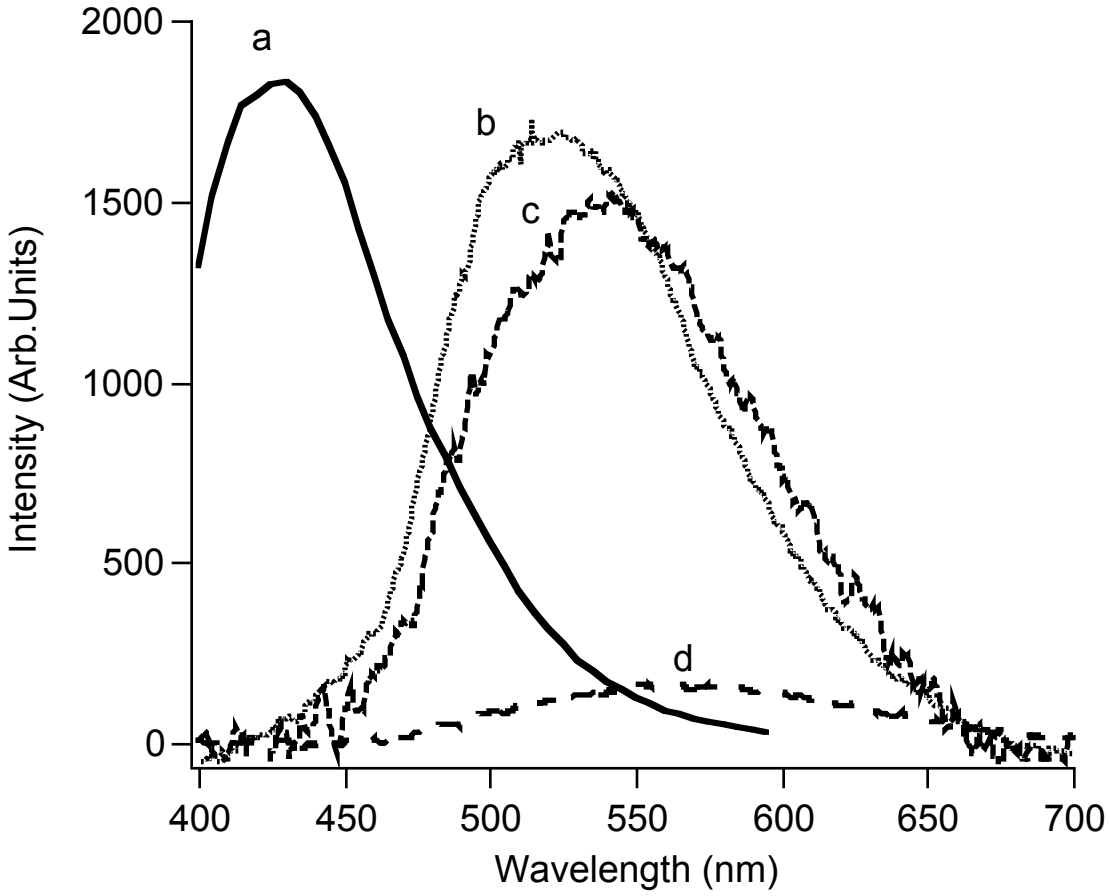

Figure 6.5. Fluorescence spectra of tholin. a) Cut through the plot in Fig. 6.2b at an excitation wavelength of 360 nm. b) Fluorescence of tholin in ice at 77K. c) Fluorescence of tholin in ice at 77K, after boiling for 5 minutes. d) Fluorescence of solid tholin at 77K.

Tholin samples were processed in a manner that might replicate conditions on the surface of Titan. There is some speculation that the surface water ice might be mixed with some percentage of ammonia (Lorenz et al. 2001; Bernard et al. 2003). To consider the possible implications of this hypothesis, tholin was extracted with a 1% by volume ammonia solution for 30 minutes, and the fluorescence spectrum of the resulting ice was obtained (spectrum not shown). The fluorescence properties appear unaltered by treatment with ammonia.

Tholin was also extracted with boiling water for 5 minutes. This may replicate events in which tholin is mixed with heated liquid water by impact (Lorenz et al. 2001; Artemieva and Lunine 2003). The fluorescence spectrum of the boiled solution in Figure 6.5 displays a red-shift of approximately 20 nm. This is suggestive of a chemical transformation of the fluorophore, such as a functional group conversion. Further boiling of the solution for up to 30 minutes resulted in no further change in the fluorescence.
A solid film of tholin was prepared by drying a drop of the saturated acetonitrile solution on a glass slide under vacuum. At 77 K, a faint fluorescence peaking at 558 nm was observed. The spectrum is shown in Figure 6.5. The fluorescence of the solid tholin, and of tholin in an ice matrix are distinct, both in intensity and wavelength, and would be easily distinguishable on Titan's surface with a simple fluorescence spectrometer.

6.7. Conclusions

Three-dimensional fluorescence spectroscopy of tholins in water and acetonitrile point to the presence of two distinct fluorescent components: a small, UV-fluorescent molecule, and a blue-fluorescent species. Both species are water soluble, and the blue-fluorescent molecule appears to form a complex with the non-fluorescent components of

the tholins. Thin layer chromatography reveals the additional presence of a green-fluorescent conjugated molecule, and a group of blue-fluorescent molecules, most likely polymeric, with a common fluorophore.

The presence of fluorescent compounds in tholins is unsurprising, considering the complexity of the material. Tholins contain a variety of fluorescent compounds, from small molecules with UV fluorescence to larger polymeric species with fluorescent components. The fluorophores are likely linear, conjugated systems, and functionalized aromatic molecules, present both as discrete compounds and as groups attached to larger molecules.

Fluorescence would be a powerful technique for locating areas of astrobiological interest on Titan's surface. A simple fiber-optic probe and spectrometer like the one used here could be integrated into almost any vehicle proposed for the exploration of Titan, and would function as a test for the presence of organics in the surface ice. When fluorescence is detected, further chemical analysis can be performed on the sample. The fluorescence itself may also provide information relating to the thermal history of the organics.

6.8. Acknowledgements

We recognize the support of the Director's Research and Development Fund at the Jet Propulsion Laboratory. We also thank Francois Raulin, Jean-Michel Bernard, and Bishun Khare for helpful comments regarding the manuscript.

6.9. References

Artemieva, N. and J. Lunine 2003. Cratering on Titan: impact melt, ejecta, and the fate of surface organics. *Icarus* **164**, 471-480.

Bernard, J.-M., Coll, P., Coustenis, A., Raulin, F. 2003. Experimetnal Simulation of Titan's Atmosphere: Detection of ammonia and ethylene oxide. *Planetary and Space Science* **51**, 1003-1011.

Berlman, I.B. 1971. *Handbook of Fluorescence Spectra of Aromatic Molecules,* 2nd ed. Academic Press, New York pp. 108, 144, 251.

Coates, J. 2000. Interpretation of Infrared Spectra, A Practical Approach. In: Meyers, R.A. (Ed.), Encyclopedia of Analytical Chemistry, John Wiley and Sons Ltd., Chichester, pp. 10815-10837.

Coll, P., D. Coscia, N. Smith, M.-C. Gazeau, S.I. Ramirez, G. Cernogora, G. Israël, F. Raulin 1999. Experimental laboratory simulation of Titan's atmosphere: aerosols and gas phase. *Planetary and Space Science* **47**, 1331-1340.

Coll, P., S. I. Ramirez, R. Navarro-Gonzalez, F. Raulin 2001. Chemical and optical behavior of tholins, laboratory analogs of Titan aerosols. *Advances in Space Research* **27**, 289-297.

D'Amico, K.L., C. Manos, R. L. Christensen 1980. Electronic Energy Levels in a Homologous Series of Unsubstituted Linear Polyenes. *J. Am. Chem. Soc.*, **102**, 1777-1782.

Dean, J. A. 1992. *Lange's Handbook of Chemistry*, 14th ed. McGraw-Hill, New York, pp. 7.25-7.27.

Imanaka, H., Khare, B.N., Elsila, J.E., Bakes, E.L.O., McKay, C.P., Cruikshank, D.P., Sugita, S., Matsui, T., Zare, R.N. 2004. Laboratory experiments of Titan tholin formed in cold plasma at various pressures: implications for nitrogen-containing polycyclic aromatic compounds in Titan haze. *Icarus* **168**, 344-366.

Khare, B.N., E.L.O. Bakes, H. Imanaka, C. P. McKay, D.P. Cruikshank, E.T. Arakawa 2002. Analysis of the Time-Dependent Chemical Evolution of Titan Haze Tholin. *Icarus* **160**, 172-182.

Lakowicz, J. R. 1999. *Principles of Fluorescence Spectroscopy*, 2nd ed. Kluwer/Plenum, New York, pp. 185-210.

Lorenz, R.D. 1996. Pillow lava on titan: expectations and constraints on cryovolcanic processes. *Planetary and Space Science* **44**, 1021-1028.

Lorenz, R.D., J.I. Lunine, C.P. McKay 2001. Geologic Setting for Aqueous Organic Synthesis on Titan Revisited. *Enantiomer* **6**, 83-96.

Sagan, C., B. N. Khare, W. R. Thompson, G. D. McDonald, M. R. Wing, J. L. Bada, T. Vo-Dihn, and E. T. Arakawa 1993. Polycyclic aromatic hydrocarbons in the atmospheres of Titan and Jupiter. *Astrophys. J.* **414**, 399-405.

Sarker, N., Somogyi, A., Lunine, J.I., Smith, M.A 2003. Titan Aerosol Analogues: Analysis of the Nonvolatile Tholins. *Astrobiology* **3**, 719-726.

Chapter 7. Gas chromatography with ultraviolet detection for the analysis of tholins

7.1. Introduction

The development of spaceflight instrumentation is challenging, due to the restrictions on power, weight, and volume that space probes necessitate. For the analysis of organics, few systems can compare to GC-MS in their ability to identify the components of complex mixtures. While GC-MS systems have been developed for spaceflight purposes, they are especially difficult to design in a way that satisfies the requirements of power, weight, and volume. The major obstacle is the necessity of vacuum for the mass spectrometer system, which requires a bulky and power-hungry pumping system.

This chapter describes an unusual instrument, a gas chromatograph coupled to a gas-phase far ultraviolet spectrometer. Examination of the gas-phase ultraviolet spectrum would allow for functional group identification of the separated compounds, although it would not necessarily permit precise identification. As well, such a system would not require vacuum, and could be miniaturized relatively easily. Since the technique is non-destructive, it could also serve as a backup detector for a more traditional mass spectrometer detector. The instrument, with minor modifications, has also been used to detect organonitrate explosives (see Appendix A).

The coupling of gas phase ultraviolet absorption with gas chromatography has been practiced sporadically for the past 40 years. Kaye reported the first GC-UV system

in 1962 [Kaye, 1962], which used ultraviolet absorption at 170 nm for the analysis of a chromatographic separation of gasoline. GC-UV systems have since been used for the analysis of wine [Cedron-Fernandez*, et al.*, 2002], indoor dust [Lagesson*, et al.*, 2000a], and proposed as a means for functional group analysis [Lagesson*, et al.*, 2000b].

We describe a GC-UV system, and its use in the identification of the products of low-temperature pyrolysis of tholins. The data obtained is compared to the data obtained by GC-MS. The spectra of a number of reference compounds have also been obtained for comparison. As well, these spectra may be useful in modeling the atmospheric properties of Titan, as the gas-phase far ultraviolet spectra of many small nitriles and amines are unknown.

7.2. Experimental

A block diagram of the experimental apparatus is shown in Figure 7.1. The laboratory-constructed pyrolyzer is shown in Figure 7.2. A 3 mm OD borosilicate glass tube is packed with a small wad of glass wool, a few milligrams of tholin, and then another wad of glass wool. The glass tube is wrapped with several turns of nichrome wire in the area of the tholin, and sealed into the injector of the gas chromatograph with a graphite ferrule and an 1/8“ Swagelok fitting. For pyrolysis, a flow of 50 mL/min of helium is passed through the pyrolyzer, and a current of 2 A is passed through the Nichrome wire for 15 s. This heats the sample to 220 °C, as determined by placing a thermocouple in the pyrolyzer and heating as above. The current is switched off, and the helium flow is stopped. The gas chromatograph program then proceeds normally. The gas chromatograph (SRI Model 8610C) is connected to a heated absorption cell via a

heated stainless steel transfer line, usually held at 100 °C. The cell consists of two aluminum blocks supporting a quartz tube (3 mm OD) between them, with silica windows on either side. The tube serves as both a light pipe and a conduit for the gas chromatograph effluent. The cell has a pathlength of ~6 cm, and is typically heated to 100 °C. Residence time in the cell is approximately 3 s, so no peak broadening due to the cell is expected.

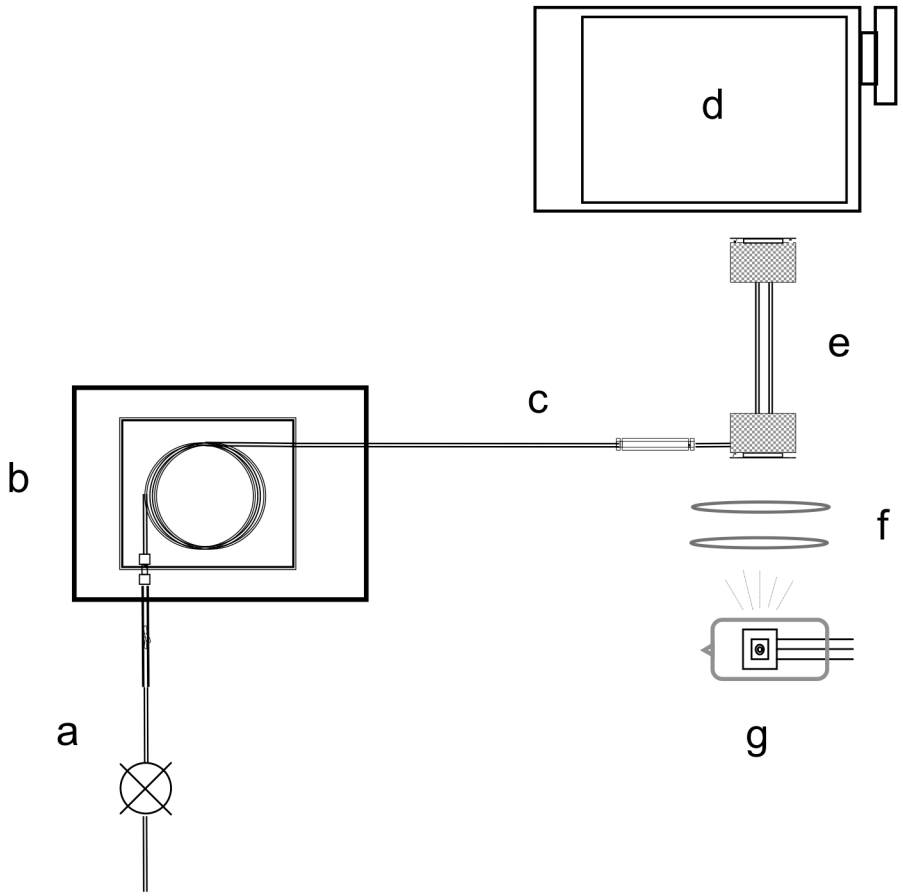

Figure 7.1. Pyrolysis-GC-UV system. a) pyrolyzer, b) SRI 8610 gas chromatograph, c) transfer line, d) Chromex 250is spectrometer, e) absorption cell, f) silica lenses, g) deuterium lamp.

The light from a 30 W deuterium lamp (Oriel 63163) is coupled into the cell using silica lenses. Unfocused light exiting the cell is directed into a Chromex 250is imaging spectrograph equipped with an Apex SPH-5 CCD detector. The resolution of the system is approximately 0.5 nm. The entire optical path, including the spectrometer, is purged with nitrogen to allow operation below 200 nm. Spectra from 185-240 nm are acquired approximately every 1.5 seconds, with an integration time of 1 s.

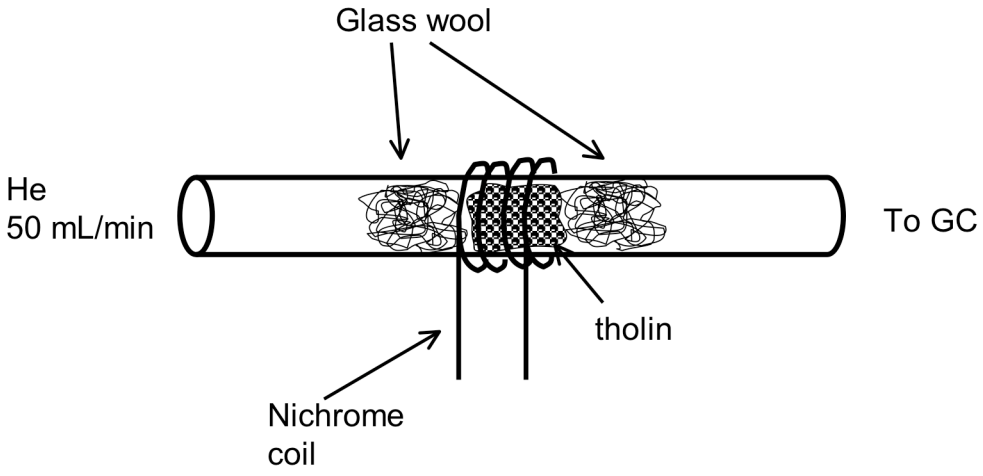

Figure 7.2. Lab-built low temperature pyrolyzer.

The gas chromatograph uses a 100% methyl polysiloxane column (MXT-1 15m × 0.53mm × 5μm film) with on-column injection. The temperature of the GC oven was ramped from 25 °C to 250 °C at 10 °C/min. Helium was used as the carrier gas with a source pressure of 10 psig.

GC-MS chromatograms were obtained in the following manner. In order to replicate the pyrolytic conditions in our lab-built pyrolyzer, the injector of the gas chromatograph was set to a temperature of 220 °C. Approximately 1 mg of tholin was

dissolved in 100 uL dichloromethane, and 1 uL of this solution was injected into the gas chromatograph, a Varian 3400 CX equipped with a Varian Saturn 2000 mass spectromter detector. The column was a DB5 capillary column. The temperature program was the same as that used above. Although the column and injection conditions are different, by keeping the temperature program the same as that used with the GC-UV system, we can make reasonable correlations between the data obtained by each method.

7.3. GC-UV of tholin pyrolysis products

Figure 7.3 is the chromatogram obtained by GC-MS. Peaks were identified by comparison with mass spectra from the NIST Chemistry WebBook library [Linstron and Mallard, 2005]. The following compounds were observed: 1) butyronitrile, 2) isobutyronitrile, 3) pentanedinitrile, 4) 2-methyl-2-butenenitrile, and 5) hexanedinitrile. The compounds are primarily alkyl nitriles and dinitriles, with some alkenes as well. These products are consistent with the results from other analyses of pyrolysis products [Coll*, et al.*, 1998]; [Ehrenfreund*, et al.*, 1994]; [Israel*, et al.*, 1997]; [Pietrogrande*, et al.*, 2001]. Examination of the spectra of some of the unidentified compounds show many of the same fragments as other, earlier eluting peaks, but with differing intensities, suggesting that they are structural isomers of the earlier peaks. For instance, the starred peaks in Figure 7.3 all have similar molecular ion masses and fragmentation spectra as peak 5, and so are identified as isomers of hexanedinitrile.

Figure 7.4 is a three-dimensional chromatogram of the products of the pyrolysis of tholin (sample CH154) obtained by GC-UV. At least a dozen distinct peaks are visible. The peaks are rather broad; this is due to the pyrolyzer, which delivers analyte to

the column over a relatively long period of time (15 s). This slow injection results in broad peaks. The initial region of very high absorbance corresponds to the period of time when the sample is being pyrolyzed. An examination of the spectrum of this region shows that is composed mostly of ammonia, which is not retained by the column. Ammonia has been shown to be released in large quantities by the tholin when heated (Chapter 4).

The spectra corresponding to selected peaks in the chromatogram are shown in Figures 7.5-7.7. Figure 7.5 and 7.6 are the spectra corresponding to peaks at

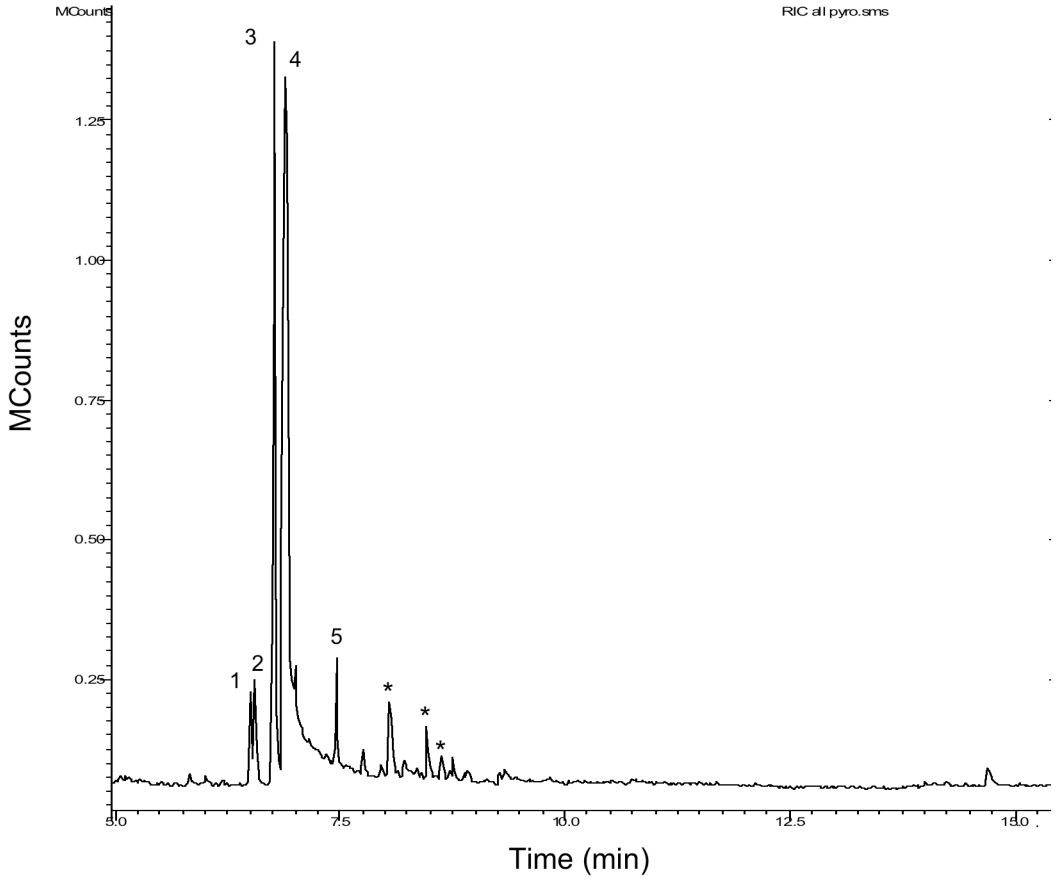

Figure 7.3. GC-MS chromatogram of the low temperature pyrolysis products of tholins.

approximately 90 s and 125 s, respectively. The peaks are broad, with structure superimposed onto the peaks at 125 s. The superimposed structure is identical to the vibrational structure present in the absorption spectrum of ammonia. This is the result of the tail of the very strong ammonia peak at the beginning of the chromatogram.

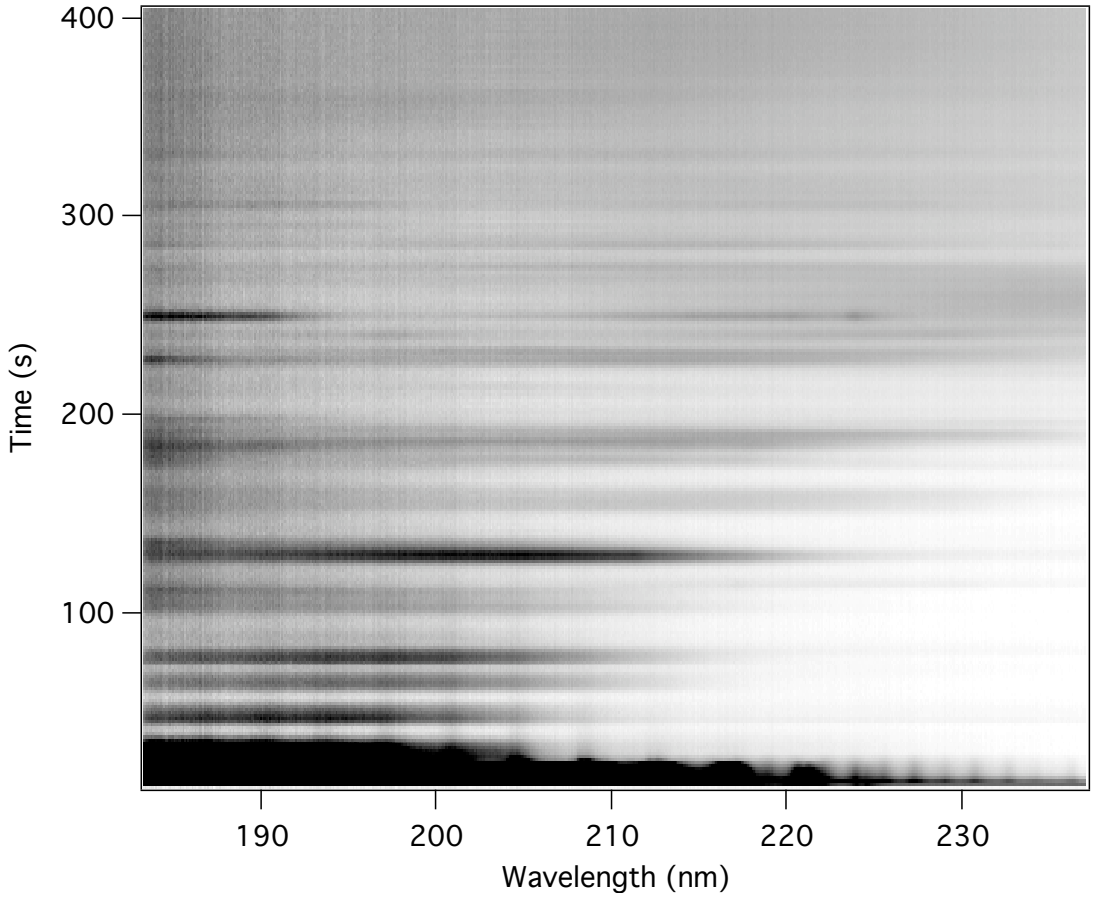

Figure 7.4. 3-D GC-UV chromatogram of tholin pyrolysis products.

Although little information on the gas-phase far ultraviolet spectra of nitriles is available, the broad peaks are consistent with the literature. Nitriles have a relatively weak $\pi \rightarrow \pi^*$ transition at around 200 nm [Robin, 1975].

The most interesting spectrum is that of the compound that elutes at approximately 250 s. The spectrum has a broad peak peaking below 190 nm, and another peak with some vibrational structure around 220 nm. For comparison, the spectrum obtained from the injection of 6-hexenenitrile is shown in Figure 7.9. The qualitative similarity of the two spectra in the region around 220 nm suggests that this peak corresponds to an alkene nitrile (not necessarily 6-hexenenitrile), as seen in the GC-MS data.

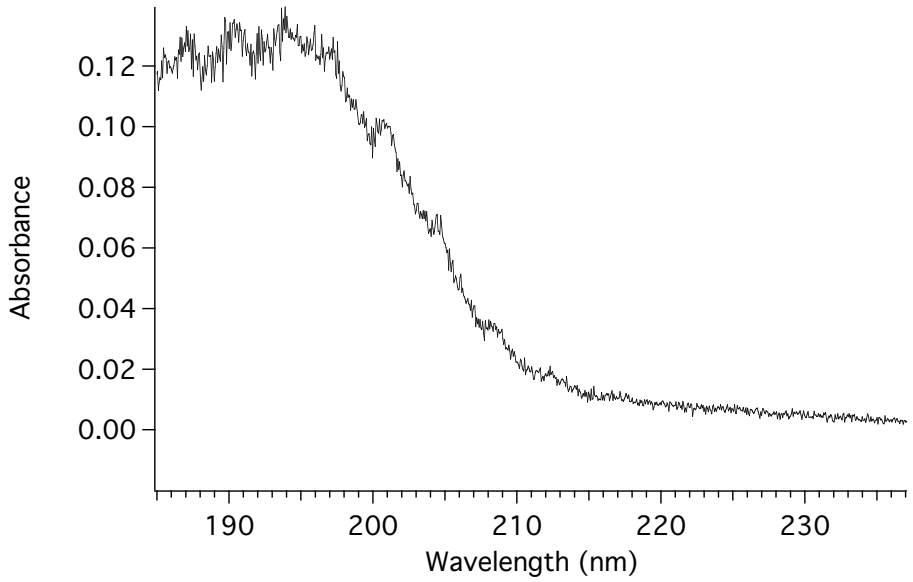

Figure 7.5. Spectrum of the peak eluting at 90 s.

The spectra from some amines and a simple alkyl olefin are shown in Figures 7.8 and 7.10-7.12. Although none of these compounds are seen in the pyrolysis data obtained by GC-MS, their distinctive spectra would enable their identification if present in another complex mixture. Even though no aromatics are seen in these low temperature pyrolytic reaction, high temperature pyrolysis does yield a number of aromatic compounds [Coll*, et al.*, 1998]; [Ehrenfreund*, et al.*, 1994]; [Israel*, et al.*, 1997];

[Pietrogrande*, et al.*, 2001]. These would also be easily distinguished by GC-UV, since they have characteristic vibrational structure in the 230-250 nm region.

7.4. Conclusions

The products of low-temperature pyrolysis of tholins have been analyzed by GC-UV. The spectra obtained with the GC-UV system are consistent with the compounds determined to be present by GC-MS. Low temperature pyrolysis produces mainly alkyl nitriles and dinitriles, with some alkene nitriles. Although amines and aromatics are absent, they would also be identifiable by their ultraviolet spectra.

A GC-UV system would be a useful addition to a probe whose mission is to explore the organic chemistry of other worlds, especially Titan. Such a system could be made small, lightweight and low-power, making it ideal for spaceflight situations. Although it would not provide exact identification of compounds, functional group identification is possible, and since the technique is non-destructive, GC-UV could serve as a backup to a more traditional GC-MS system.

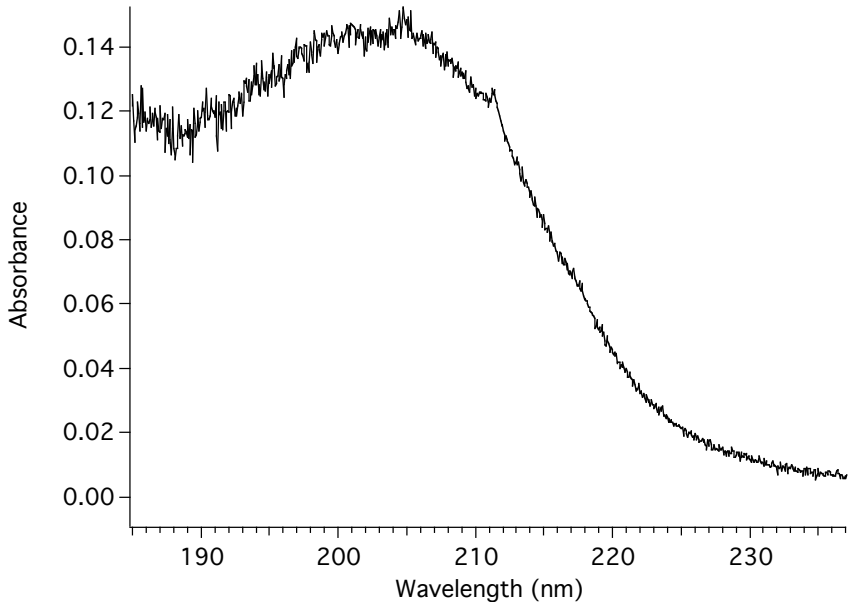

Figure 7.6. Spectrum of the peak eluting at 125 s.

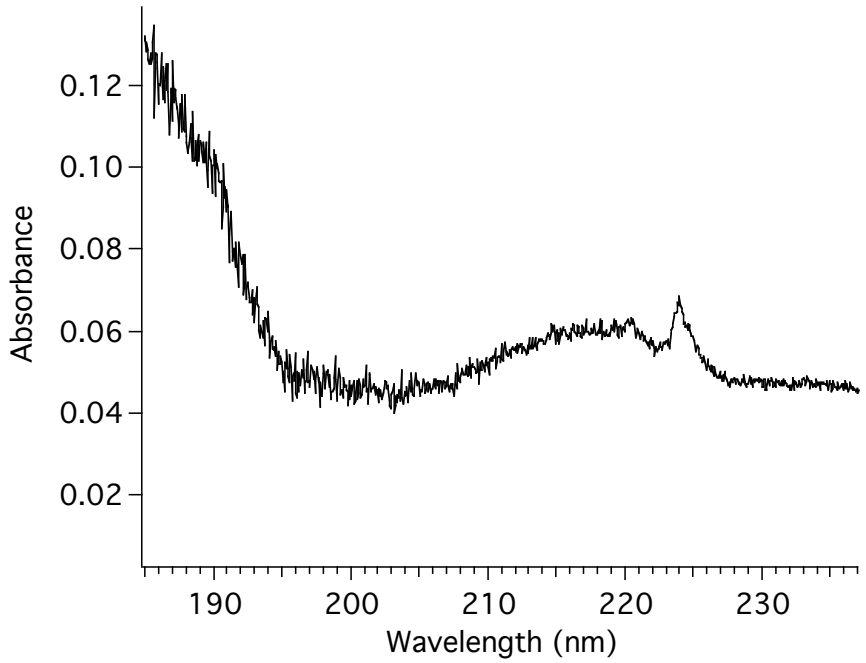

Figure 7.7. Spectrum of the peak eluting at 250 s.

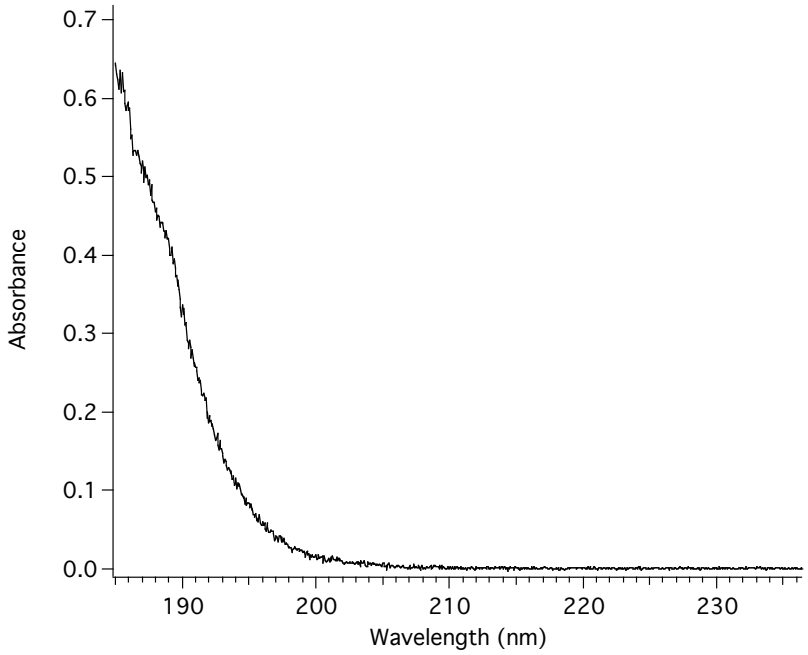

Figure 7.8. Gas-phase ultraviolet spectrum of 1-hexene.

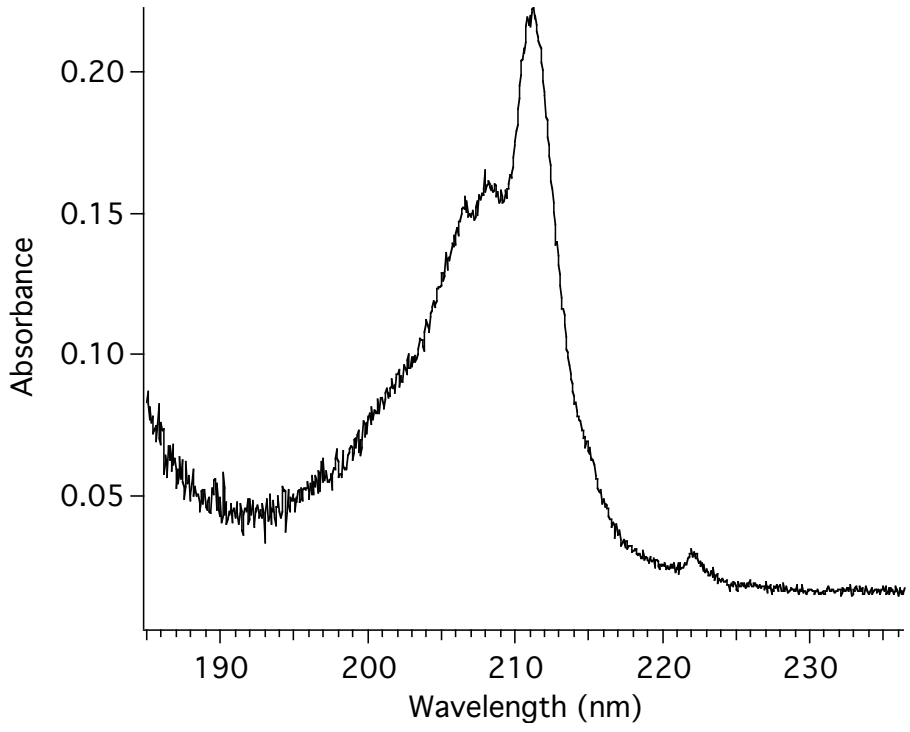

Figure 7.9. Gas-phase ultraviolet spectrum of 5-hexenenitrile.

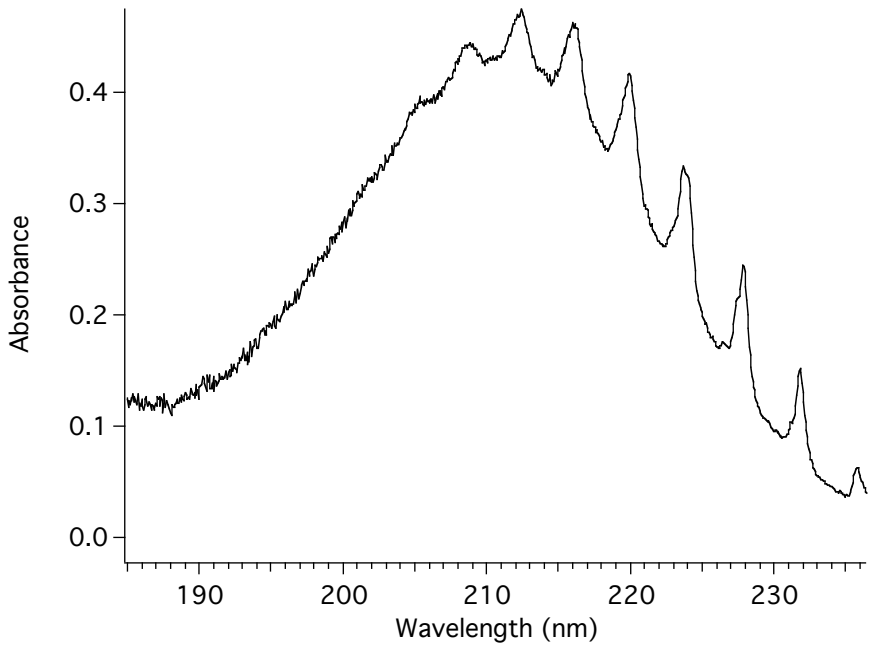

Figure 7.10. Gas-phase ultraviolet spectrum of tert-butylamine.

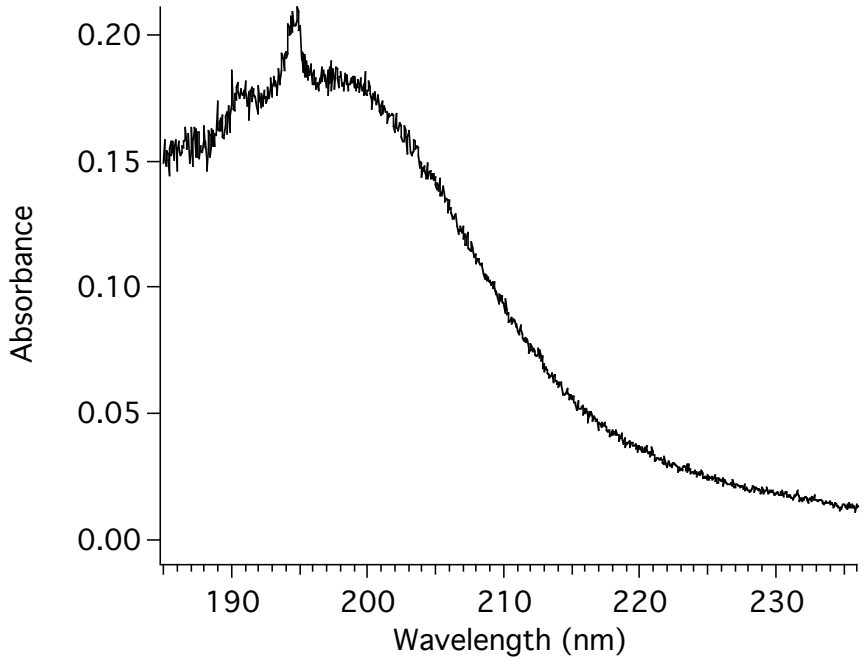

Figure 7.11. Gas-phase ultraviolet spectrum of diethylamine. The peak at 194 nm is due to interference from acetone.

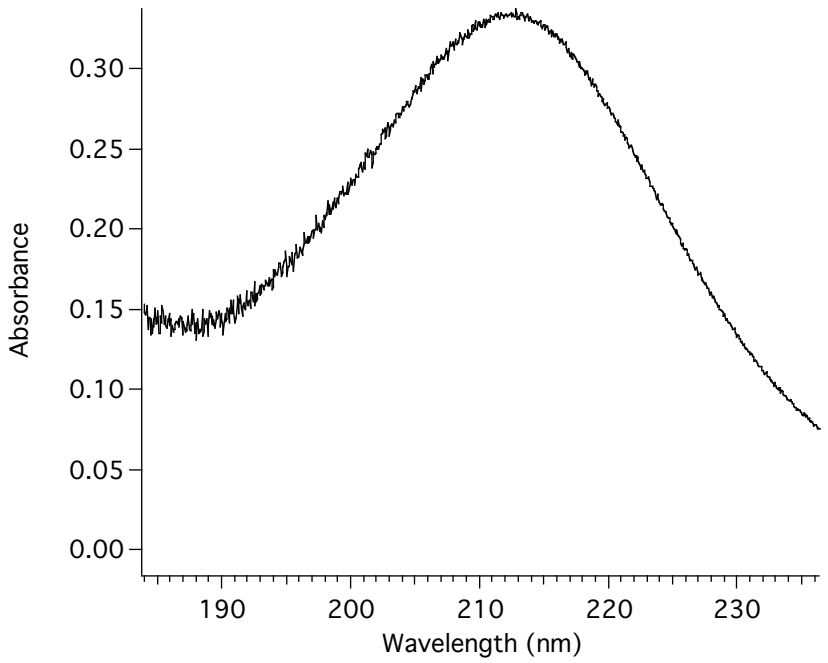

Figure 7.12. Gas-phase ultraviolet spectrum of triethylamine.

7.5. References

Cedron-Fernandez, T., et al. (2002), Separation and determination of volatile compounds in synthetic wine samples by gas chromatography using UV-visible molecular absorption spectrometry as detector, *Talanta*, *57*, 555-563.

Coll, P., et al. (1998), Review and latest results of laboratory investigations of Titan's aerosols, *Origins of Life and Evolution of the Biosphere*, *28*, 195-213.

Ehrenfreund, P., et al. (1994), Analytical Pyrolysis Experiments of Titan Aerosol Analogs in Preparation for the Cassini Huygens Mission, *Life Sciences and Space Research XXV (4)*, *15*, 335-342.

Israel, G., et al. (1997), The Aerosol Collector Pyrolyser (ACP) Experiment for Huygens, in *Huygens: Science, Payload and Mission*, ESA Publications Division, Noordwijk, The Netherlands.

Kaye, W. (1962), Far-Ultraviolet Spectroscopic Detection of Gas Chromatograph Effluent, *Analytical Chemistry*, *34*, 287.

Lagesson, H. V., et al. (2000a), Qualitative determination of compounds adsorbed on indoor dust particles using GC-UV and GC-MS after thermal desorption, *Chromatographia*, *52*, 621-630.

Lagesson, H. V., et al. (2000b), Identification of compounds and specific functional groups in the wavelength region 168-330 nm using gas chromatography with UV detection, *Journal of Chromatography A*, *867*, 187-206.

Linstron, P. J., and W. G. Mallard, eds,. (2005), *NIST Chemistry WebBook, NIST Standard Reference Database Number 69*, National Institute od Standards and Technology, Gaithersburg, MD.

Pietrogrande, M. C., et al. (2001), Analysis of complex mixtures recovered from space missions - Statistical approach to the study of Titan atmosphere analogues (tholins), *Journal of Chromatography A*, *939*, 69-77.

Robin, M. B. (1975), *Higher Excited States of Polyatomic Molecules*, Academic Press, San Francisco.

Chapter 8. Progress towards detectors for the determination of enantiomeric excess

8.1. Introduction

One of the most fascinating questions in prebiotic chemistry is that of the origin of homochirality. All life on Earth is based on the L-amino acids and D-sugars. There is no particular reason for these choices; the combination of the D-amino acids and L-sugars should work just as well. The intriguing facet of this characteristic of life is the idea that life is unlikely to evolve from a racemic mixture of compounds. Homochirality in the amino acids that led to the first peptides and proteins would have been necessary to insure that the polymer would fold into the proper secondary and tertiary conformations to function properly. [Ehrenfreund, et al., 2004]

There have been many theories as to how homochirality could have developed prior to the origin of life. [Podlech, 2001]; [Siegel, 1998] The most likely candidates seem to be some form of amplification of an initial small excess, or the action of polarized light to selectively destroy one enantiomer over the other. [Avalos, *et al.*, 2000] Of course, the actual events that led to homochirality on Earth are impossible to determine. As well, experiments that replicate prebiotic conditions are impractical, given the large volumes and long timescales that would be necessary. As discussed in Chapter 2, these experiments have probably been performed on Titan naturally over the course of millions of years. Examination of the frozen melt pools of Titan, paying special attention

to the enantiomeric excess of any chiral compounds, could provide valuable insights into the origin of homochirality and the origin of life.

There are a great variety of methods for the determination of enantiomeric excess [Schreier*, et al.*, 1995], but few are suitable for spaceflight applications. Polarimetric methods are not very sensitive. NMR techniques require the bulk of an NMR magnet. The most developed of the chiral separation techniques, gas chromatography, is suitable for spaceflight, but unsuitable for the analysis of complex mixtures, such as would be found on Titan. While GC-MS with a chiral column would separate the components of a complex mixture as well as separate any chiral compounds that are present, the resulting chromatogram will likely be too complex to be easily interpretable.

A different approach to this problem is outlined below. Instead of a chiral column, the gas chromatograph is equipped with a standard, non-chiral column. Two detectors are used. The second detector is a standard mass spectrometer detector to enable identification of the compounds. Prior to the mass spectrometer is an enantiomeric excess detector. Such a detector would be nondestructive, and would signal when an enantiomeric excess is detected. Racemic chiral compounds passing through the detector would not result in a signal.

This chapter describes an approach to the development of a detector for the determination of enantiomeric excess. The sensor is composed of two quartz crystal microbalances (QCMs). [Lu and Czanderna, 1984] A QCM is a thin plate of quartz, with a metal electrode plated on each side. When placed in the proper circuit, the QCM resonates at a specific frequency proportional to its mass. The relationship between frequency and mass is given in equation (8.1), where Δf(Hz) is the change in frequency, f

is the fundamental frequency of the crystal, d_q is the density of quartz (2.65 g cm^{-3}), N is the frequency constant for an AT-cut crystal (1.670 x 10^5 cm Hz), Δm (g cm^{-2}) is the added mass per unit area, and m (g cm^{-2}) is the mass per unit area of quartz [Edmonds, 1988]. In order to create a chemical sensor, the QCM is coated with an absorbent film (either selective or non-selective). When the coated QCM is exposed to analyte, the film absorb some of the analyte, the mass of the device increases, and the frequency drops. QCMs are capable of mass resolution in the nanogram range.

$$\Delta f = - \{f^2 / d_q N\} \{\Delta m / [1 + \Delta m / m]\} \quad (8.1)$$

To function as enantiomeric excess detector, one crystal is coated with an enantiomeric film that selectively adsorbs one enantiomer of an analyte in greater quantity than the other. The other crystal is coated with a film of the opposite enantiomer. The output of the two crystal oscillators is subtracted, and this final frequency is monitored. In this configuration, the difference frequency is a direct measure of the enantiomeric excess.

Enantiomerically selective QCMs have been developed by a number of other groups, although mainly for use in liquids, not gases. Bodenhoffer described a sensor based on the chiral GC phase Chirasil-Val that was able to distinguish between the enantiomers of methyl lactate and certain amino acid derivatives. [Bodenhofer*, et al.*, 1997a]; [Bodenhofer*, et al.*, 1997b] However, a dual QCM sensor that utilizes a pair of enantiomeric sensors was not developed.

We describe progress in the development of the kind of sensor described above. The gold electrode of the QCM is coated with a self-assembled monolayer that is derivatized with a chiral selector. The response of the sensor to the enantiomers of methyl lactate is presented. As well, we also present data for a similar piezoelectric sensor system based on a monolayer derivatized surface acoustic wave (SAW) device. SAW sensors are similar to QCMs in that both are piezoelectric mass sensors [Edmonds, 1988], but SAWs are several orders of magnitude more sensitive, smaller and would result in an improved sensor system.

8.2. Experimental

A block diagram of the QCM apparatus is shown in Figure 8.1. Two 15 MHz quartz crystal microbalances (International Crystal Manufacturing, Oklahoma City, OK) are held in an aluminum cell with an internal volume of approximately 10 mL. Analyte vapor is delivered to the cell with a Model 1010 Precision Gas Diluter (Custom Sensor Solutions, Inc., Oro Valley, AZ). Stock vapor samples were prepared in Tedlar bags for delivery to the diluter. The dilution gas used was nitrogen. Each crystal was connected to a lab-built Colpitts oscillator. The circuit diagram for the oscillators is shown in Figure 2. The output of both oscillators is fed to an SLB-1 frequency mixer (Mini-Circuits, Inc., Brooklyn, NY), and its output is fed to an Agilent 53131A frequency counter. The difference frequency determined by the counter is recorded once each second using custom software written with Labview (National Instruments, Austin , TX).

Experiments with SAW devices utilized a commercial dual crystal SAW sensor system obtained from Microsensor Systems, Inc. (Bowling Green, KY). The system

integrates two 250 MHz SAWs in a small brass chamber directly mounted on a circuit board. The circuitry oscillates both SAWs and outputs their difference frequency. Analyte vapor was delivered to the SAWs using the gas dilution system described above.

The following procedure was used to apply a monolayer on the surface of the gold electrode of the QCM (Scheme 8.1). The QCM was cleaned by applying a drop of piranha solution (3:1 concentrated H_2SO_4: 30% H_2O_2) to each side for 1 minute, followed by a thorough rinse with deionized water. (Caution! Piranha solution is a strong oxidizer and extremely corrosive, and can react violently with organics. Use with care.) The QCM was then immersed in a 5 mM solution of 16-mercaptohexadecanoic acid in methanol for 2 hours. A decanethiol monolayer was applied to some crystals by using a 5 mM solution of decanethiol.

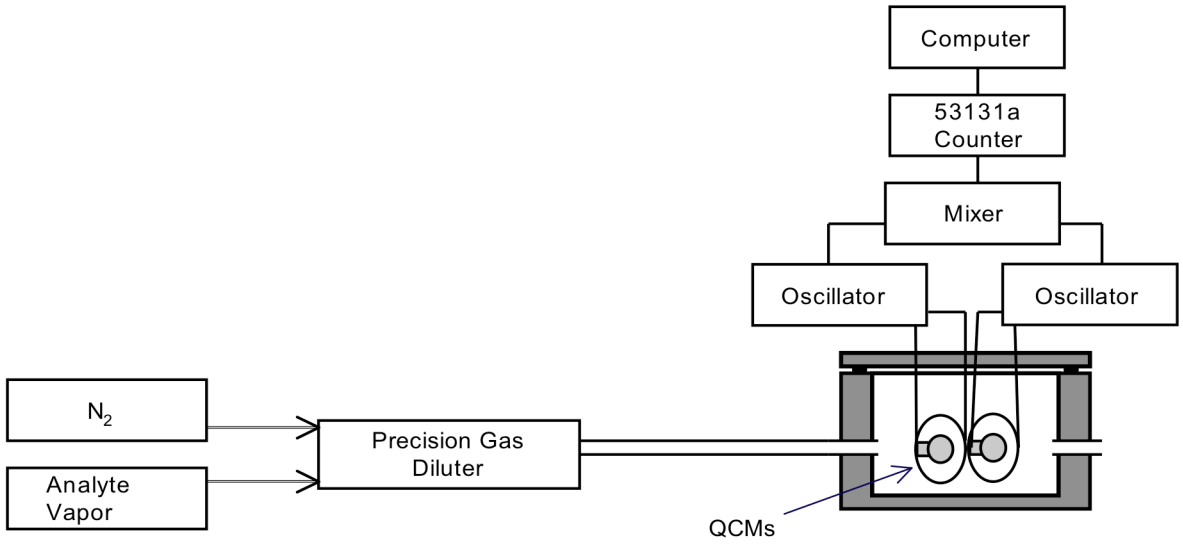

Figure 8.1. Block diagram of the QCM apparatus.

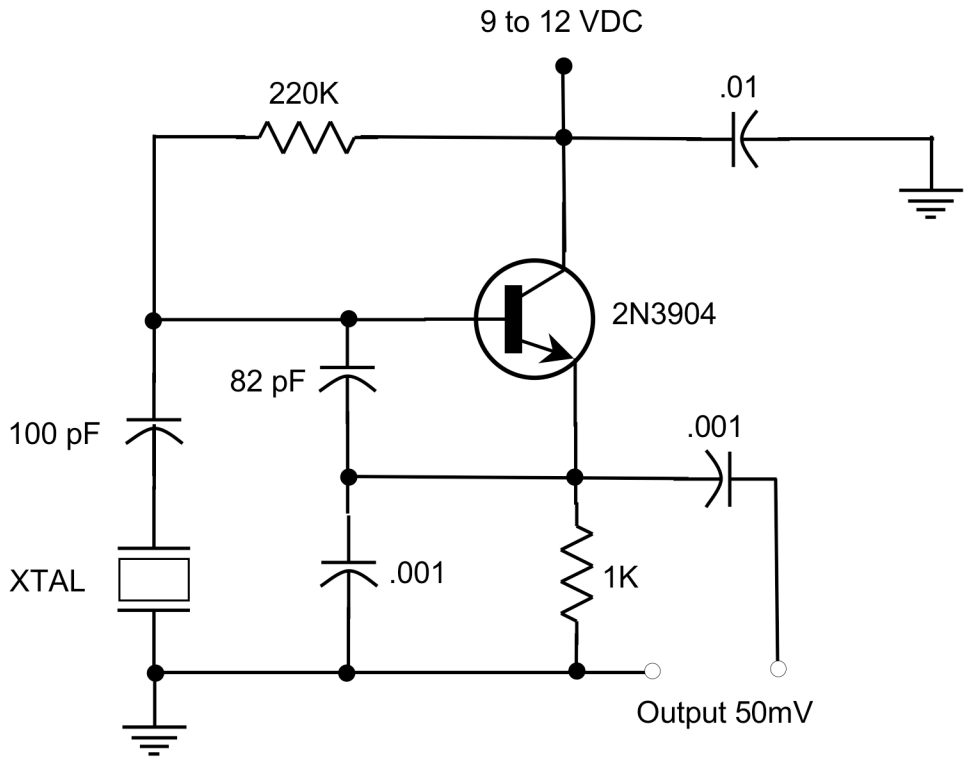

Figure 8.2. Colpitts oscillator used to drive the QCMs.

The crystal is then rinsed with methanol, and immersed in a solution of L-valine-tert-butylamide, triethylamine, and dicyclohexylcarbodiimide in dichloromethane for 12 hours. The synthetic procedure is illustrated in Scheme 8.1.

SAW devices require a different derivatization strategy, illustrated in Scheme 8.2, since the surface to be derivatized is quartz, rather than gold. The SAW device is cleaned with piranha solution for 2 minutes, then rinsed with water and dried under a stream of nitrogen. The SAW is then placed in a 10% solution of (3-aminopropyl)triethoxysilane for 6 hours. The SAW is rinsed with actone, and then placed in a solution of 19.6 mg 1-(3-dimethylaminopropyl)-3-ethylcarbodiimide hydrochloride (EDC), 32.8 mg N-

hydroxysuccinimide (NHS), and 31.2 mg (R)-(3,5-dinitrobenzoyl-α-phenylglycine) in 10 mL of water for 1 hour. The SAW is rinsed with water and dried under a stream of nitrogen.

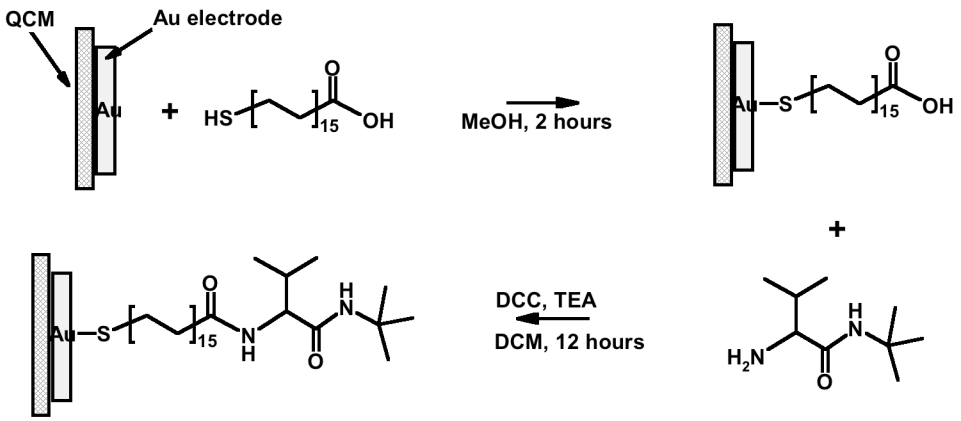

Scheme 8.1. Synthesis of an L-valine-tert-butylamide monolayer on a QCM electrode.

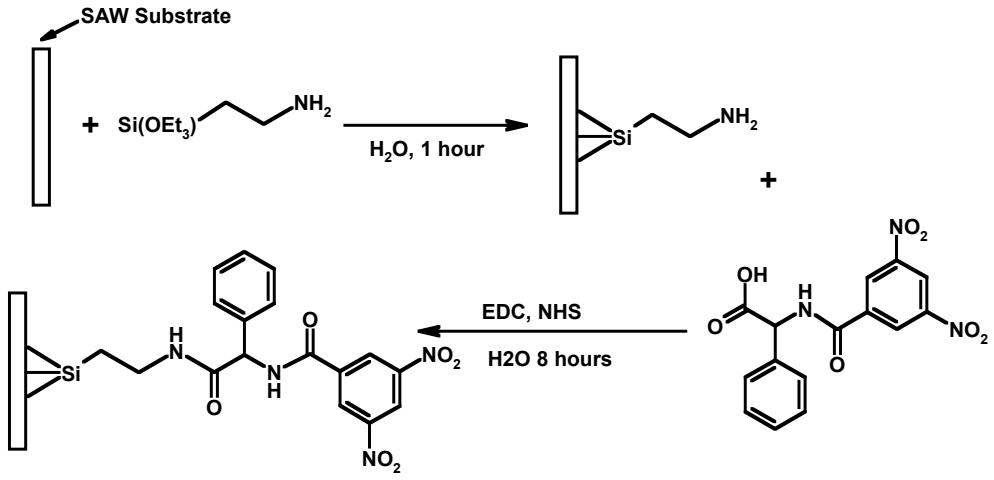

Scheme 8.2. Synthesis of an N-[(3,5-dinitrobenzoyl)phenyl]glycine monolayer on a SAW substrate.

8.3. Results and discussion

Figure 8.3 is a graph of the change in difference frequency of the crystal pair on exposure to each enantiomer of methyl lactate vapor, at several different concentrations. In this experiment, a crystal with an L-valine tert-butyl amide derivatized monolayer was paired with a decanethiol monolayer crystal. This allows for non-specific interactions, and the effects of temperature variations, to be canceled out. The response to the S enantiomer of methyl lactate is greater than the response to the R enantiomer. Valine tert-butyl amide was chosen as the chiral selector because its efficacy has been proven through its use in the popular GC stationary phase Chirasil-Val.

Experiments in which one crystal was derivatized with L-valine-tert-butylamide, and the other D-valine-tert-butyl amide yielded inconsistent results. This is likely due to difficulties in creating monolayers of the different enantiomers that are sufficiently identical to yield the proper differential response. More consistent monolayers could be created by preparing a chiral selector that incorporates a thiol moiety. The chiral monolayer would then be prepared in a single step, and the difficulties that arise from multiple reaction steps on monolayers could be avoided.

Figure 8.4 is graph of the change in difference frequency for the SAW sensor pair. One SAW is coated with a derivatized monolayer of N-[(3,5-dinitrobenzoyl)phenyl]glycine, and the other SAW is left uncoated, to serve as a reference. While enatioselectivity was not observed, we can see the much greater sensitivity of the SAW sensors. A 16 ppm exposure results in a 450 Hz frequency shift on the SAW, while a similar exposure of the QCM sensor results in a 3 Hz shift.

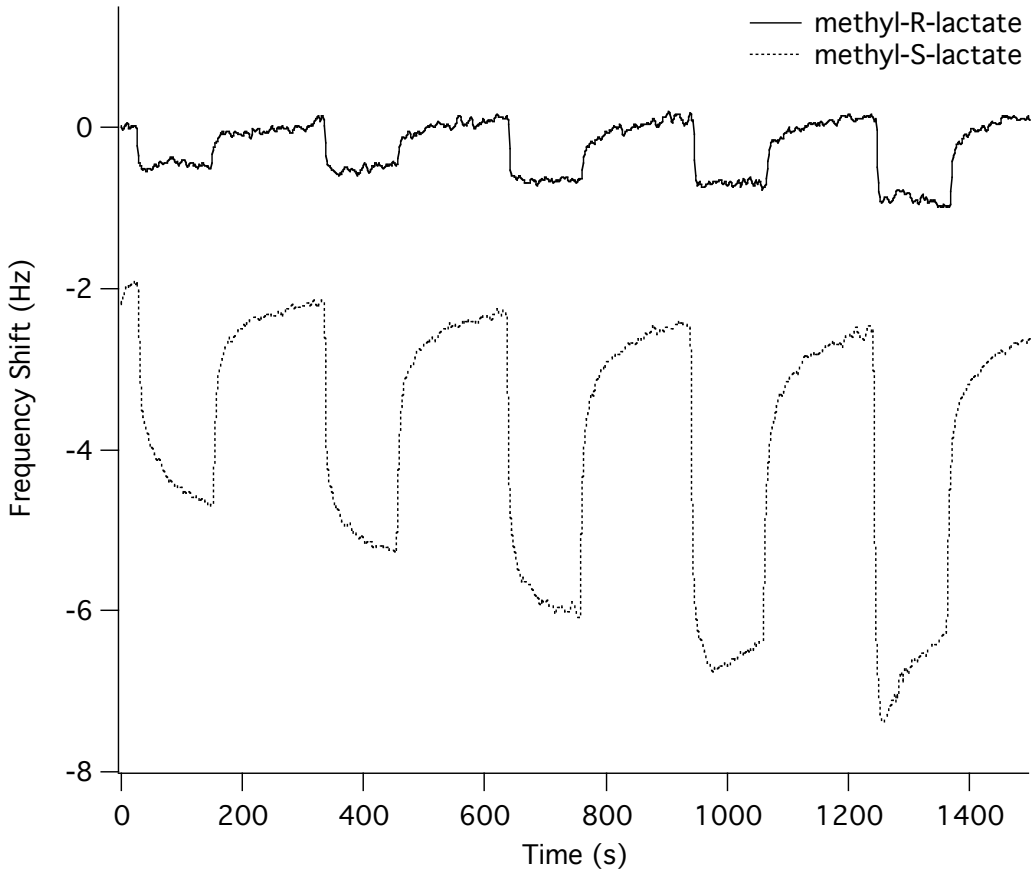

Figure 8.3. Responce of the QCM sensor to methyl lactate vapor. Concentrations are 16, 32, 64, 128, and 256 ppm, in that order.

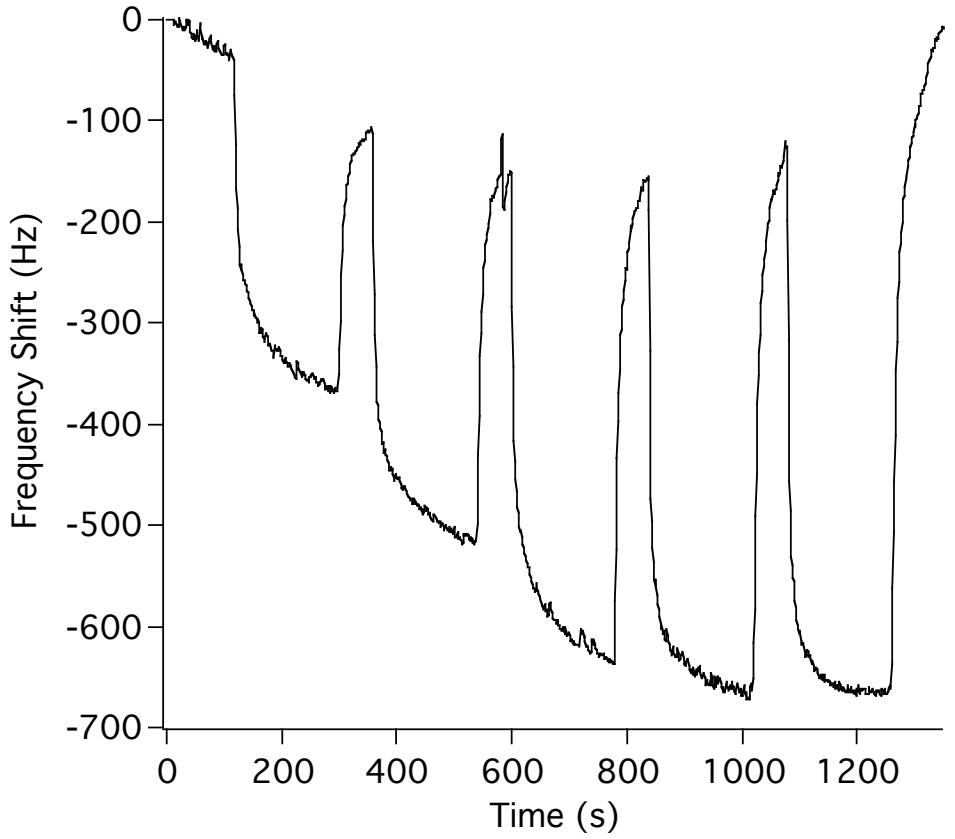

Figure 8.4. Response of a N-[(3,5-dinitrobenzoyl)phenyl]glycine derivatized SAW sensor to R-methyl lactate vapor. Concentrations are 3.9, 7.8, 11.7, 15.6 and 19.5 ppm.

8.4. Conclusions

Enantiomerically derivatized monolayers on the electrodes of a quartz crystal microbalance are capable of distinguishing between the enantiomers of methyl lactate. The sensor utilizes an L-valine tert-butyl amide selector. Unfortunately, the synthesis of the monolayer on the QCM electrode is too inconsistent to allow the construction of a sensor composed of two enantiomeric QCMs. Such a sensor would allow for the direct determination of enantiomeric excess.

This work represents progress towards the development of such a sensor. In its final incarnation, surface acoustic wave sensors, instead of QCMs may be used. The greater sensitivity of these devices (as shown here) would allow for more precise determination of enantiomeric excess, and the analysis of smaller quantities of material.

8.5. References

Avalos, M., et al. (2000), From parity to chirality: chemical implications revisited, *Tetrahedron-Asymmetry*, *11*, 2845-2874.

Bodenhofer, K., et al. (1997a), Chiral discrimination in the gas phase using different transducers: Thickness shear mode resonators and reflectometric interference spectroscopy, *Analytical Chemistry*, *69*, 3058-3068.

Bodenhofer, K., et al. (1997b), Chiral discrimination using piezoelectric and optical gas sensors, *Nature*, *387*, 577-580.

Edmonds, T. E., ed. (1988), *Chemical Sensors*, Blackie and Son: New York, NY.

Ehrenfreund, P., et al., eds. (2004), *Astrobiology: Future Perspectives*, Kluwer Academic Publishers: Boston.

Lu, C., and A. W. Czanderna, eds. (1984), *Applications of Piezoelectric Quartz Crystal Microbalances*, Elsevier: New York.

Podlech, J. (2001), Origin of organic molecules and biomolecular homochirality, *Cellular and Molecular Life Sciences*, *58*, 44-60.

Schreier, P., et al. (1995), *Analysis of Chiral Organic Molecules*, Walter de Gruyter: New York.

Siegel, J. S. (1998), Homochiral imperative of molecular evolution, *Chirality*, *10*, 24-27.

Appendix A. Multi-Dimensional Detection of Nitro-Organic Explosives by Gas Chromatography-Pyrolysis-Ultraviolet Detection (GC-PUD)

A.1. Abstract

We describe a new methodology for the trace detection of organic explosives containing nitro functionalities. Conventional gas chromatography separates the components of an explosive mixture. Effluent from the gas chromatograph is pyrolyzed by passage over a heated nichrome wire. Nitric oxide produced on pyrolysis of a nitro-organic compound is then detected by ultraviolet absorption spectroscopy between 180 and 240 nm, using a deuterium lamp as the light source. Nitric oxide exhibits a sharply banded, characteristic spectrum in this region, enabling detection of nitro-organics. The system is tested using the explosive simulants nitrobenzene and 2,4-dinitrotoluene, and with the nitramine explosive tetryl. Detection limits are 25 ng for nitrobenzene, and 50 ng for 2,4-dinitrotoluene. Tetryl is detected with a detection limit of 50 ng. The system is both easy to implement and could be built as a compact, low power device.

A.2. Introduction

Explosives detection is an urgently needed capability that is now at the forefront of many research efforts. An ideal explosives detection system would be reliable, simple and provide an unambiguous signal when explosives are detected. We report here a new methodology for the detection of nitro-organic explosives based on the ultraviolet

detection of NO produced in the thermal decomposition of explosive compounds separated by gas chromatography.

Trace explosives detection methodologies commonly make use of the fragmentation of the target molecules (with the notable exception of ion mobility spectrometry systems[1]), followed by sensitive detection of the released gaseous products. Since many explosive compounds are based on nitro-organics, NO is a common product of decomposition, and a good target for sensitive detection. Both Steinfeld[2] and Moore[3] have recently reviewed the wide variety of techniques used to detect explosives. NO has been detected as the product of thermal decomposition of nitro-organics by IR spectroscopy, microwave spectroscopy, and fluorescence. A number of non-optical techniques, such as mass spectrometry, have also been used.

One of the more successful techniques to detect NO is the use of chemiluminescence. The EGIS system, manufactured by Thermo Electron Corporation, utilizes this type of detector[4]. The chemiluminescence detector, also known as a thermal energy analyzer[5], operates by pyrolyzing the sample in a catalytic reactor to release NO. The NO is subsequently reacted with ozone to produce excited NO_2 which emits infrared radiation that is detected with a photomultiplier. The EGIS system is selective for nitro-organics and is highly sensitive, able to respond to a few picograms of analyte.

The coupling of gas phase ultraviolet absorption with gas chromatography has been practiced sporadically for the past 40 years. Kaye reported the first GC-UV system in 1962[6], which used ultraviolet absorption at 170 nm for the analysis of a chromatographic separation of gasoline. GC-UV systems have since been used for the analysis of wine[7], indoor dust[8], and proposed as a means for functional group analysis[9].

The nitro-organic explosives possess strong absorptions in the UV[10,11,12], and their direct detection by GC-UV is possible. However, the spectra are broad and featureless, and overlap with the absorptions of many other organic compounds. The ultraviolet absorption spectra of the nitro-organic explosives themselves cannot provide unambiguous detection of explosives in the presence of other organics.

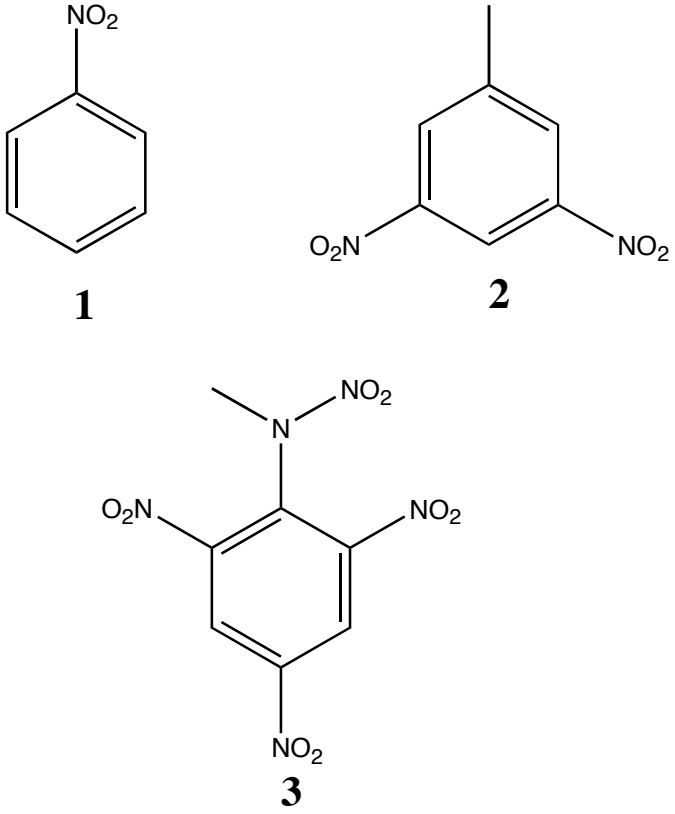

1 **2** **3**

Scheme A.1. Nitrobenzene (**1**), 2,4-dinitrotoluene (**2**), and tetryl (**3**).

The multidimensional[13] technique employed here, gas chromatography-pyrolysis-ultraviolet detection (GC-PUD), overcomes this limitation. After separation by gas chromatography, explosive vapors are pyrolysed on a heated nichrome wire. NO produced in the pyrolysis is subsequently detected by ultraviolet spectroscopy. Explosive simulants nitrobenzene and 2, 4-dinitrotoluene, as well as the explosive tetryl, all yield detectable NO on pyrolysis (Scheme A.1). Linearity of response and sensitivity are good,

with a limit of detection of ~50 ng for tetryl. GC-PUD is technically simple, and provides a clear signal for the presence of explosives.

A.3. Experimental

A block diagram of the experimental apparatus is shown in Figure A.1. The gas chromatograph (SRI Model 8610C) is connected to the pyrolysis tube via a heated stainless steel transfer line, usually held at 250 °C. The homemade pyrolysis tube is comprised of a Kimax glass envelope, ~5 mm in diameter, inside of which is a coil of nichrome wire. The tube is sealed using a high temperature ceramic putty. A current of 2-2.5 A is passed through the coil, heating it to a temperature of 900-1200 °C. The temperature was measured with a Micro-Optical Pyrometer, Pyrometer Instrument Co., Inc., Bergenfield, NJ. The gaseous products from pyrolysis flow to a heated absorption cell. The cell consists of two aluminum blocks supporting a quartz tube (3 mm OD) between them, with silica windows on either side. The tube serves as both a light pipe and a conduit for the pyrolysis products. The cell has a pathlength of ~6 cm, and is typically heated to 150 °C. Residence time in the cell is approximately 3 s, so no peak broadening due to the cell is expected.

The light from a 30 W deuterium lamp (Oriel 63163) is coupled into the cell using silica lenses. Unfocused light exiting the cell is directed into a Chromex 250is imaging spectrograph equipped with an Apex SPH-5 CCD detector. The resolution of the system is approximately 0.5 nm. The entire optical path, including the spectrometer, is purged with nitrogen to allow operation below 200 nm. Spectra from 180-240 nm are acquired approximately every 1.5 seconds, with an integration time of 1 s.

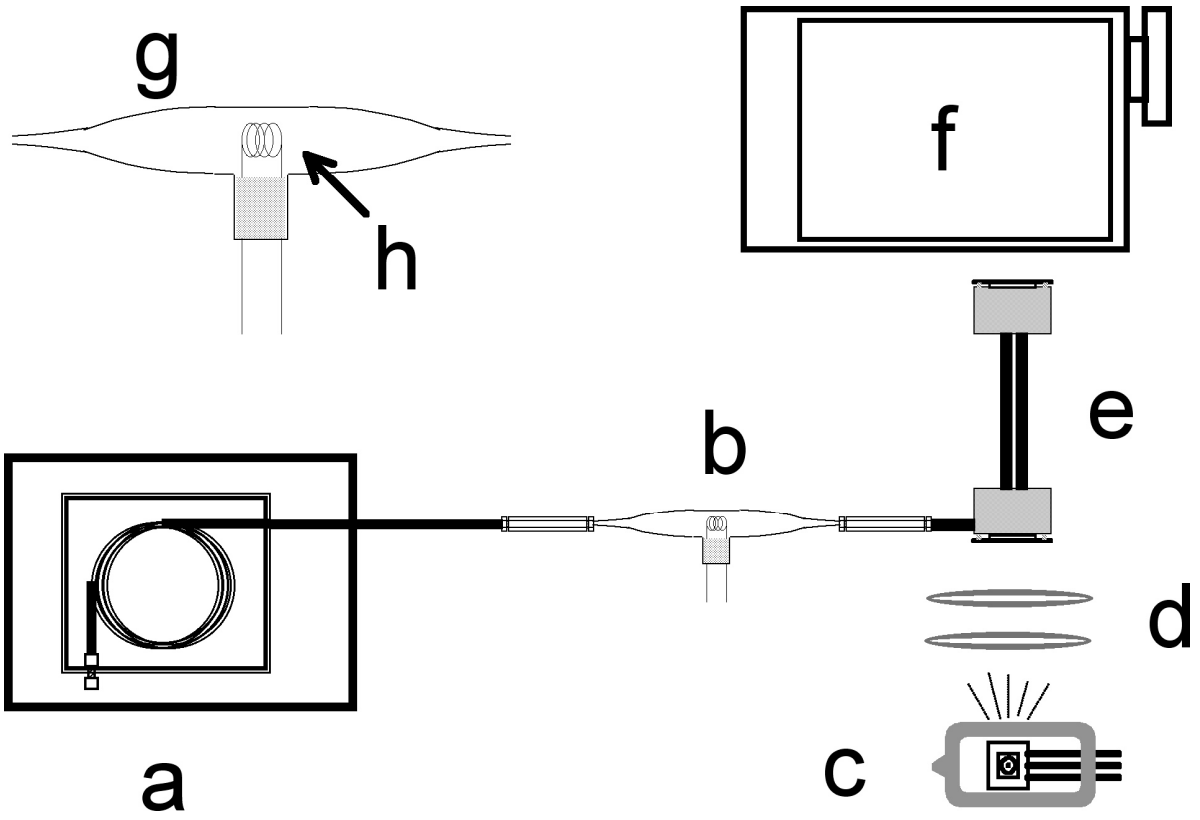

Figure A.1. Block diagram of GC-PUD system. a) SRI 8610C gas chromatograph. b) pyrolyzer tube. c) D_2 lamp. d) silica lenses. e) ultraviolet absorption cell. f) Chromex 250 is/sm spectrometer. Inset shows details of the pyrolyzer. g) Kimax evelope. h) Nichrome coil.

The gas chromatograph uses a 100% methyl polysiloxane column (MXT-1 15m × 0.53mm × 5μm film) with on-column injection. For nitrobenzene and 2,4-dinitrobenzene, the temperature of the GC oven was ramped from 50 °C to 250 °C at 15 °C/min. The temperature program for tetryl was as follows: 100 °C for 2 minutes, then ramped at 10 °C/min to 200 °C, then ramped at 20 °C/min to 250°C, and held for 5 minutes. Helium was used as the carrier gas with a source pressure of 5 psig.

Nitrobenzene and 2, 4-dinitrobenzene (Aldrich) are used without further purification. Acetonitrile was obtained from EM Science. Tetryl was acquired as a 1mg/mL solution in acetonitrile from Supelco.

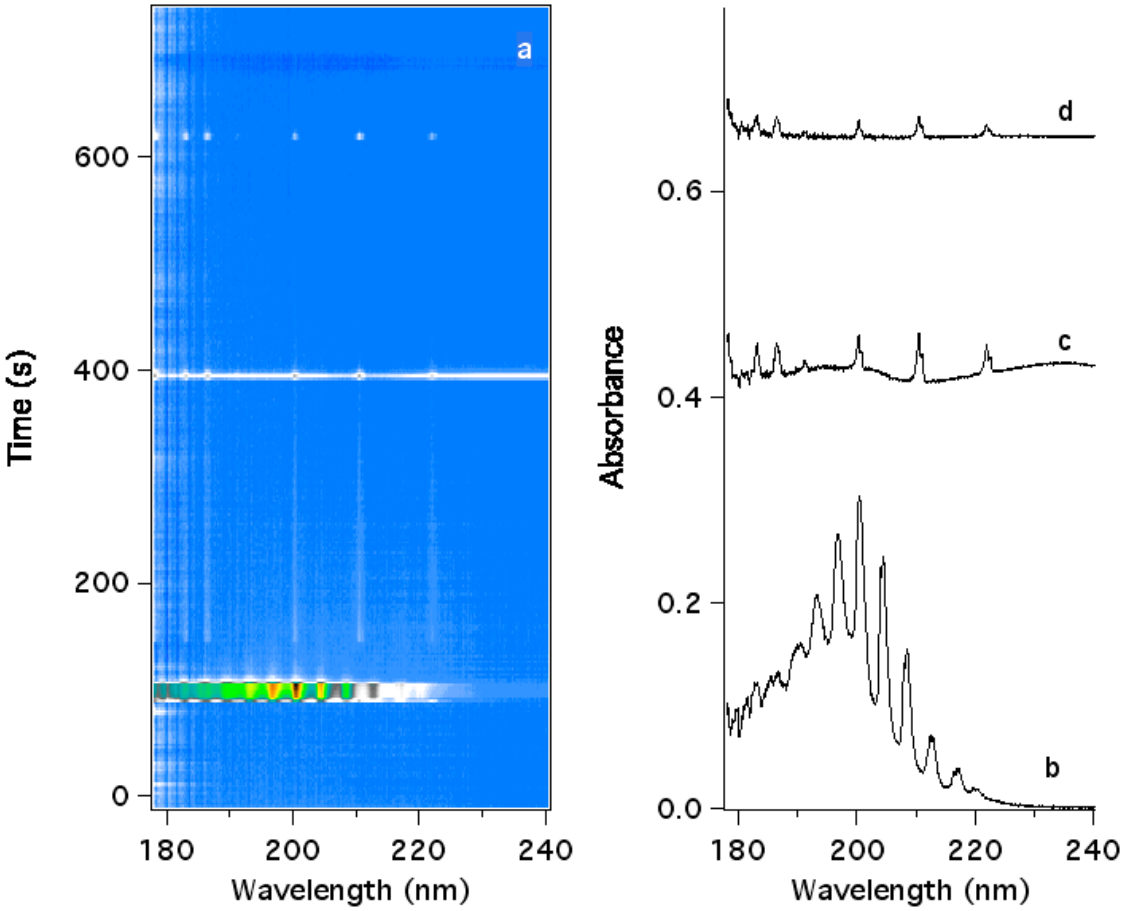

Figure A.2. a) 3-D GC-PUD chromatogram 500 ng each of nitrobenzene (elutes at 395 s) and 2, 4-dinitrotoluene (620 s). Acetonitrile elutes at 100 s. b) Ultraviolet spectrum obtained at 100 s, showing ammonia formed on the pyrolysis of acetonitrile. c) Ultraviolet spectrum obtained at 395 s, showing NO formed on the pyrolysis of nitrobenzene. d) Ultraviolet spectrum obtained at 620 s, showing NO formed on the pyrolysis of 2, 4-dinitrotoluene. Spectra b, c, and d have the same scale and have been shifted vertically for clarity.

A.4. Results and discussion

Figure A.2a shows a representative 3-D chromatogram of 500 ng each of nitrobenzene (NB) and 2,4-dinitrotoluene (2,4-DNT) obtained by GC-PUD. The sample was injected as 1 μL of a 1 mg/mL solution of NB and 2,4-DNT in acetonitrile. Clear signals are visible due to acetonitrile, NB, and 2,4-DNT at retention times of 100 s, 395 s, and 620 s, respectively. Figures A.2b, c, and d show horizontal slices through the chromatogram at these retention times. The spectrum shown in Figure A.2b is identical to that of ammonia, indicating that ammonia is a product of the pyrolysis of acetonitrile. The spectra in Figures A.2c and A.2d match the spectrum of NO^{14}, indicating that NO is produced by the pyrolysis of NB and 2,4-DNT.

Figure A.3 shows the relationship between peak area and the mass of analyte injected into the gas chromatograph for NB, 2,4-DNT and tetryl. Peak areas were determined by taking a vertical slice through the 3-D chromatogram at the maximum of the 215 nm band of NO. This generates a chromatogram equivalent to an experiment where one monitors the absorbance of the eluent at 215 nm only. The 215 nm band was chosen because it has the largest absorbance in our experiment. The area of the peak representing the eluted compound was then determined for several injections of different masses of each compound.

The peak areas for all three analytes tested are linear with mass below approximately 5 micrograms. At higher concentrations, NB and 2,4-DNT showed a small negative deviation from linearity. The slope of the curves for NB and 2,4-DNT are essentially identical, while the slope for tetryl is significantly greater. The correspondence between the slopes of NB and 2,4-DNT shows that the number of nitro

groups on the molecule is not related to the amount of NO generated by pyrolysis in our system. The steeper slope of the curve for tetryl may be due to the presence of both nitro and nitramine functionalities in this compound, altering its pyrolysis behaviour. Limits of detection (LOD), determined as three times the noise, were 50 ng for tetryl and 2,4-DNT, and 25 ng for nitrobenzene.

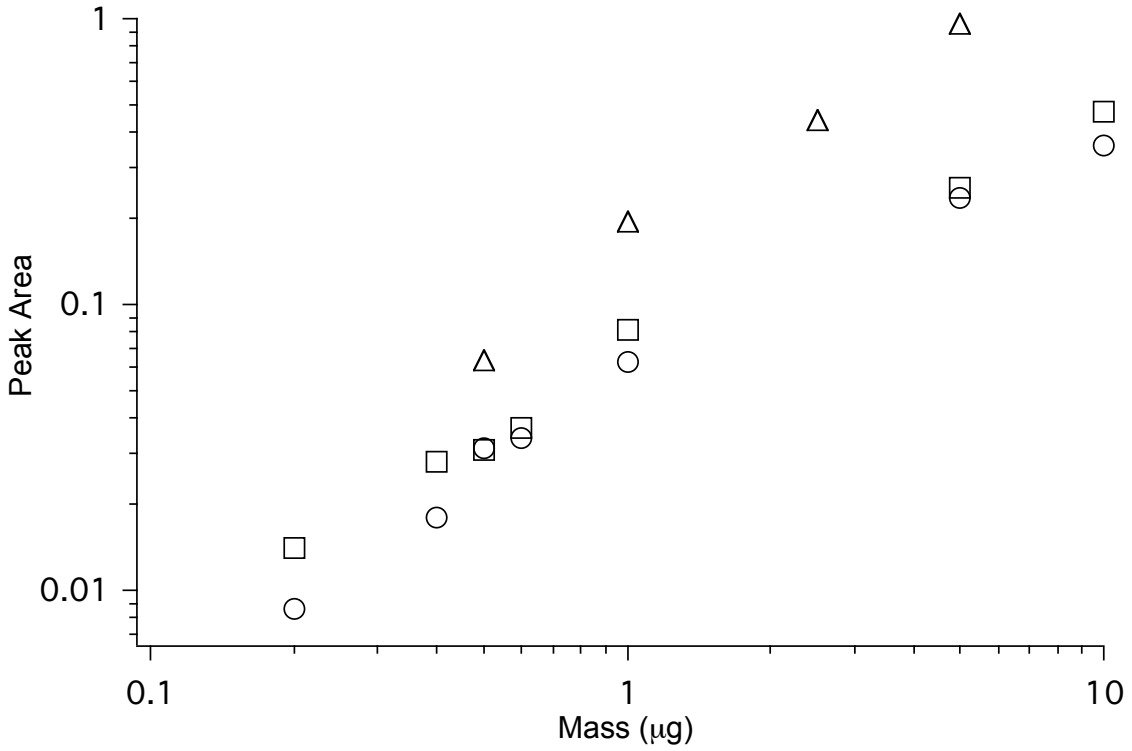

Figure A.3. Peak area vs. mass of analyte injected for NB (circles), 2,4-DNT (squares) and tetryl (triangles). Note the log scale.

Two major factors contribute to the observed LODs. The most important issue is the efficiency of the pyrolyzer. The current delivered to the pyrolyzer, and thus its temperature, is set by increasing the temperature until no absorbance due to the analyte remains, and only NO absorbance is observed. This was found to occur at temperatures between 900 °C and 1200 °C, depending on the amount of analyte injected. These

temperatures are much higher than those required for pyrolysis of most nitroarenes[15]. This suggests that much of the analyte is not passing close enough to the nichrome wire to be pyrolyzed, necessitating a high temperature in order to completely pyrolyze the analyte.

A second issue is that of peak width in the chromatogram. Since the detector is measuring the instantaneous concentration of NO in the cell, broad peaks will lead to less signal than narrow peaks, even though the total amount of analyte in each peak is the same. This accounts for the lower LOD for nitrobenzene, which elutes early and has a rather narrow peak, compared to 2,4-DNT, which exhibits a broader peak under these chromatographic conditions.

Organic compounds containing both nitrogen and oxygen, such as amides, will also produce NO on pyrolysis, leading to possible interferences. These interferences can be reduced by the use of sampling techniques that pre-select for explosives, or by using a catalytic pyrolyzer[5], as is used in the EGIS system. The catalytic pyrolyzer operates at much lower temperatures (275 °C), and produces NO only from nitro-organic compounds.

A.5. Conclusions

We have developed a system, gas chromatography-pyrolysis-ultraviolet detection, for the selective detection of nitro-organic explosives in the presence of other organics. After separation by gas chromatography, explosive compounds are pyrolyzed by passage over a hot wire, and the resulting NO is detected by its characteristic ultraviolet absorption spectrum. Nitrobenzene, 2,4-dinitrotoluene and tetryl are all detected with a

linear response, and limits of detection of 25 ng for nitrobenzene, and 50 ng for tetryl and 2,4-dinitrotoluene.

The GC-PUD system is technically simple and provides a clear signal of the presence of nitro-organics. While the current detection limits are not sufficient for the detection of common real-world samples, optimization of the system would provide the necessary sub-nanogram to picogram sensitivity. Increases in sensitivity could be achieved by using a multi-pass cell, a more sensitive UV spectrometer, and by improving the efficiency of the pyrolyzer. The use of fast GC techniques[16] would improve the speed of the analysis.

Other diagnostic pyrolytic reactions may exist that can be probed with this technique. For instance, the production of ammonia from acetonitrile on pyrolysis suggests that all nitriles may form ammonia when pyrolyzed. The study of the pyrolysis products from a wide variety of compounds would enable the GC-PUD technique to be used for the functional group analysis of complex mixtures.

A.6. Acknowledgements

We gratefully recognize the support of the Director's Research and Development Fund at the Jet Propulsion Laboratory.

A.7 References

[1] Eiceman, G.A.; Karpas, Z. *Ion Mobility Spectrometry;* CRC Press: Ann Arbor, 1994.

[2] Steinfeld, J.I.; Wormhoudt, J.; *Annu. Rev. Phys. Chem.* **1998**, *49*, 203-232.

[3] Moore, D.S.; *Rev. Sci. Instr.* **2004**, *75*, 2499-2512.

[4] Fine, D.H.; Wendel, G.J. *SPIE Substance Detection Systems* **1993**, *2092*, 131-136.

[5] Fine, D.H.; Rufeh, F.; Lieb, D.; Rounbehler, D.P. *Anal. Chem.* **1975**, *47*, 1188-1191.

[6] Kaye, W. *Anal. Chem.* **1962**, *34*, 287-293.

[7] Cedron-Fernandez, T.; Saenz-Barrio, C.; Cabredo-Pinillos, S.; Sanz-Vicente, I. *Talanta* **2000**, *57*, 555-563.

[8] Lagesson, H.V.; Nilsson, A.; Tagesson, C. *Chromatographia* **2000**, *52*, 621-630.

[9] Lagesson, V.; Lagesson-Andrasko, L.; Andrasko, J.; Baco, F. *J. Chromatogr.* **2000**, *867*, 187-206.

[10] McQuaid, M.J.; Sausa, R.C. *Appl. Spectrosc.* **1991**, *45***,** 916-917.

[11] Usachev, A.D.; Miller, T.S.; Singh, J.P.; Yueh, F.; Jang, P.; Monts, D.L. *Appl. Spectrosc.* **2001**, *55***,** 125-129.

[12] Schroeder, W.A.; Wilcox, P.E.; Trueblood, K.N.; Dekker, A.O. *Anal. Chem.* **1951**, *23*, 1740-1747.

[13] Hill, Jr., H.H.; Martin, S.J. *Pure Appl. Chem.* **2002**, *74*, 2281-2291.

[14] Thompson, B.A.; Hartek, P.; Reever, R.R. *J. Geophys. Res.* **1963**, *68*, 6431-6436.

[15] Brown, R.F.C. *Pyrolytic Methods in Organic Chemistry*; Academic Press: San Francisco, 1980.

[16] Mastovskw, K.; Lehotay, S.J. *J. Chromatogr. A* **2003**, *1000*, 153-180.

Appendix B. Simple Optical Sensor for Amine Vapors Based on Dyed Silica Microspheres

B.1. Abstract

A new optical sensing method for sensitive detection of amine vapors down to ppb levels is described. The sensor is based on the pH indicator Bromocresol green, adsorbed onto a silica sphere matrix. When the amines adsorb onto the matrix, the color changes from orange to blue. The color change is detected with a fiber optic spectrometer. Sensor performance is demonstrated for the aliphatic amines tert-butylamine, diethylamine and triethylamine and also for ammonia, pyridine and aniline. The response for the aliphatic amines is linear with concentration up to 2 ppm with a detection limit of approximately 1.4 ppb for tert-butylamine. The microsphere sensor is more sensitive than other optical amine sensor designs described in the literature. The sensor response varies with temperature, with lower sensitivity and faster response at higher temperatures allowing for adjustment to prioritize sensitivity or speed. At 80 ºC the response time is 2-20 s, with maximum signal after approximately 2 min and a recovery time of 2–10 min depending on concentration of amine vapor. Sensor response is highly reproducible and fully reversible.

B.2. Introduction

Sensing low concentrations of chemical vapors is an area of great interest with many practical applications. Amine vapors are of particular interest since both aliphatic and

aromatic amines can induce toxicological responses at low concentrations.[1,2] Aliphatic amines can be found in many wastewater effluents from industry, agriculture, pharmacy, and food processing.[3] Hence sensitive and rapid detection of amines is valuable in environmental and industrial monitoring as well as in food quality control.[4] Simplicity, robustness, low weight and high sensitivity are attractive characteristics for chemical sensors in virtually all applications. In addition, the ideal sensor should be capable of continuously monitoring specific analyte levels free from interference with other common organic vapors.

Several different techniques have been developed for amine sensing. Conventional real-time monitoring of gases has commonly been performed employing electrochemical sensors.[5] These are usually based on the oxidation of amines on various anode materials or on chemically modified electrodes.[6,7,8] Biosensors have been constructed employing immobilized amine oxidases or amine dehydrogenases.[9] Other methods of sensing include piezo crystal detectors with PVP (polyvinylpyrrolidone) coating[10] and measurements of resistance in polypyrrole films[11]. Several of these techniques have inherent disadvantages such as the need for reference electrodes, the development of surface potentials and irreversibility. Many of these problems can be circumvented by employing fiber-based optical sensing.

Numerous amine and ammonia sensors employ optical transduction methods. Charlesworth et al. described a fiber optic fluorescence based sensor for amine vapors utilizing a film of the pH-sensitive molecule 2-napthol and reported a sensitivity of 24 ppm.[12] Qin et al. designed an optical sensor for amine detection based on dimer-monomer equilibrium of indium(III) octaethylporphyrin in a polymeric film and reported a

sensitivity of 0.1 ppm (detection limit of 50 ppb) for the most lipophilic amines.[13] McCarrick et al. constructed a visual indicator based on a calix[4]arene, bearing nitrophenylazophenol chromogenic functionalities, complexed with lithium. The modified calixarene underwent a color change from yellow to red for trimethylamine concentrations above 20 ppb. The color change results from deprotonation of an acidic chromophore.[14]

Silica microspheres have been widely employed for the construction of gas-phase chemical sensors.[15,16,17] Their popularity is a result of the ease with which silica sphere matrices are prepared and modified. Silica spheres are easily derivatized and due to the mild reaction conditions it is possible to incorporate various molecules, dyes, organic and organometallic reagents into the silica matrix. Silica sphere matrices are also chemically and mechanically stable and the average pore size, pore size distribution, surface area, refractive index, and polarity of the resultant matrix can be controlled and tailored.[18] These properties enable construction of selective chemical sensors. In a recent paper Onida et al. described a neutral amine-templated mesophorous silica system, impregnated with Reichardt's dye.[19] The resulting material is pink when dehydrated, but turns white when air is readmitted or polar solvents adsorbed. The non-dehydrated system changes color reversibly when exposed to amines and ammonia, but is not affected by other polar or non-polar substances. The system was proposed as a possible ammonia gas sensor.

The amine sensor we describe is based on optical monitoring of micron-sized silica spheres dyed with the pH indicator bromocresol green, spread in a multilayer on a glass slide. This multilayer responds optically to gas-phase sub-ppm (down to 1.4 ppb) concentrations of amines with an increase in absorbance at 620 nm.

B.3. Experimental

Reagents. Silica microspheres (5 μm diameter) were obtained from Alfa Aesar. All amines were analytical or reagent grade products and used without further purification. Triethylamine, tert-butylamine and aniline were obtained from Aldrich, diethylamine from Sigma and pyridine from EM Science. The pH indicator dye Bromocresol green was purchased from Sigma.

Silica bead sensors. The amine sensor comprised a thin multilayer of silica spheres with an adsorbed indicator dye. A uniform suspension was obtained by sonicating a mixture of 60 mg silica spheres, 24 mg bromocresol green and 400 μL acetone for 2 min. Glass plates were cleaned in piranha solution (3:1 conc. H_2SO_4:30% H_2O_2) and stored in methanol until used. (Caution! Piranha solution reacts violently with organics. Use with care.) A couple of drops of silica suspension (total volume 10 μL) were manually applied to a clean glass plate kept tilted at an angle of ~11°. This created a thin, locally uniform layer of silica spheres (1 to 3 layers of spheres deep), as the drop spread and dried. The sensor was allowed to dry overnight in a desiccator. The sensing films were a deep orange color, which changes to blue when exposed to amine vapors.

Instrumentation. Figure B.1 shows a schematic of the optical sensor system. Nitrogen was used as the carrier gas for all experiments. Amine vapor samples were prepared in Tedlar bags at concentrations between 500 ppm and 70 ppb. The amine vapor was diluted with a gas diluter (Custom Sensor Solutions, Model 1010 Precision Gas Diluter) before entering the system through a glass tube (c). The flow rate of diluted amine vapor through the glass tube was 1300 mL/min. This is high enough to saturate the space around the sensor with diluted amine vapor at the desired concentration, and so the sensor is not

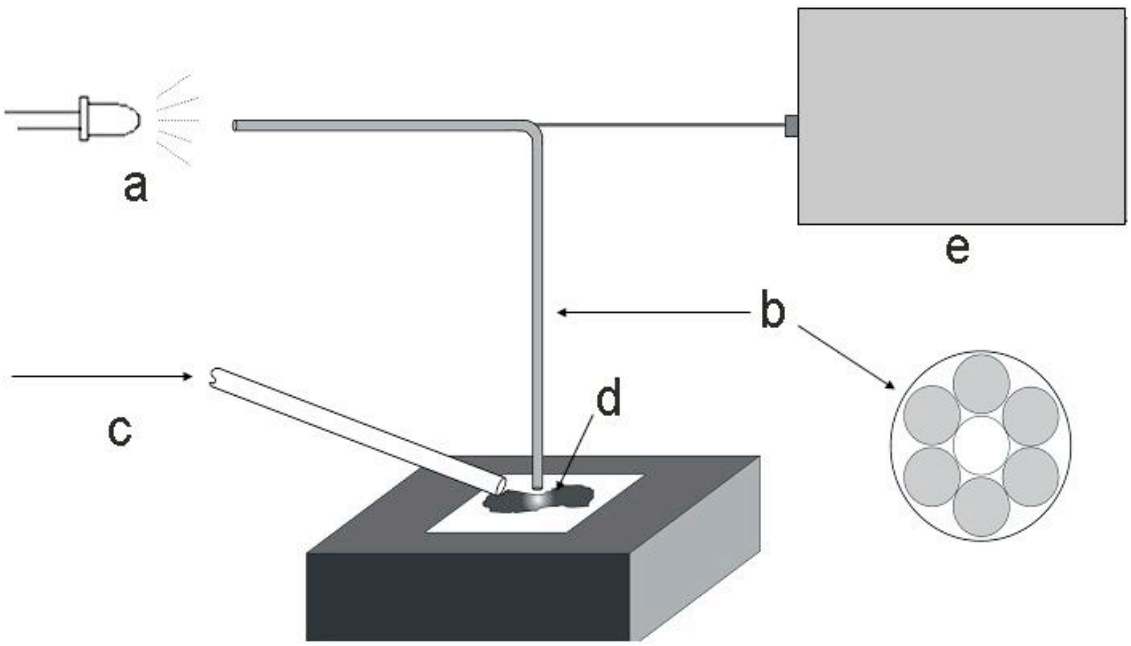

Figure B.1 Schematic diagram of the optical sensor system. An optical fiber (b) carries both incoming light from the LED source (a) and the reflected light from the sensor (d) to the spectrometer (e). The amine vapor is diluted in nitrogen and flows to the sensor through the glass tubing (c).

enclosed in a chamber. The amine sensor (d) (approximately 5 x 10 mm) is mounted on a temperature controlled aluminum block. A white LED (a) was employed as the light source. The output of the LED is passed into the excitation bundle of a six-around-one fiber optic probe (b). The inset of Figure B.1 shows a view of the end of the fiber optic probe facing the sample. Six illumination fibers surround a single read fiber. The diameter of each individual optical fiber was 0.5 mm. The end of the probe is held a few

millimeters above the amine sensor. Reflected light is collected by the read fiber of the probe and is analyzed with a fiber optic spectrometer (e) (Ocean Optics S-2000 fiber optic spectrometer). The absorbance of the light by the sensor over time was analyzed as described below using software supplied by Ocean Optics Inc.

Each new amine sensor was activated by flushing with 5-10 ppm tert-butylamine before use. This was necessary to achieve reproducible results and maximum sensitivity. The activation was only necessary prior to the first use of the sensor. The reason for the enhanced sensitivity after activation with amine is unclear.

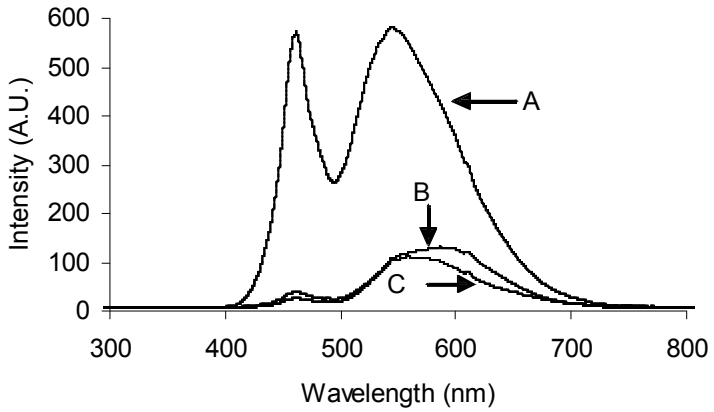

Figure B.2 The diffuse reflectance spectrum of the LED from a white surface (A), the activated sensor (B) and the sensor exposed to 3.5 ppm tert-butylamine adsorbed onto it (C). The absorbance reported in this paper is the change in reflected light intensity between the activated sensor and the sensor with adsorbed amine.

Data acquisition. The reported absorbance in this paper is the change in light absorption between the activated sensor and the sensor with analyte amines adsorbed onto it, where absorbance is defined as $A = -\log (I/I_o)$. Conventionally, light absorbance of

a substance is compared to absorbance of a white surface, i.e. I_o is the intensity of the light reflected off a white surface. In this sensor system it is more convenient to employ the clean sensor as the absorbance reference, I_o. The main advantage is that the difference in the intensity of reflected light between the sensor with and without amine is much smaller than the intensity difference between the sensor and the white background. Figure B.2 gives the raw diffuse reflectance spectra. Curve A shows the reflectance spectra of the LED source from a white surface. Curves B and C show the reflectance from the activated sensor and the sensor with absorbed amine, respectively. The figure also shows that the maximum intensity difference with and without amine adsorbed onto the sensor occurs around 620 nm. Hence all absorbance data was acquired at 620 nm, except for spectra covering the whole wavelength region, with curve B used as the absorbance reference, I_o.

To determine the effect of temperature variations, the sensor system was tested with 1.4 ppm of various amines for 2 min at temperatures between 20 ºC and 120 ºC. All other experiments were performed at the optimal temperature of 80 ºC. The sensitivity was examined for tert-butylamine, diethylamine and triethylamine with concentrations ranging between 0.1 and 2 ppm for diethyl and triethylamine and 1.4 ppb to 28 ppm for tert-butylamine. The aromatic amines pyridine and aniline were only briefly examined at much higher concentrations (approximately 40 and 200 ppm).

For each series, the sensor was exposed to amine vapor for 2 min at each concentration. After the amine vapor was turned off, the sensor was flushed with pure nitrogen until at least 95% of the original signal was recovered.

B.4. Results and discussion

Sensor Response Mechanism. The sensor is based on the spectral properties of pH indicator bromocresol green. Like most pH indicators, bromocresol green (tetrabromo-m-cresolsulfonphthalein) is a weak organic acid whose absorbance spectrum is quite different from the absorbance spectrum of its conjugate base. The structure of bromocresol green and its conjugate base are shown in Figure B.3. A bromocresol green solution changes from yellow to blue over the pH range 3.8-5.4, as the equilibrium shifts to the deprotonated, arylmethine form of the dye. [20] Bromocresol green was selected as the pH indicator because of its appropriate endpoint and the high uptake by the silica beads, probably due to its many polar groups. Other indicators proved to be less effective.

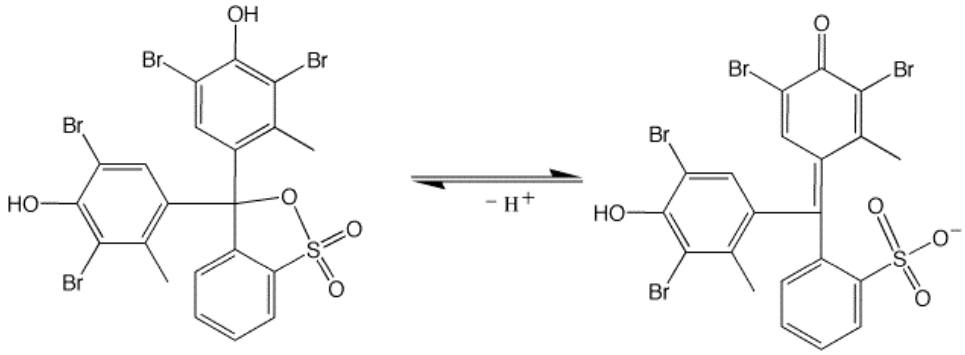

Figure B.3. Bromocresol green and its conjugate base.

Characteristics of the Optical Amine Sensor. Figure B.4 shows the response of the sensor to diethylamine, triethylamine, tert-butylamine and ammonia. By using the sensor itself as a reference, the baseline is set to zero and the absorbance peaks are clearly defined. The maximum absorbance is located at 620 nm for all amines. Thus the

absorbance at 620 nm was monitored to evaluate the response of the sensor to temperature and concentration, as well as saturation and recovery times. Figure B.4 also demonstrates a sensitivity difference between diethylamine, triethylamine, tert-butylamine and ammonia. In particular the response is significantly lower for ammonia. In addition, the sensor was also tested with aniline and pyridine, with the resulting relative sensitivity: diethylamine > triethylamine ≥ tert-butylamine > ammonia >> aniline > pyridine.

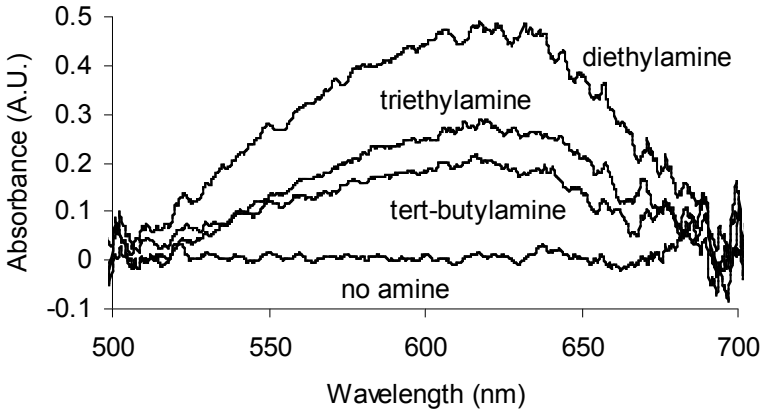

Figure B.4. Absorbance spectra of the sensor with 5 ppm of tert-butylamine, diethylamine and triethylamine, employing the sensor as absorption reference. The response varies significantly between the amines and the difference is correlated to the amines $k_{B,}$ not their acidity in the gas phase.

The response depends ultimately on two factors, the basicity and the hydrogen bonding capability in relation to adsorption of the amine on the silica surface. In solution the dialkyl amines have the highest pK_a while in the gas phase the trialkyl amines are the most basic. The tendency of alkyl groups to stabilize charge through a polarization

mechanism accounts for the basicity of triethylamine in the gas phase. The combined effects of polarization and solvent stabilization due to hydrogen bonding result in a leveling of amine basicities in solution compared to the gas phase[21]. For example, solvent stabilization by hydrogen bonding results in dialkylamines being slightly more basic than trialkylamines. The response pattern, from the relative absorbance strength diethylamine > triethylamine > tert-butylamine > ammonia, suggests an environment where hydrogen bonding is important, similar to that of a solution. It is likely that the amines are hydrogen bonded to hydroxyl groups on the silica surface, which corroborates

Table B.1. Table of pK_a and gas basicity constants for the investigated amines. The amines are ordered from highest to lowest response.

Amine	pK_a[22]	Gas Basicity (kJ/mol)[23]
Diethylamine	10.84	919.4
Triethylamine	10.75	951.0
Tert-butylamine	10.68	899.9
Aniline	5.23	850.6
Pyridine	4.58	898.1

studies suggesting that interaction of adsorbates with the hydroxyl sites on the silica surface generally accounts for the major part of adsorption.[24] The response for pyridine and aniline was orders of magnitude smaller than for the aliphatic amines. The detection limit for aniline is approximately 200 ppm while no response was detected for 230 ppm pyridine. This can be explained by the lower basicity of these compounds (Table B.1).

The correlation between basicity and response indicates that response is mainly determined by basicity of the amine. There is also a difference in adsorption of the amines, however. The strength of the hydrogen-bond interaction between a silica surface and an amine can be measured using spectroscopic methods. Van Cauvelaert et al. measured a significantly stronger interaction between silica and triethylamine compared to butylamine.[25] They concluded that the strength of the interaction depended both on the acid-base properties of the molecule and the steric effects between large groups and the silica surface. This suggests that it should be possible to enhance the selectivity of the sensor by employing a derivatized silica surface, which could select for not only the acid-base properties of the amine, but the shape as well.

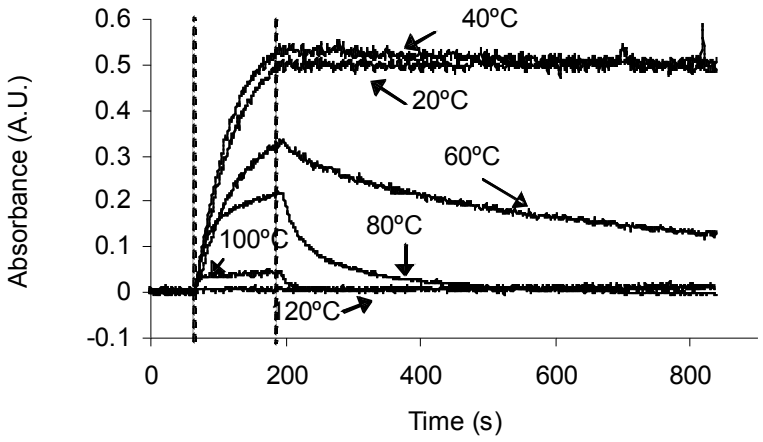

Figure B.5. Absorbance versus time at different temperatures for 1.4 ppm tert-butylamine. Both signal strength and the recovery time depends on temperature. The amine is flowed over the sensor for 2 min (between the dashed lines in the figure) and then turned off. For the lowest two temperatures, 20 ºC and 40 ºC, very little recovery occurred due to evaporation within 10 min of the turn-off of amine vapor. In the range 60–100 ºC evaporation occurs at increasing rates at the cost of decreasing signal. At 120 ºC there is no signal for 1.4 ppm tert-butylamine.

Temperature Dependence. The effect of temperature on the operation of the sensor system was investigated by comparing sensitivity and detection time at 620 nm for 1.4 ppm tert-butylamine vapor at temperatures between 20ºC and 120ºC (Figure B.5). For each temperature, the amine vapor was flowed over the sensor for 2 min followed by 10 min of recovery time. Sensitivity, response time and recovery time are all dependent on temperature. At temperatures below 60ºC the evaporation of amine within 10 min is neglible and the sensor is very sensitive but effectively irreversible. Above 60ºC, the

sensitivity and recovery time both decrease with temperature. At 120ºC there is no longer any response for an amine vapor concentration of 1.4 ppm and hence no higher temperature was investigated. For all experiments described in the next section, 80ºC was employed as the operational temperature as a compromise between a reasonable recovery time of ~10 min and loss of sensitivity at higher temperatures.

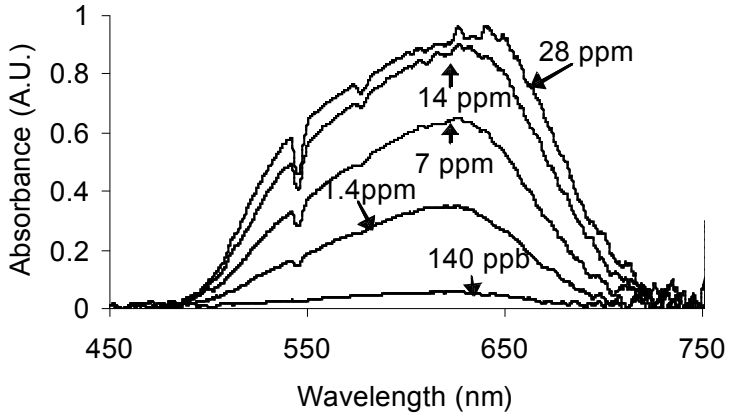

Figure B.6. The absorbance curves concentrations between 0.14 and 28 ppm of tert-butyl amine. The number of adsorption sites seem close to saturation at 28 ppm. The absorbance curves are similar for all concentrations.

Concentration Dependence. Tert-butylamine was detected with a range of concentrations from 140 ppb to 28 ppm (Figure B.6). At 28 ppm the system appears close to saturation and no higher concentrations were tested for the aliphatic amines. The signal strength is clearly dependent on the amine concentration. The maximum absorbance is essentially constant at 620 nm, however, and hence for all other measurements only the peak intensity at 620 nm as a function of time was recorded. Additional data were acquired for tert-butylamine, triethylamine and diethylamine in the low concentration

region of 0.11 to 0.54 ppm. Figure B.7 shows the sensor response at 620 nm for triethylamine at 2 min amine exposures between 0.11 and 0.54 ppm.

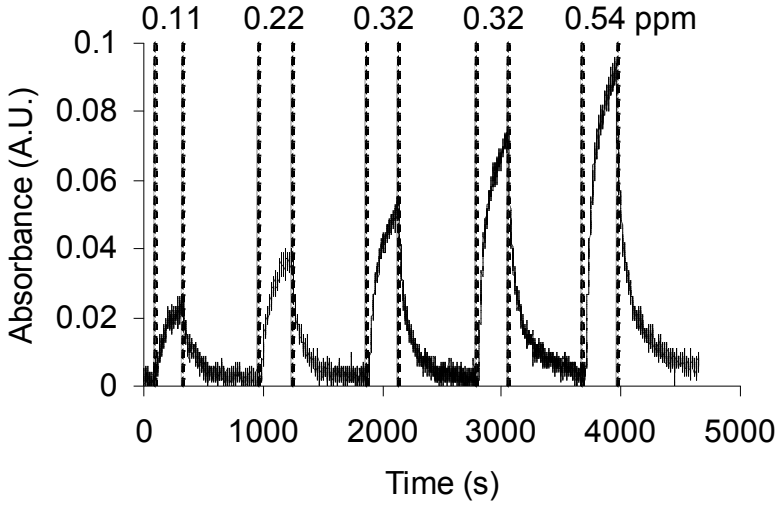

Figure B.7. Successive sensor response at 620 nm for triethylamine at the concentrations 0.11, 0.22, 0.32, 0.43 and 0.54 ppm respectively. This demonstrates sensor reversibility as well as ability to acquire repeated measurements.

A least square regression was employed to model the detector response as a function of concentration for each amine at concentrations between approximately 0.1 and 1 ppm. Figure B.8 shows the response of the sensor after two minutes of amine exposure to different concentrations of tert-butylamine, diethylamine and triethylamine. Linear regression fits the sensor response at low concentrations very well, with a regression constant larger than 0.99 for all three amines. The sensitivity of the sensor, measured by the slope of the regression, differs between the amines. An unexpected feature is the intercept for the tert-butylamine data. The trend lines for triethylamine and diethyl amine pass through the origin, but the tert-butylamine trend line exhibits a non-zero intercept.

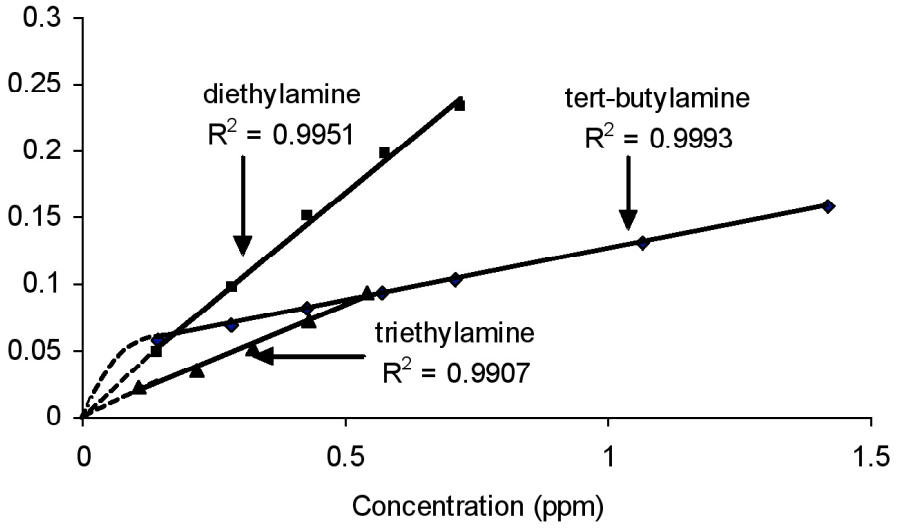

Figure B.8. The relationship between absorbance and concentration of tert-butyl amine, diethylamine and triethylamine. The relationship is linear within the limited domain 0.14 to 1.4 ppm. All correlation coefficients are larger than 0.99. Extrapolated curves are represented by dashed lines.

Activating the sensor with triethylamine yielded the same curve for tert-butylamine as activating with tert-butylamine. To examine if the non-zero intercept was a general feature for primary amines the behavior of ethylenediamine was investigated. The result was a very similar curve to tert-butylamine with a non-zero y-axis intercept. We naturally expect the response of the sensor to be zero at zero concentration. One possible explanation for the result is that at the concentrations used here for tert-butylamine, we have begun to saturate the sensor, and enter a second region of linear response, leading to a flatter curve with a non-zero intercept. This conjecture necessarily leads to a steep slope for the tert-butylamine curve at concentrations below 0.14 ppm (the lowest

concentration shown on the graph). Extrapolated curves that intersect the origin and illustrate this possibility are shown in Figure B.8 as dashed lines. Unfortunately, concentrations lower than about 0.14 ppm are unreliable in our setup, due to the difficulties associated with serial dilution and surface adsorption in the gas diluter tubing. The slopes at these low concentrations would be ordered tert-butylamine > diethylamine > triethylamine.

The complexity of the system makes it difficult to ascertain the origin of the two prominent features of the concentration dependence, the faster saturation of binding sites for primary amines than for secondary and tertiary amines, and the relative steepness of the slopes. The bromocresol green very likely interacts with the silica surface by hydrogen bonding involving the OH and SO_3 functional groups on the molecule. The color change is associated with the deprotonation of the dye by the adsorbed amines and presumably the conjugate acid of the amine interacts both with the surface hydroxyls and the dye molecules by strong hydrogen bonding. The nature of the surface hydroxyls is a key factor to consider. Hertl[22] defined two types of hydroxyls possible on the surface. A-type hydroxyls do not participate in hydrogen bonding interactions, and are "free." B-type hydroxyls are those that are participating in a hydrogen bond. It has been suggested that primary amines have an extended interaction with B-type hydroxyls (hydrogen bonded hydroxyls) on the silica surface compared to secondary and tertiary amines, which interact more with A-type hydroxyls (free hydroxyls)[23]. If there are fewer B-type hydroxyls available, primary amines would saturate faster. This would lead to the non-zero intercept described above. The ordering of the slopes implies that primary amines

adsorb and react with the dye at a faster rate than secondary amines, which are faster than tertiary amines.

A concentration series was also produced for ammonia, with concentrations ranging from 1 to 20 ppm (data not shown). The response of the sensor was linear in this region with $R^2 = 0.98$. The sensor was less sensitive to ammonia than to the alkylamines studied. As previously mentioned, this is due to two factors: the lower basicity of ammonia (Table B.1), and the much higher vapor pressure of ammonia, which results in less adsorption onto the silica surface.

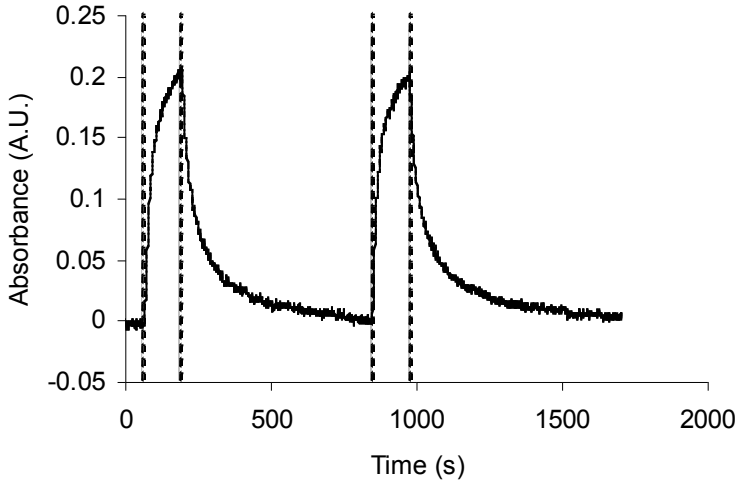

Figure B.9. Absorbance at 620 nm verses time for a pair of 1.4 ppm tert-butyl measurements at 620 nm. The difference in absorbance between the first and second flow of amine is within the error of the gas-diluter.

Reproducibility and recovery time. Figure B.9 demonstrates the reproducibility of the sensor, exposed to 2 min of 1.4 ppm tert-butylamine twice with 12 min between each exposure. The difference in absorbance for detection 1 and 2 is well within the error of

the gas diluter, which is 15% at these concentrations (from the model specifications). The variation between the two measurements is here 1% of the maximum absorbance.

The recovery time is defined as the time from turn-off of amine vapor to the time when the signal has decreased 95%. The recovery time is a function of concentration, with a value of 8 min for 1.4 ppm tert-butylamine (Figure B.9). This is typical for ppm concentrations. Measurements on sub-ppm concentrations typically had a recovery time of less than 5 min and approached 3 min for ppb concentrations.

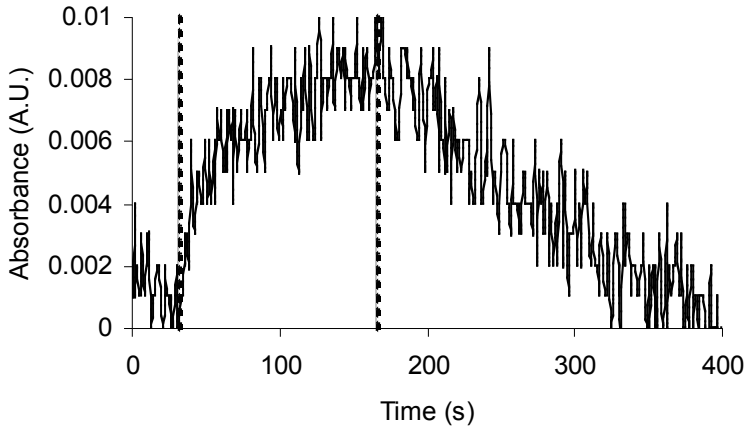

Figure B.10. Detector response for 1.4 ppb tert-butylamine, which approaches the detection limit for this sensor configuration, shown in Figure B.1. The lines marks the time of the flow of amine.

Detection Limit. At 1.4 ppb tert-butylamine vapor the absorbance was approximately 5 times the noise level (Figure B.10) and 1 ppb is hence the detection limit for the experimental arrangement employed in these studies. For these small concentrations it is

important to not let the sensor dry out between measurements since the dry sensor is less sensitive than the sensor recently flushed with amine vapor.

Interferences. Analytes other than amines and ammonia could theoretically interfere with the sensor. Water, due its presence in most settings, is one of the most likely molecules that could present interference. Flushing the sensor with water vapor in ppm concentrations had little effect on the sensor response, however. In addition comparable gas concentrations of methanol, acetone, ether and dichloromethane showed no detectable response from the sensor.

Onida et al[19]. investigated a similar silica system and also did not see any interference from common polar molecules and concluded that the basicity of the amine was responsible for the color change. The only compounds that would interfere with the amine measurements would then be substances more basic than the adsorbed dye. Very few molecules have comparable basicities and interference is hence not expected to be a problem in common settings.

B.5. Conclusions

A new optical sensing method for detecting low-concentration amine vapors down to ppb levels has been described. The sensor is based on the spectral properties of the pH indicator Bromocresol green, adsorbed onto a silica sphere matrix. The sensor's inherent simplicity and ease of manufacturing should make it attractive for further development.

The sensor easily detects sub ppm concentrations of common aliphatic amines and has a linear response up to 2 ppm. The detection limit is below 1.4 ppb, which makes this sensor more sensitive than comparable optical amine sensors in the literature. The

response varies with temperature, allowing for adjustment to prioritize sensitivity or speed. The responses for each sensor were reproducible and fully reversible.

The sensor displays different levels of sensitivity for each amine tested. This is due to the basicity of the amine and its ability to hydrogen bond to the silica surface. Derivatization of the silica would enable the creation of sensors that are more selective. An array of chemical sensors, each with a different derivatization, could then determine both the concentration and identity of amines.

B.6. Acknowledgements

We gratefully recognize the support of the Director's Research and Development Fund at the Jet Propulsion Laboratory and ASTID grant No. NNG04GJ00G. We also thank Ron Grimm for his assistance.

B.7. References

[1] Page, E.H. et al. Occupational and Environmental Medicine 2003, 60, 69-75

[2] Greim H. et al. Chemosphere, 1994, 36, 2, 271-295,

[3] Gong W.L. et al. Environ. Toxicol. Chem,. 2004, 23 2, 239-244

[4] Shakila, R.J.; Vijayalakshmi, K.; Jeyasekaran, G. Food Chemistry 2003 82, 3, 347-352

[5] Opdycke, W.N.; Parks, S.J.; Meyerhoff, M.E. Anal Chim Acta 1983, 155, 11-20

[6] Surmann, P. ; Peter, B. Electroanalysis 1996, 8, 685-691.

[7] Koppang, M. D.; Witek, M.; Blau, J.; Swain, G. M. Anal. Chem. 1999, 71,1188-1195.

[8] Casella, I. G.; Rosa, S.; Desimoni, E. Electroanalysis 1998, 10, 1005-1009.

[9] Niculescu, M.; Nistor, C.; Frebort, I.; Pec, P.; Mattiasson, B.; Csoregi, E.Anal. Chem. 2000, 72, 1591-1597.

[10] Mirmohseni A.; Oladegaragoze A. Sensors and Actuators B-Chemical, 2003, 89 (1-2), 164-172

[11] Ratcliffe, N. M. Anal. Chim. Acta, 1990, 239, 257-262

[12] Charlesworth, J. M.; McDonald, C. A. Sens. Actuators, B 1992, 8, 137-152

[13] Qin, W.; Parzuchowski, P.; Zhang, W.; Meyerhoff, M. E. Anal. Chem, 2003, 75, 332-340

[14] McCarrick, M.; Harris, S. J.; Diamond, D. J. Mater. Chem. 1994, 4, 217-221

[15] Collinson, M. M. Critical review of Analytical Chemistry, 29 (4) 1999 289-311

[16] von Bultzingslowen, C. et al. Analyst, 127 (11) 2002 1478-1483

[17] Makote R, Collinson M.M. Anal. Chim. Acta 394 (2-3): 195-200 AUG 9 1999

[18] Collinson, M. M. Critical Reviews in Analytical Chemistry, 1999, 29(4):289–311

[19] Onida, B., Fiorilli, S., Borello, L., Viscardi, G., Macquarries, D., Garrone, E. J. Phys. Chem. B, 2004, 108:16617-16620

[20] Wang, E.; Zhisheng, S. Anal. Chem. 1987, 59, 1414-1417

21 Arnett, E.M.; Jones, III, F.M.; Taagepera, M.; Henderson, W.G.; Beauchamp, J.L.; Holtz, D.; Taft, R.W.; J. Am. Chem. Soc. 1972, 94, 4724-4726.

[22] Handbook of Chemistry and Physica, 82nd edition, CRC Press LLC, 2001

[23] Hunter, E.P.; Lias, S.G. J. Phys. Chem. Ref. Data, 1998, 27, 3, 413-656.

[24] Hertl, W.; Hair, M. L.; Journal of Physical Chemistry 1968, 72, 4676-4683

[25] van Cauvelaert, F.H.; Vermoortele, F.; Uytterhoeven, J.B. Discussions of the Faraday Society, 1976, 52: 66-76